AIX-MARSEILLE UNIVERSITÉ
ÉCOLE DOCTORALE SCIENCES POUR L'INGÉNIEUR
Mecanique, Physique, Micro et Nanoelectronique / ED353
LABORATOIRE DE MÉCANIQUE ET D'ACOUSTIQUE - UMR CNRS 7031

WAVE PROPAGATION IN PERIODIC STRUCTURES APPLIED TO WOODWIND TONEHOLE LATTICES

HOW THE CUTOFF FREQUENCY BALANCES SOUND PRODUCTION AND RADIATION

Erik Alan PETERSEN

Doctoral Dissertation / Thése de doctorat

Discipline : Engineering sciences
Specialty : Acoustics

Defended on 20 November 2020 in Marseille, France in front of the jury:

DALMONT, Jean-Pierre	Université du Maine	Rapporteur
SHARP, David	Open University	Rapporteur
CHABASSIER, Juliette	INRIA	Examinateur
HÉLIE, Thomas	IRCAM	Examinateur
POCHEAU, Alain	Aix-Marseille Université	Examinateur
GUILLEMAIN, Philippe	CNRS, LMA	Directeur du thèse
KERGOMARD, Jean	CNRS, LMA	Invité
JOUSSERAND, Michaël	Buffet Crampon	Invité

AFFIDAVIT

I, Erik PETERSEN, hereby declare that the work presented in this manuscript is my own work, carried out under the scientific supervision of Philippe GUILLEMAIN, in accordance with the principles of honesty, integrity and responsibility inherent to the research mission. The research work and the writing of this manuscript have been carried out in compliance with both the French national Charter for Research Integrity and the Aix-Marseille University Charter on the fight against plagiarism.

The work presented in this manuscript has not been submitted previously either in France or in another country in the same or in a similar version as part of another examination or defence process.

Place date

Signature

ABSTRACT

The research goal of this dissertation is to evaluate how the tonehole lattice cutoff frequency affects the sound production and radiation of woodwind instruments. Below the cutoff, waves entering the tonehole lattice are evanescent, where as above cutoff waves can propagate freely within the lattice. Therefore, the low frequency response of the resonator that determines the playing frequency of a woodwind is set by the length between the reed and the first open tonehole, while the high frequency response is governed by the remaining open toneholes downstream on the instrument. A study of the cutoff frequency that separates these two bands is, in effect, a study of how this 'unused' portion of the tonehole lattice may influence the sound of the instrument. Following the work of Benade in the 1960s, studies on this subject have been rare, despite its central importance to the sound of woodwind instruments. This dissertation includes analytical, numerical, and experimental advances on the subject of the cutoff frequency, approached in three published studies. In the first, cylindrical academic resonators are analytically designed to have specific cutoffs while maintaining the same first resonance frequency. They are then compared using digital synthesis based on a physical model of the instrument. The cutoff is found to have a modest impact on sound production, evaluated using the pressure and flow waveforms within the mouthpiece, where the greatest effect is a randomization of the relative amplitude of even and odd harmonics above the cutoff. There is little evidence that the 'ease of playing' of the resonators is affected by the cutoff. In the second study, the academic resonators are played by a musician using a clarinet mouthpiece during *in situ* measurements. The radiated sound demonstrates a 'region of reinforced spectra,' for which there is an amplitude increase of both even and odd harmonics around the cutoff of each resonator. The third study derives the cutoff theory for conical resonators and introduces new quantitative descriptors to estimate the cutoff of acoustically irregular lattices. An analysis of the saxophone demonstrates that the cutoff varies considerably over the first register of the instrument. The results also demonstrate ways in which the theory of wave propagation in periodic media can succeed or fail when applied to real instruments. Preliminary results for two additional studies are presented. In the first, the methods developed for the saxophone are applied to another conical instrument, the bassoon. The results show that, compared with the saxophone, the cutoff of the bassoon is homogeneous across different fingerings of the first register. In the second, the effect of diffraction from a simplified resonator is evaluated using a boundary element method. The results are compared with a simplified analytical radiation model and anechoic measurements, showing that the more efficient simple model is generally sufficient. This dissertation demonstrates ways in which the cutoff affects both internal waveforms and, more importantly, the radiated soundfield of woodwind-type instruments. It also advances the theoretical basis for incorporating the cutoff into a tonehole lattice conception, which is of practical use for instrument manufacturers.

Key words: musical acoustics; periodic waveguides; woodwinds; tonehole lattice cutoff frequency

RÉSUMÉ

L'objectif de cette thèse est de contribuer à évaluer comment la fréquence de coupure créée par un réseau de trous latéraux ouverts dans un instrument de musique de la famille des bois agit sur la production et le rayonnement du son produit par ces instruments. En dessous de cette fréquence de coupure, les ondes pénétrant dans le réseau de trous ouverts sont évanescentes, tandis qu'au delà de cette fréquence les ondes peuvent se propager dans le réseau. Par conséquent, la réponse basse fréquence du résonateur qui détermine la fréquence de jeu est directement reliée à la longueur entre l'anche et le premier trou ouvert, tandis que la réponse à haute fréquence est déterminée par le réseau de trous ouverts. Une étude de la fréquence de coupure séparant ces deux bandes de fréquence correspond donc à comprendre comment cette partie "inutilisée" du résonateur joue sur le son produit. Depuis les travaux de Benade dans les années 1960, les études sur ce sujet ont été rares bien qu'il s'agisse d'un sujet central sur le son des instruments à vent. Ce manuscript comprend des études analytiques, numériques et expérimentales relatives à la fréquence de coupure et est étayé par trois articles de revues. Tout d'abord, des résonateurs cylindriques "académiques" sont conçus analytiquement de sorte à fixer leurs fréquences de coupure tout en maintenant la première fréquence de résonance constante. Ces résonateurs sont ensuite comparés en utilisant une synthèse numérique reposant sur un modèle physique de fonctionnement. Un premier résultat est que la fréquence de coupure a très peu d'effet sur la production du son, calculée grâce à la pression et au débit interne dans l'embouchure de l'instrument. Au delà de la fréquence de coupure, on assiste à une répartition aléatoire des amplitudes des harmoniques pairs et impairs. Il y a donc très peu d'effet de cette fréquence de coupure sur la "facilité de jeu" d'un instrument. Dans une seconde étude, les résonateurs sont réalisés physiquement et joués par un musicien grâce à l'ajout d'un bec de clarinette. Le spectre externe présente une région où il y une augmentation du niveau des harmoniques, tant pairs qu'impairs, au voisinage de la fréquence de coupure. La troisième étude étend la théorie de la fréquence de coupure au cas de résonateurs coniques et introduit de nouveaux descripteurs pour estimer la fréquence de coupure de réseaux acoustiquement irréguliers. Une analyse sur le saxophone montre que la fréquence de coupure évolue de note à note au long du premier registre. Nous montrons également dans quelle mesure la théorie de propagation d'ondes dans des milieux périodiques peut fonctionner ou échouer dès lors que l'on s'intéresse à un instrument existant. Des résultats préliminaires de deux autres études dont également présentés. La première concerne le basson, pour lequel on applique les méthodes développées pour le saxophone. Les résultats montrent que, contrairement au saxophone, la fréquence de coupure reste quasiment constante tout au long du premier registre. La deuxième concerne l'utilisation d'éléments finis de frontière (BEM) pour étudier la diffraction d'un resonator muni de trous. Ce calcul est comparé avec celui produit par un calcul analytique simple et une expérience en chambre anéchoïque, qui montre qu'un modèle simple est suffisant. Dans cette thèse, nous montrons comment la fréquence de coupure agit sur les formes d'onde et le spectre de la pression et du débit internes et plus significativement sur le champ rayonné. Nous avançons également sur les bases théoriques permettant d'inclure ce critère dans un objectif de conception, à destination des facteurs.

Mots clés acoustique musicale; guides d'onde periodiques; instrument de la famille des bois; fréquence de coupure d'un reseau du trous latéraux

ACKNOWLEDGMENTS

I had the good fortune of spending my three years of doctoral research in the Laboratoire de mecanique et d'acoustique on the coast of the mediterranean in Marseile, France. This opportunity alone, learning a new language, experiencing a different culture, and access to all of Europe is reason enough to be thankful.

All of this was possible grace a mon directeur du these, Philippe Guillemain, who agreed to supervise my research and integrate me into the research group at LMA. I appreciate his guidance both academically as well as his insistence on weekly group lunches and communal coffee breaks. I must also thank my *de factor* co-adviser Jean Kergomard who contributed considerably to the direction of my research often pushing it towards the physics and acoustics direction over signal processing, and a never ending source of historical information and relevant citations. I am also grateful to Jean-Pierre Dalmont and David Sharp who agreed to serve as rapporteurs in my jury, as well as the other members Julieete Chabassier, Thomas Helie, Alain Pocheau, and Michael Jousserand for their comments and questions regarding my manuscript.

I am also grateful to the many other people with whom I worked over these three years. At a greater distance (3.5 hrs by train) I appreciate the collaboration of Michael Jousserand at Buffet Crampon, providing the occasional reminder that the work relates to real instruments. Christophe Vergez and Fabrice Silva both helped with their insights on many topics as well as graciously agreeing to comment on my dissertation manuscript despite very busy schedules. Thank you to Patrick Sanchez for his 'get er done' attitude (what is the french equivalent of that expression?). Of course Marc Pachebat and Regine Guillern must be acknowledged for agreeing to collaborate on an inter-term project between the acousticians and mechanics people!

The greater environment of researchers and engineers in the equipe SONS and at LMA in general also provided many opportunities for useful and pleasant interactions over a petit cafe, in addition to tangible help. I think for example about the Guy Rabau and the shop team for drilling plenty of holes through plastic tubes and Jaques Chatron for generously lending microphones and expertise at a moments notice.

I appreciate the interaction, both collegial and social with the other graduate students in the lab. I had the good opportunity to engage in a recipe exchange with Louis Guillot. A great thank you to Tom Colinot, with whom I frequently collaborated, both for his contribution to my research projects but also as a friend. Within the social aspect, I also want to thank the members of my orchestra OSAMU for accepting a violist who spoke no French at first, and for the many after rehearsal 'coups' that they invited me to, even if it was usually too late for me to accept.

Nearing the end, I thank my family - my father Trond Petersen, mother Mary Visher, and sister Janneke Petersen - for their constant support and occasional interest in this work. They have put up with my interest in acoustics for many years now. I want to thank Karin Sveen and Liv Duesund for generously loaning their koselig house in the Norwegian mountains during the final preparation of my dissertation and defense. There was no better place to be for those final weeks.

And finally, I must thank my partner Gabriella Smith for everything. Agreeing to move to Europe with me now more than three years ago, even when her career is centered

in the United States. Her patience and interest in hearing about my research, which may not be that exciting for non-acousticians. And for generally being the best coatch in the world.

Table of Contents

Chapter 1

Introduction

This research begins with the question: what are the factors that balance sound production and radiation of woodwind instruments? It is clear that both are necessary. An instrument must function sufficiently well in order to be played by a musician, but it must also sound good enough to be acceptable to the musician and audience alike. However, instruments evolved over centuries following a primarily empirical design process. Manufacturers modified instruments based on experience and intuition, and the modifications that 'improved' the instrument in one way or another were generally favored. A modern understanding of acoustics played a relatively small role in the evolution of musical instruments. Therefore, the acoustical analysis of sound production and radiation of existing instruments is inherently an *a posteriori* study - an attempt to explain how these are balanced which was not likely understood at the time of its conception.

Current knowledge of acoustics and access to scientific tools allows this question to be treated in a new way. For example, sound production can be probed using various synthesis algorithms to evaluate playing characteristics such as sounding frequency and the emergence of higher registers. Modern computers and recording equipment allow for easy spectral analysis of the radiated sound, which can be used as a quantitative complement to the observations of a skilled listener. Lastly, the development in other areas of physics over the last century, such as the theoretical basis of wave propagation in periodic structures, can be applied to the study of musical acoustics. These relatively new tools can be used to analyze the acoustics of empirically evolved existing instruments in addition to aiding new instrument conception.

1.1 A bit of history

Treating woodwind tonehole lattices as a periodic structure that can be studied through the perspective of wave propagation in periodic media began with Arthur Benade [1]. Based on his experience as a physicist, he observed a cutoff frequency type phenomenon that is characteristic to periodic media in many different fields [2, p. vii-viii]. He came to the conclusion that [3, p. 485]

> ...we can go so far as to use the cutoff frequency as a number that implies a great deal about the entire musical personality of the instrument...

and used this hypothesis as the basis for many studies, up to his final, posthumous articles [4, 5].

The cutoff observed by Benade separates the acoustical response of a woodwind resonator into two different frequency bands. At low frequencies, below the cutoff, a wave is not able to propagate in the portion of the instrument that has open toneholes, while above the cutoff, waves are able to propagate within the lattice. The effect of these two bands is readily observed through many measurable characteristics of the instrument [3], for which many examples are provided in Chapter 2 of this dissertation.

Stop and pass bands of this type are observed in many areas of physics benefiting from a rich, interdisciplinary theoretical and practical development. As is often the case for acoustics, these methods were developed in other disciplines of physics such as solid state physics and the study of crystal lattices, and then applied to new areas such as acoustics. In the foreword of his book [2, p. vii-viii], Brillouin observes

> All problems discussed [in this book] deal with periodic structures of various kinds, and they all lead to similar results: these structures, be they electric lines or crystal lattices, behave like band-pass filters. If energy dissipation is omitted, there is a sharp distinction between frequency bands exhibiting wave propagation without attenuation (passing bands) and those showing attenuation and no propagation (stopping bands).

He continues with a short historical review of how this has been discovered in different disciplines. The application of this theory to woodwind toneholes by Benade follows a path that is more general than the discipline of acoustics, let alone the niche of musical acoustics.

Benade's studies on the cutoff generally fall into two categories: first as an immutable characteristic of a resonator that is defined solely by its geometry, and second through its influence on the spectral characteristics of internal waveforms and the sound radiated from an instrument under playing conditions. A full account encompasses nearly three decades of publications and presentations, many of which are vulgarizations targeted towards intrepid musicians, not all of which will be presented here.

In the first category, Benade's contributions include a derivation for the cutoff based on the geometry of a lattice of open toneholes, in addition to a derivation for how waves propagate through a lattice of closed toneholes, a topic that is not treated in the current work [1]. Also in this category, he observed that real instruments do not have geometrically periodic lattices, so different fingering of an instrument may have a different cutoffs. From input impedance measurements, he estimated the cutoffs across the first register of many different instruments. From this, he produced charts of the cutoffs as a function of fingering, which can be used to compare subtle differences between instruments of the same type, as well as identify global trends that distinguish different instrument families [3]. He comments that many instruments have very little evolution of the cutoff across different fingerings,[1] and postulates that this is a desirable quality in an instrument.

The second category of Benade's research on the cutoff involved the sound radiated from real and "academic" resonators [7]. Many of these studies were qualitative, focusing

[1] However, Chapter 5 [6] of the current document provides a counter example for a common woodwind, the saxophone.

musicians' response to changes in the cutoff. In one project, he modified two B♭ clarinets in such a way that the cutoff of one was lowered by about 2 percent while the other was raised by about 2 percent [8]. He had musicians with different backgrounds play both instruments and found that classically trained musicians preferred the instrument with a lower cutoff and jazz musicians preferred the instrument with a higher cutoff, with both groups deeming the other instrument unusable. In another study, he created an "isospectrum clarinet" for which the cutoff changed with each note in such a way that there were always (only) three strong input impedance peaks below the cutoff [9]. This instrument is reported to sound particularly 'dark' and the high notes 'bright,' albeit without elaborating on a criteria evaluating the sound. These types of experiments provide strong qualitative evidence for the centrality of the cutoff in determining an instrument's character, but fall short of establishing a direct, quantitative link. It is in his final two articles that a quantitative assessment is attempted, first for a clarinet and then for a saxophone [4, 5]. These studies are based on *in situ* measurements followed by an analysis of the spectral characteristics of the radiated sound. While the results are impressive and musically relevant, the fact that real instruments do not necessarily have well defined cutoffs leads to a certain ambiguity of the results, particularly for the saxophone.

In his dissertation research Worman, advised by Benade, approached the problem of sound production in single reed instruments, including some discussion of the tonehole lattice cutoff [10, 11, 12]. The effect of the cutoff frequency was evaluated using three academic resonators that had respectively one, two, and three input impedance peaks below the cutoff, and observing the pressure waveform inside the mouthpiece. The first resonator had a nearly sinusoidal waveform, whereas the resonators with two and three peaks became progressively more harmonically rich. This includes the growth of even harmonics, attributed to the nonlinear coupling between odd harmonics [13]. He observes that the 'ease of oscillation' or 'regeneration' appears to be proportional to the number of input impedance peaks below the cutoff. This includes a discussion regarding the effect of the input impedance peak harmonicity on the flexibility of playing frequency, also of importance for higher registers [14]. However, Worman remarks that if there are too many peaks below cutoff, which would be the case for a cylinder without a lattice, the radiated tone becomes so rich in harmonics as to sound unpleasant or harsh. This is an important comment regarding the competition between sound production and radiation, directly linking the 'ease of playing' and the produced sound, although he does not further develop the subject.

Following these first two decades of research, some additional studies on the cutoff were published by Kergomard and Keefe, among others, mainly focusing on its impact on radiation [15, 16, 17] although with some aspects of sound production [18, 19, 20, 21]. More recently, Moers demonstrated the link between academic periodic lattices and the complicated tonehole lattices of real instruments, a theoretical advance that opens many possible research questions [22, 23]. Also relating to real instruments, Wolfe showed that the cutoff of flutes has increased over centuries of instrument development, likely to match changing musical needs and evolving timbre preferences [24].

Despite these more recent studies, the sustained level of interest in the tonehole lattice cutoff frequency dropped drastically as the researchers after Benade carved out other

areas of expertise. One is left with many analytical tools for understanding the tonehole lattice cutoff and thoroughly convinced that it has a large impact on the character of an instrument. However, the link between sound production and radiation is not fully developed, nor has the theoretical basis for controlling the cutoff been explicitly adopted by instrument manufacturers, although the cutoff may be accounted for in numerical optimization of woodwind resonators [25].

This dissertation presents a series of studies that seek to understand the balance between sound production and radiation of woodwind instruments approached using the theory of wave propagation in periodic structures.

1.2 Document organization

The remainder of the manuscript is organized as follows:

Chapter 2: This chapter presents both the classical theory of the tonehole lattice cutoff frequency in addition to developing new interpretations, particularly with respect to comparing academic resonators with real woodwind instruments.

- First, the theory of acoustic propagation in periodic air columns is reviewed including a derivation of the tonehole lattice cutoff frequency.
- Next, an exploration of how the cutoff affects wave propagation in simplified resonators demonstrates the phenomena through controlled, academic examples. This includes examples of internal characteristics such as the input impedance and reflection coefficient. External characteristics are also presented, such as the directivity and transfer function between internal and external pressure and flow variables.
- The final section repeats the above analysis for internal and external variables, but this time applied to a clarinet. This is to highlight the ways in which the theory of wave propagation in periodic media can succeed and fail when applied to real instruments.

Chapter 3: [Article] The effect of the cutoff frequency on sound production of a clarinet-like instrument

- An analytical model is developed for resonators with independently variable first input impedance peaks and cutoff frequencies. The input impedances of three resonators with the same first peak and 1.0, 1.5, and 2.0 kHz cutoffs are simulated.
- The internal pressure and flow waveforms are simulated using digital synthesis. The effect of the cutoff on sound production is evaluated by comparing the playing frequency, spectral centroid, odd/even harmonic parity, and attack time.

Chapter 4: [Article] The link between the tonehole lattice cutoff frequency and clarinet sound radiation: a quantitative study

- Resonators with 1.0, 1.5, and 2.0 kHz cutoffs are manufactured and played using a clarinet mouthpiece. The effect of the cutoff is evaluated using *in situ* measurements and analyzed in terms of spectral characteristics of the radiated sound.
- Experimental results are replicated by simulation using a digital synthesis model coupled with a simple analytic radiation model. Qualitatively similar results are presented for the radiated sound of a real clarinet.

Chapter 5: [Article] On the tonehole lattice cutoff frequency of conical resonators: applications to the saxophone

- The theory of acoustically regular lattices is derived for a conical lattice, including the analytic formulation for designing resonators with variable first input impedance and cutoff frequencies, as was done in Chapter 5.
- Then the theory is applied to the geometry of an alto saxophone. New descriptors of the cutoff are developed to account tonehole lattices that are not strictly periodic, as is the case for the saxophone.

Chapter 6: General conclusion and suggestions for future work

The Appendices: In addition to the main chapters of this dissertation, two projects are presented in the appendices. Here, preliminary results are provided to demonstrate additional topics and techniques used in this dissertation.

- **Appendix A** examines the passive radiation properties of the academic resonators used in Chapter 4. A BEM radiation model that accounts for diffraction is compared with a simple analytic radiation model and anechoic measurements.
- **Appendix B** applies the methods developed in Chapter 5 to the measured geometry and input impedance of a bassoon. Additional cutoff descriptors are also introduced.

Chapter 2

Wave propagation in periodic acoustic lattices: applications to woodwind resonators

The purpose of this chapter is to orient the reader to the topic of the tonehole lattice cutoff frequency, and how it applies to woodwind instruments. This is accomplished in three basic steps, involving a review of wave propagation in periodic waveguides, followed by a series of examples of the implications of this theory using academic waveguides and, in a third step, comparing the results demonstrated for the academic resonators to the behavior of real instruments. This chapter does not attempt to provide a comprehensive overview of the functioning of a woodwind instrument, and notably ignores any detailed discussion regarding the coupling of the nonlinear excitation mechanism with the resonator that facilitates auto-oscillation, for which there are many examples in the literature [26] (see also [23, 27]). This aspect of musical woodwind acoustics is not particularly concerned with the details of the resonator: the primary importance of the resonator feedback for auto-oscillation is limited to several of its lowest resonances. From this perspective, the influence of the resonator is determined by the distance between the reed and the first open tonehole while the lattice is essentially ignored. Here, the purpose is to study the effect of the lattice, a rich topic on its own. Therefore, a detailed development of the lattice theory is considered the to be foundational material of this manuscript.

The first task in orienting the reader is a reproduction and synthesis of previous research regarding acoustic waveguides from the literature. This is accomplished by first presenting some necessary tools and notations, including the linear acoustic wave equation and the transfer matrix method used to simulate acoustic waveguides. This formalism is then used to derive the acoustic propagation equations of a periodic waveguide, which constitute the theoretical basis of the cutoff frequency of a tonehole lattice [3, 23, p. 377]. Both of these are mature topics, having been developed in the beginning and middle of last century. These sections serve two purposes: an explicit statement of the simulation model, and a full derivation of the cutoff frequency, which is presented only in abridged versions in the publications that make up this manuscript. From here, the relevant bibliography becomes more recent with the introduction of a variation of the transfer matrix method developed in the last decade that accounts for external tonehole interactions [28]. This variation does not differ fundamentally from the classic method,

so the discussion in this text does not focus on the mathematical details. Instead, an explanation is provided for how this variant may be exploited in ways that the classic method can not, and why it is particularly suited for simulating periodic lattices. Finally, a recent interpretation of the cutoff frequency links the classical theory of wave propagation in periodic media to acoustic waveguides that are not geometrically periodic, but are acoustically periodic, a result that provides the foundation for the research in this dissertation [22, 23, p. 383]. Taken together, Sections 2.2 and 2.3 present the principle concepts and sufficient mathematical details that link together these approximately 100 years of research.

The second task in orienting the reader is to demonstrate some of the characteristics of wave propagation in periodic acoustic waveguides. This is accomplished by presenting a series of examples that are chosen to illustrate these characteristics on internal and external acoustic variables. Here, the academic resonators are designed using original results which form part of the publication in Chapter 3 [29]. However, in Section 2.4, the academic resonators are used to demonstrate characteristics of woodwind instruments that have been known for decades [15, 17], in addition to new observations and contributions. The purpose of this section is to provide very clear examples of cutoff behavior, explore some of the different possible data representations, and highlight some of the possible pitfalls when studying the cutoff, all of which is to help the reader interpret the results of subsequent chapters.

The third and final task necessary to orient the reader is to apply the above theory to real woodwind resonators. Real instruments do not have geometrically or acoustically periodic lattices and generally have other geometric features that are not accounted for in the derivation of the cutoff frequency, so their acoustic response is influenced by additional factors. This discussion is caste predominantly in comparison with the previous theoretical considerations: in what ways does a real instrument resemble the academic resonators, and in what ways do they differ? Do the characteristics of a cutoff that are easily recognized with academic resonators present in the same manner on a real instrument, and in what ways might the observer be fooled by phenomena observed on real instruments that are unrelated to the lattice? These questions are explored for both internal and external acoustic pressure and flow variables. This is an important perspective that allows the reader to differentiate between competing factors when considering a real instrument.

2.1 The wave equation

The following exposition of wave propagation in acoustic waveguides and the derivation of the cutoff frequency requires some equations from acoustics in fluid media.[1] The (linearized) hydrodynamic equations of acoustics in a homogeneous and quiescent fluid without a source are

$$\frac{\partial \rho}{\partial t} + \rho_0 \nabla \cdot v = 0, \tag{2.1}$$

[1] The following sequence of equations follows Pierce [30, p. 18], but the general derivation in various forms dates back several centuries.

$$\rho_0 \frac{\partial v}{\partial t} = -\nabla p, \tag{2.2}$$

$$p = c^2 \rho, \tag{2.3}$$

for acoustic pressure $p(x,t)$, acoustic particle velocity $v(x,t)$, acoustic density $\rho(x,t)$, ambient density ρ_0, and speed of sound c. These equations are often referred to as the Equation of Continuity (conservation of mass), Euler's Equation, and the Equation of State. Through substitution, they may be used to derive the one dimensional plane wave equation

$$\frac{\partial^2}{\partial x^2} p(x,t) - \frac{1}{c^2} \frac{\partial^2}{\partial t^2} p(x,t) = 0, \tag{2.4}$$

which has solutions of the form $p(x,t) = Ae^{j(x-ct)} + Be^{j(x+ct)}$, corresponding to the superposition of outgoing and incoming waves. Here, A and B are amplitudes, j the imaginary unit.

Assuming time harmonic signals, the frequency domain Helmholtz equation is

$$\frac{\partial^2}{\partial x^2} P(x,\omega) + k^2 P(x,\omega) = 0, \tag{2.5}$$

where $P(x,\omega)$ is the frequency domain acoustic pressure, $\omega = 2\pi f$ the angular frequency, and $k = \omega/c$ the wave number. For the case of progressive waves, the frequency domain acoustic velocity is $V(x,\omega) = P(x,\omega)/z_\mathrm{s}$ where $z_\mathrm{s} = \rho c$ is the characteristic impedance of air. The acoustic flow $U(x,\omega) = V(x,\omega)S$ is the acoustic velocity multiplied by a surface S. Here, the surface is taken as the cross section of the duct at the location for which $V(x,\omega)$ is defined. For the remainder of the manuscript the acoustic pressure $P(\omega)$ and flow $U(\omega)$ are the primary acoustic variables, treated in the frequency domain, where the spatial dependency x is omitted in favor of a discrete spatial index w or n [2]. Additionally, the rest of the manuscript uses ρ instead of ρ_0 to denote the ambient fluid density because the acoustic fluctuation of density is no longer needed.

2.2 Modeling an acoustic waveguide

A tool used in the current work to calculate the response of an acoustic waveguide is the Transfer Matrix Method (TMM) [31, 32] and a variant, the Transfer Matrix Method with external Interactions (TMMI) [28]. Here, the basic equations for the TMM are provided, which can be easily adapted for the TMMI with minimal modification. None of Section 2.2 is new with the exception of the adaption of the TMMI to simulate radiation described qualitatively in Section 2.2.5.

For an acoustic waveguide with various basic elements (Section 2.2.1), the TMM uses transfer matrices that have analytic solutions relating the input and output of each w^{th} element. The variables used in this work are acoustic pressure $P(\omega)$ and flow $U(\omega)$, although there exist analogous formulations for electrical and mechanical systems using

[2] The distinction between w or n is detailed in Section 2.2.4.

voltage/current and force/velocity variables [33]. More generally, the TMM is suited to resolve a wide range of wave propagation topics outside of acoustics, including elastic waves, electromagnetic waves, and problems in quantum mechanics.

2.2.1 Passive response of a generic waveguide

The transfer of pressure and flow across the w^{th}-element is written generically

$$\begin{pmatrix} P_w(\omega) \\ U_w(\omega) \end{pmatrix} = M_w(\omega) \begin{pmatrix} P_{w+1}(\omega) \\ U_{w+1}(\omega) \end{pmatrix}, \tag{2.6}$$

where

$$M_w(\omega) = \begin{pmatrix} A_w(\omega) & B_w(\omega) \\ C_w(\omega) & D_w(\omega) \end{pmatrix}. \tag{2.7}$$

The coefficients $A_w(\omega)$, $B_w(\omega)$, $C_w(\omega)$, $D_w(\omega)$ depend on the geometry of the element and generally vary with frequency $f = \frac{\omega}{2\pi}$. Different types of elements can be concatenated to form more complex waveguides consisting of a total W elements. The pressure and flow variables at the input of the first element are related to the pressure and flow variables at the output of the W^{th} element by the matrix multiplication of the transfer matrix across each w^{th} element

$$\begin{pmatrix} P_1(\omega) \\ U_1(\omega) \end{pmatrix} = M(\omega) \begin{pmatrix} P_{W+1}(\omega) \\ U_{W+1}(\omega) \end{pmatrix}, \tag{2.8}$$

where

$$M(\omega) = \prod_{w=1}^{W} M_w(\omega) = M_1(\omega)M_2(\omega)M_3(\omega)\cdots M_W(\omega). \tag{2.9}$$

More generally, once the pressure and flow is determined at one position it is possible to calculate the pressure and flow at any other location by accounting for the successive impact of each intermediary element. The basic elements used in this work are cylindrical ducts, conical ducts, discontinuities of the duct radius, and short branches that terminate either in open space or a rigid cap, referred to as toneholes in the musical community. Waves are assumed to propagate only along the axis of the waveguide. The curvature seen on the saxophone, for example, is ignored [34]. If the element is reciprocal its transfer matrix will have a determinant equal to unity and if the element is symmetric then coefficients $A_w(\omega) = D_w(\omega)$ [35]. The current section treats only cylindrical ducts with short branches that terminate in open space, because these are the building blocks of an acoustically periodic cylindrical waveguide.

2.2.2 Basic acoustic elements

The transfer matrix $M^{\ell}(\omega)$ for a lossless cylindrical duct of length ℓ and radius a is

$$M^{\ell}(\omega) = \begin{pmatrix} \cos(\omega\ell/c) & jz_{\text{c}}\sin(\omega\ell/c) \\ \frac{j}{z_{\text{c}}}\sin(\omega\ell/c) & \cos(\omega\ell/c) \end{pmatrix}, \tag{2.10}$$

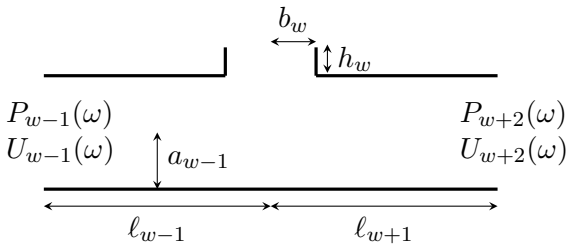

Figure 2.1: Schematic of a waveguide composed of three basic elements. The $(w-1)^{\text{th}}$ and $(w+1)^{\text{th}}$ elements are identical cylindrical ducts with radii $a_{w-1} = a_{w+1}$ and lengths $\ell_{w-1} = \ell_{w+1}$. The w^{th} element is a tonehole with radius b_w and chimney height h_w.

where $z_{\text{c}} = \rho c/(\pi a^2)$ is the characteristic impedance of the duct [36]. A tonehole with radius b and chimney height h is treated as a shunt acoustic mass

$$M^{\text{h}}(\omega) = \begin{pmatrix} 1 & 0 \\ Y^{\text{h}}(\omega) & 1 \end{pmatrix}, \tag{2.11}$$

where $Y^{\text{h}}(\omega) = j\omega m_{\text{h}}$ is the admittance of the tonehole with acoustic mass $m_{\text{h}} = \rho h/(\pi b^2)$ [37, 38], see Figure 2.1. Implicit in this assumption is that the acoustic pressure inside the main bore just to the left and right of the tonehole is continuous, and that the acoustic flow coming from one duct equals the sum of the flow in the other two ducts. More complete models of the tonehole exist, but the improvements concern mainly the effect of closed toneholes. Because the cutoff arises from a lattice of open toneholes, the simpler model is sufficient in the current work [39, 17, 40]. Similar matrices can be written for other elements such as conical sections and radius discontinuities, but are not necessary for the development of this topic [41, 42, 43].

2.2.3 Solving for pressure and flow

As noted earlier, once the pressure and flow at one location is known the pressure and flow at any other location can be determined. In general the pressure and flow are not known. However, the pressure and flow within the waveguide can be solved at the input of the w^{th} element

$$\begin{pmatrix} P_w(\omega) \\ U_w(\omega) \end{pmatrix} = M_w(\omega) M_{w+1}(\omega) \cdots M_W(\omega) \begin{pmatrix} Z_{\text{rad}}(\omega) \\ 1 \end{pmatrix}, \tag{2.12}$$

by imposing a radiation impedance $Z_{\text{rad}} = P_{W+1}(\omega)/U_{W+1}(\omega)$ at the output of the last W^{th} element. It is often convenient to ignore $P_{W+1}(\omega)$ and $U_{W+1}(\omega)$, and instead use an analytic or numerical model for Z_{rad}, for which there are many examples in the literature. Unless otherwise noted, the TMM and TMMI (see Section 2.2.5) simulations in this dissertation use an approximate formula assuming an unflanged radiating aperture

of circular cross section for the radiation impedance [44].[3]

The special case $w = 1$ is often referred to as the input impedance of the waveguide $Z_{\text{in}}(\omega) = P_1(\omega)/U_1(\omega)$, but can be equivalently defined for any other element $Z_w(\omega) = P_w(\omega)/U_w(\omega)$.

2.2.4 A comment regarding notation: elements and cells

A note on notation is necessary at this point. In discussing the TMM, basic elements were assigned the subscript w, and a finite lattice is comprised of W elements. The remainder of this exposition adopts the subscript n, which can correspond to the transfer across a cell that is comprised of multiple basic elements. In Figure 2.1, for example, the transfer from the input to the output of the cell can be written

$$\begin{pmatrix} P_{w-1}(\omega) \\ U_{w-1}(\omega) \end{pmatrix} = M_{w-1}(\omega)M_w(\omega)M_{w+1}(\omega) \begin{pmatrix} P_{w+2}(\omega) \\ U_{w+2}(\omega) \end{pmatrix}, \tag{2.13}$$

where $M_{w-1}(\omega) = M_{w+1}(\omega) = M^{\ell}(\omega)$ account for the section of duct to the left and right of the tonehole $M_w(\omega) = M^{\text{h}}(\omega)$. Using n notation, the transfer across the same cell simplifies to

$$\begin{pmatrix} P_n(\omega) \\ U_n(\omega) \end{pmatrix} = M_n(\omega) \begin{pmatrix} P_{n+1}(\omega) \\ U_{n+1}(\omega) \end{pmatrix}, \tag{2.14}$$

where $M_n(\omega) = M^{\ell}(\omega)M^{\text{h}}(\omega)M^{\ell}(\omega)$, see Figure 2.2. The input impedance to the n^{th} cell is $Z_n(\omega) = P_n(\omega)/U_n(\omega)$ The original notation using w is helpful to illustrate the components of the TMM. The n notation, however, facilitates the introduction of cells comprised of multiple elements as the basic building blocks of a lattice. This is important because it is a necessary transformation used by the simulation method described in Section 2.2.5, and because it casts the TMM into a form that can be applied to wave propagation in periodic media, as is done in Section 2.3.

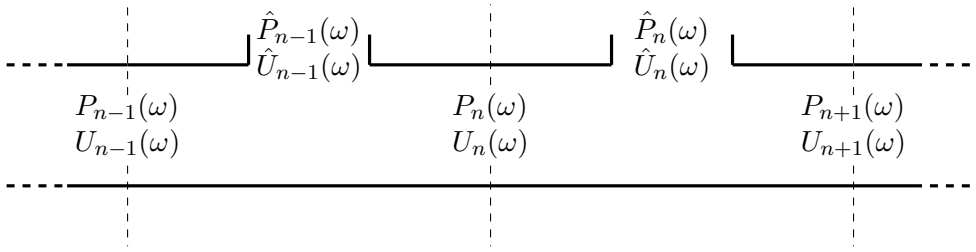

Figure 2.2: The $(n-1)^{\text{th}}$ and n^{th} neighboring cells of an infinite, geometrically regular lattice. Pressure and flow variables inside the main duct are denoted by $P(\omega)$ and $U(\omega)$, and in the toneholes by $\hat{P}(\omega)$ and $\hat{U}(\omega)$.

[3] This article proposes multiple approximations. The one used in this manuscript is Eq. (3) with the non-causal model proposed in Table 1, which is appropriate for frequency domain analysis.

2.2.5 External interactions

The TMM described above is simple, efficient, and adequately relates $P_n(\omega)$, $U_n(\omega)$ and $Z_n(\omega)$ at some location n to any other location in the waveguide for many musical acoustics applications. However, in this dissertation, simulations are executed using the Transfer Matrix with external Interactions (TMMI) [28], except when otherwise noted. The TMMI operates in essentially the same way as the TMM: the pressure and flow variables are translated across discrete sections of a waveguide by including the influence of individual elements whose contributions have analytic solutions. However, the TMMI uses a coordinate system with pressure $\hat{P}_n(\omega)$ and flow $\hat{U}_n(\omega)$ reference variables in the toneholes shown in Figure 2.2, rather than within the bore of the main duct. This facilitates some improvements over the TMM.

The TMMI was developed in order to more accurately simulate the input impedance of a woodwind-type resonator by accounting for the mutual impedance of toneholes that radiate into the same space [45, 46, p. 368], which is ignored in the TMM. Accounting for the mutual impedance results in a subtle improvement over the TMM, with a greater impact for resonators with closely spaced toneholes because the mutual loading is assumed to be inversely proportional to the distance between toneholes.[4] Accounting for external interactions has a minimal effect at low frequencies for which the radiation is primarily through the first tonehole, with only minor contributions from the remaining lattice. The first several input impedance peaks are essentially unaltered in frequency, modulus, and quality factor when comparing TMM and TMMI simulations [29]. In many cases only the low frequency input impedance peaks are needed due to their strong impact on sound production, in which case the TMM is a fine choice due to its simplicity and efficiency. The TMMI has a stronger effect for frequencies above the tonehole lattice cutoff (see Section 2.3), resulting in lower impedance peaks due to increased radiation [28, 29]. Therefore, the TMMI is an appropriate choice for input impedance simulations that require accuracy above the cutoff.

The reference coordinates of the TMMI are convenient because they provide the acoustic variables $\hat{P}_n(\omega)$ and $\hat{U}_n(\omega)$ that correspond to the radiating apertures. As shown in Chapter 4 and Appendix A, these variables can be used to generate a very simple radiation model treating each flow $\hat{U}_n(\omega)$ through the n^{th} aperture as a monopole. The external pressure $P_O(\omega)$ at any observation point O is a simple superposition of the contribution of each monopole [30, p. 189]. Although this radiation model ignores diffraction of the resonator body and reduces each tonehole radiation to a monopole type source, Appendix A demonstrates that the results are satisfactory in comparison with measurements. A major advantage of this simple radiation model, available through the extension by using the TMMI, is that it links the internal variables $P_{\text{in}}(\omega)$ and $U_{\text{in}}(\omega)$ to the external variable $P_O(\omega)$. This is an advantage when comparing sound production and radiation of different resonators and, to the best of the current author's knowledge, is a new extension of the TMMI.

[4] The actual mutual loading is a more complicated expression relating the tonehole radius, inter-hole spacing, and wavelength, but this approximation works reasonably well for woodwind type resonators.

2.3 Acoustically periodic waveguides

In the previous section the TMM and TMMI were developed to translate acoustic variables $P_n(\omega)$ and $U_n(\omega)$ across individual elements, or groups of elements, that constitute a waveguide. The full system is resolved at any point by imposing a radiation condition at the termination of the final element. This is a common approach for modeling the passive response of an acoustic waveguide composed of a finite number of elements.

The purpose of this section is to derive the equations relating to wave propagation in a periodic medium [2, p. 17], and therefore the analysis is applied to an arbitrary cell n and the neighboring $(n-1)^{\text{th}}$ and $(n+1)^{\text{th}}$ of an *infinite* lattice [47, 23, p. 377-384]. The relation between acoustic variables in an infinite lattice is determined using much of the same formalism as for a finite lattice. One difference is that, in contrast with the finite waveguide, there is no meaning to imposing a final radiation impedance because there is no last element. Instead, an iterative impedance is assumed such that the input impedance into cells n and $(n+1)$ is the same, justified by the infinite nature of the lattice. From this assumption, the TMM formalism may be used to determine propagation characteristics inside an infinite waveguide from the geometry of a single cell [1] ignoring thermoviscous and radiation losses. Sections 2.3.1 and 4.2.1 follow the form of existing derivations, but include additional mathematical steps than are not provided in previous articles and books for this specific problem [2, 3, 38, 23].

2.3.1 Geometrically periodic lattices

A periodic lattice can be designed using the transfer matrices for a length of cylindrical duct $M^{\ell}(\omega)$ and a tonehole $M^{\text{h}}(\omega)$ to generate a unit cell with transfer matrix

$$M^{\text{cell}}(\omega) = M^{\ell}(\omega)M^{\text{h}}(\omega)M^{\ell}(\omega) = \begin{pmatrix} A(\omega) & B(\omega) \\ C(\omega) & D(\omega) \end{pmatrix}, \tag{2.15}$$

with generic coefficients $A(\omega)$, $B(\omega)$, $C(\omega)$, and $D(\omega)$ that depend on the geometry of the cell. The subscript n is not used with the matrix variables because all the cells are identical. From Eq. (2.14)

$$\begin{aligned} P_{n-1}(\omega) &= A(\omega)P_n(\omega) + B(\omega)U_n(\omega) \\ U_{n-1}(\omega) &= C(\omega)P_n(\omega) + D(\omega)U_n(\omega) \end{aligned} \quad ; \quad \begin{aligned} P_n(\omega) &= A(\omega)P_{n+1}(\omega) + B(\omega)U_{n+1}(\omega) \\ U_n(\omega) &= C(\omega)P_{n+1}(\omega) + D(\omega)U_{n+1}(\omega). \end{aligned} \tag{2.16}$$

Equations (2.16) are simplified through substitution and setting $A(\omega) = D(\omega)$ (symmetry) and $A^2(\omega) - B(\omega)C(\omega) = 1$ (reciprocity) [23, p. 379],

$$\begin{aligned} 2A(\omega)P_n(\omega) &= P_{n-1}(\omega) + P_{n+1}(\omega) \\ 2A(\omega)U_n(\omega) &= U_{n-1}(\omega) + U_{n+1}(\omega). \end{aligned} \tag{2.17}$$

From here, the analysis is continued in terms of the pressure variable, although it is equivalent to continue with flow. Solutions at the n^{th} cell are assumed to be a superposition

of forward and backward propagating waves

$$P_n(\omega) = P^+(\omega)e^{-n\Gamma} + P^-(\omega)e^{n\Gamma}, \tag{2.18}$$

where Γ is the complex propagation constant of the lattice wave $P_n(\omega)$, and can strongly vary with frequency. The conditions for propagation are evident in Eq. (2.18): if Γ is purely imaginary the wave will propagate in the lattice from index 1 to index n. However, if Γ is real + j$m\pi$ for an integer m, then the wave is evanescent. When losses are ignored Γ is either purely real or purely imaginary for a given frequency, and when losses are included Γ is typically complex with both real and imaginary components for all frequencies. It is possible to derive an analytic formulation for Γ, in terms of the cell geometry, and trace it through the complex plane to identify the frequencies for which it changes from real to imaginary [23, p. 379].

The solutions at the $(n-1)^{\text{th}}$ and $(n+1)^{\text{th}}$ cells are

$$\begin{aligned} P_{n-1}(\omega) &= P^+(\omega)e^{-(n-1)\Gamma} + P^-(\omega)e^{(n-1)\Gamma}, \\ P_{n+1}(\omega) &= P^+(\omega)e^{-(n+1)\Gamma} + P^-(\omega)e^{(n+1)\Gamma}, \end{aligned} \tag{2.19}$$

which, inserted into Eq. (2.17), yields

$$2A(\omega)P_n(\omega) = P_n(\omega)e^{\Gamma} + P_n(\omega)e^{-\Gamma}. \tag{2.20}$$

Therefore, the propagation constant Γ depends on the matrix coefficient $A(\omega)$ by

$$A(\omega) = \frac{1}{2}\left[e^{\Gamma} + e^{-\Gamma}\right], \tag{2.21}$$

and from the definition of the hyperbolic cosine,

$$A(\omega) = \cosh(\Gamma). \tag{2.22}$$

Eq. (2.22) relates the wave propagation constant Γ, which describes the frequency dependent wave propagation in the lattice, directly to the geometry of the constituent cell described by $A(\omega)$. Following the evolution of $A(\omega)$ with frequency is sufficient to determine the bands for which Γ is real and imaginary:

$$\begin{aligned} |A(\omega)| < 1: &\quad \Gamma \text{ is imaginary, the wave propagates} \\ |A(\omega)| > 1: &\quad \Gamma \text{ is real + j}m\pi\text{, the wave is evanescent} \\ |A(\omega)| = 1: &\quad \text{corresponds to cutoff.} \end{aligned} \tag{2.23}$$

Equivalent expressions can be found for an asymmetric cell by retaining $A(\omega) \neq D(\omega)$ in Eq. (2.17), in which case the left hand side of Eq. (2.22) is replaced by $\frac{1}{2}\left[A(\omega) + D(\omega)\right]$ [48]. Equation (2.23) defines an important set of conditions used throughout this dissertation. A lattice is said to have a stop band for frequencies corresponding to $|A(\omega)| > 1$ because a wave entering the lattice is evanescent. Conversely, a lattice is said to have a pass band for frequencies corresponding to $|A(\omega)| < 1$ because wave entering the lattice continues to propagate [23, p. 379]. The frequency for which $|A(\omega)| = 1$, referred to as the tonehole

lattice cutoff frequency, separates these two bands.[5] Evaluating the importance of the cutoff on sound production and radiation is a key aspect of this research.

2.3.2 The tonehole lattice cutoff frequency of an infinite, lossless lattice

In this section, the cutoff frequency is determined by tracing the evolution of $A(\omega)$ with frequency. From Eqs. (2.10,2.11,2.15), the exact form of $A(\omega)$ is the product of the transfer matrices across the components of a unit cell

$$A(\omega) = 1 - 2\sin^2(\omega\ell/c) + jY^{\mathrm{h}}(\omega)z_{\mathrm{c}}\sin(\ell\omega/c)\cos(\ell\omega/c). \tag{2.24}$$

From Eq. (2.23), the cutoff frequency occurs when $|A(\omega_{\mathrm{c}})| = 1$, so

$$2\sin^2(\omega_{\mathrm{c}}\ell/c) = jY^{\mathrm{h}}(\omega_{\mathrm{c}})z_{\mathrm{c}}\sin(\ell\omega_{\mathrm{c}}/c)\cos(\ell\omega_{\mathrm{c}}/c), \tag{2.25}$$

which simplifies to

$$\cot(\omega_{\mathrm{c}}\ell/c) = \frac{2\omega_{\mathrm{c}}m_{\mathrm{h}}}{z_{\mathrm{c}}}, \tag{2.26}$$

provided that the sine function is not equal to zero. This transcendental equation is solved using a Taylor expansion of the cotangent

$$\frac{1}{(\omega_{\mathrm{c}}\ell/c)} = \frac{2\omega_{\mathrm{c}}m_{\mathrm{h}}}{z_{\mathrm{c}}} + \mathcal{O}(\omega_{\mathrm{c}}\ell/c), \tag{2.27}$$

and solving for ω_{c}

$$\omega_{\mathrm{c}}^2 \approx \frac{cz_{\mathrm{c}}}{2\ell m_{\mathrm{h}}}. \tag{2.28}$$

Remembering the definition $z_{\mathrm{c}} = \frac{\rho c}{\pi a^2}$ and recognizing the acoustic compliance $C_{\mathrm{a}} = \frac{2\ell\pi a^2}{\rho c^2}$, the cutoff frequency is written

$$f_{\mathrm{c}} \approx \frac{1}{2\pi}\left[\frac{1}{C_{\mathrm{a}}m_{\mathrm{h}}}\right]^{1/2}. \tag{2.29}$$

This is recognized as the Helmholtz resonance of the cell considering rigid boundary conditions at the input and output locations n and $n+1$ with the main bore acting as a compliant volume and the tonehole as a rigid acoustic mass [22, 49].

2.3.3 Geometric and acoustic regularity

The previous section follows a derivation for the cutoff frequency of an infinite, periodic lattice. It is interesting to compare the assumptions in Eq. (2.15) at the beginning and the result for the cutoff frequency in Eq. (2.29). The derivation begins assuming a lattice of repeating, geometrically identical cells. The derivation relies on this assumption to relate the pressure and flow variables between the $(n-1)^{\mathrm{th}}$, n^{th}, and $(n+1)^{\mathrm{th}}$ elements. Lattices of this form may be considered *geometrically regular*. However, the result in Eq. 2.29 is cast not in terms of geometric variables, but in terms of acoustic mass and

[5] For a discussion on other stop bands see Section 2.3.4.

compliance. An acoustical periodicity exists as long as the product of the acoustic mass and compliance remains constant for all cells, forming an *acoustically regular* lattice [22]. Geometrically regular lattices are a subset of acoustically regular lattices, assuming that the cells can be described by lumped elements.

The interpretation of acoustic regularity is important because it justifies applying the theory of wave propagation in periodic media to waveguides that are decidedly not geometrically periodic, such as woodwind instruments. On real instruments, the size and spacing of toneholes is generally not constant across the body of the resonator, and may in fact vary considerably to achieve a desired intonation or timbre. The interpretation of a woodwind resonator as a geometrically periodic lattice is not justified. However, some instruments, notably the clarinet, have tonehole lattices that demonstrate considerable acoustic regularity. It is this interpretation of Eq. (2.29) that serves as a starting point when applying the theory to musical instruments.

2.3.4 Nomenclature regarding stop bands, pass bands, and the reflection coefficient

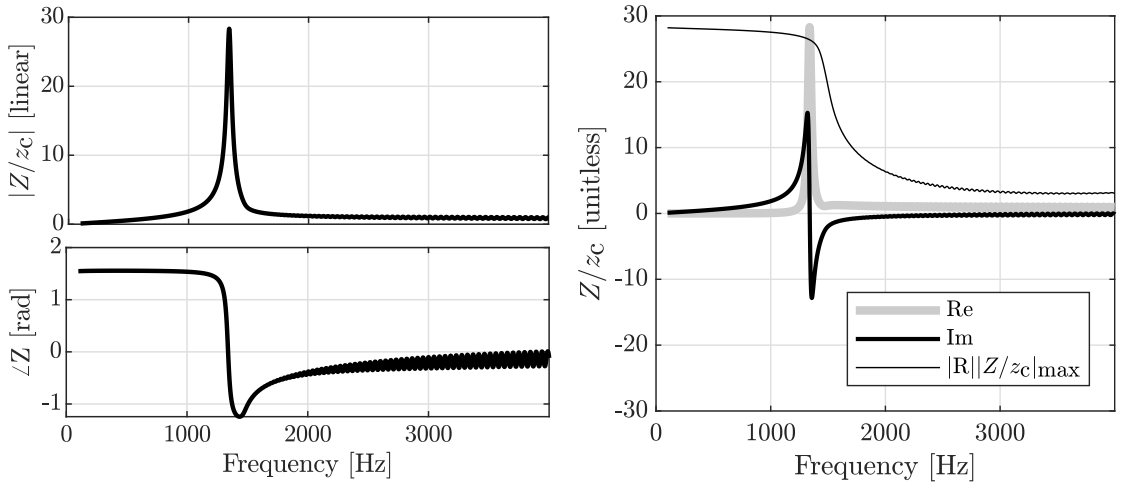

Figure 2.3: Simulated (TMMI) input impedance of a lattice comprised of 100 identical cells and a cutoff frequency around 1500 [Hz]. Upper left: modulus; lower left: argument; right: real and imaginary components. Also on right, reflection coefficient modulus multiplied by input impedance modulus maximum for readability. Below cutoff the impedance is predominantly imaginary, indicating a reactive load, while above cutoff it is predominately real, indicating transmission of energy. Numerically the lattice is 'infinite' because a propagating wave is very strongly attenuated over the long propagation distance. A 'finite' version of this lattice with 10 holes has a peak structure above cutoff due to successive reflections from the termination.

It is appropriate at this point to make a comment about vocabulary that sometimes leads to miscommunication when discussing wave propagation in lattices. As explained in Section 4.2.1, the lattice has a stop band below the cutoff and a pass band above

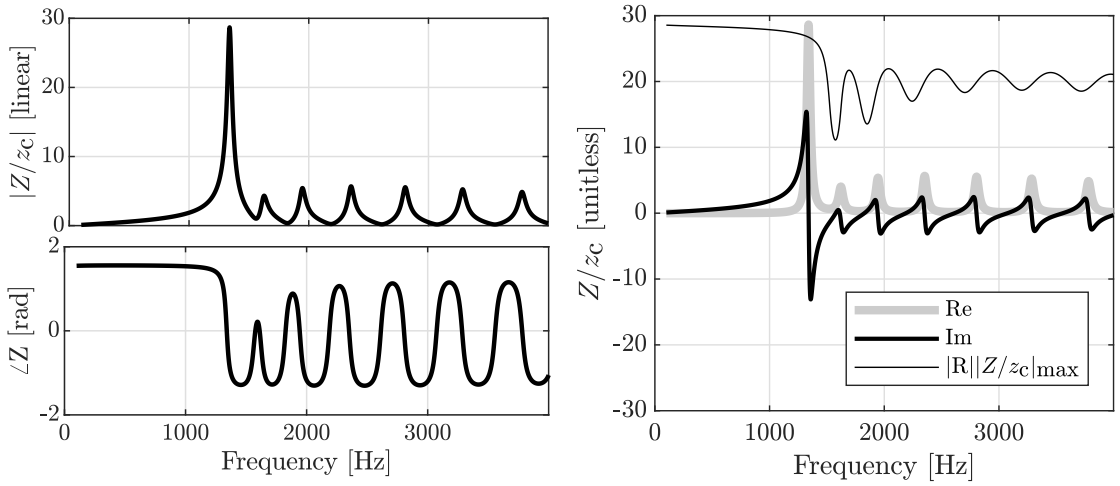

Figure 2.4: The same representation as Figure 2.3, but here for a lattice comprised of 10 cells. The peak structure above cutoff is due to resonances that are proportional to the total length of the lattice.

the cutoff. Figures 2.3 and 2.4 show the input impedance modulus and argument (left) and real and imaginary components (right) simulated for a 100 cell ('infinite') lattice and 10 cell (finite) lattice. As seen in the right panels, the input impedance below the cutoff is predominantly imaginary, suggesting a reactive load, while above the cutoff the impedance is predominantly real, suggesting transmission of energy into the lattice. From this interpretation the vocabulary 'stop band' is clear: it is the frequency band for which waves are not able to propagate into the lattice. However, the stop band of the lattice appears as a pass band in the reflection coefficient

$$R(\omega) = \frac{Z(\omega)/z_c - 1}{Z(\omega)/z_c + 1}, \tag{2.30}$$

because most of the energy that is stopped at the input of the lattice (at the first open tonehole) is strongly reflected back into the resonator. The modulus of the reflection coefficient, multiplied by the input impedance modulus maximum value for readability, is plotted on the right panel in both figures. In the current document stop and pass bands will always refer to the response of a wave entering the lattice (first case), and never to the apparent pass and stop bands of the reflection coefficient: the stop band refers to a wave that does not propagate into the lattice and a pass band refers to wave that does propagate in the lattice.

Note that Figure 2.3 is an idealized case due to the large number of cells. However, it does not correspond directly to the results in Section 2.3 because the TMMI accounts for thermoviscous losses and the theory is for a lossless lattice. For the 100 cell lattice, the transmitted wave is strongly attenuated by thermovisous losses over the 'infinite' propagation path. In contrast, peaks above cutoff in Figure 2.3 are due to reflections from the termination of the 10 cell lattice.

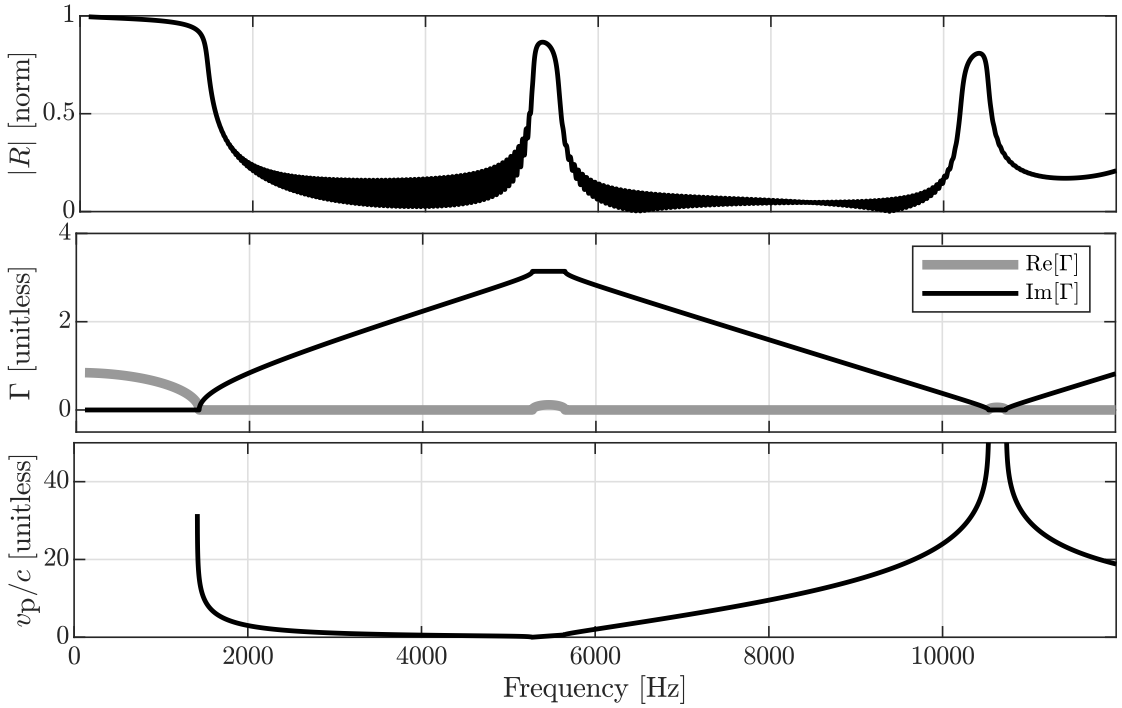

Figure 2.5: Simulations of a lattice comprised of 100 identical cells and a cutoff frequency around 1500 [Hz] (same as Figure 2.3). The reflection coefficient modulus (top) is simulated using the TMMI, while the wave propagation constant Γ (middle) and phase velocity v_p (bottom) are derived from the geometry of a constituent cell using Eqs. (2.22,2.24,2.33). The frequency range is intentionally very large to capture additional stop bands at 5200 [Hz] and 10500 [Hz].

2.3.5 Other stop bands

In musical acoustics, the tonehole cutoff frequency is the one described by Eq. 2.29, or at least an approximate, empirically observed version of this phenomenon. However, there are other types of cutoff frequencies that may be observed with these types of periodic lattices. In particular, additional stop bands at frequencies whose corresponding wavelengths are proportional to the inter-hole spacing have been observed in both simulations and measurements. Figure 2.5 demonstrates these two types of stop bands using the reflection coefficient modulus, the wave propagation constant Γ, and the phase velocity v_p (see Eq. (2.33)). The reflection coefficient is traced from the same TMMI simulation used for the 100 cell lattice shown in Figure 2.3. The propagation constant and phase velocity are properties that can be derived from the geometry of a single cell.

The second type of stop band typically spans several hundred Hz and is centered at a frequency

$$f_\mathrm{B} = \frac{c}{\lambda_\mathrm{B}}, \tag{2.31}$$

where

$$\lambda_{\mathrm{B}} = 2 \cdot 2\ell \tag{2.32}$$

is recognized as the Bragg wavelength[6] [2, p. 115]. Similar stop bands occur at integer multiples of f_{B} if the lattice is geometrically regular. The second stop band corresponds to the case $\Gamma = \text{real} + ja\pi$ in Eq. (2.23), and at these frequencies the flow through neighboring toneholes have a phase shift of approximately π radians. It is also interesting to note the variation of the phase velocity [2, p. 69]

$$v_{\mathrm{p}} = \omega / \mathrm{Im}[\Gamma], \tag{2.33}$$

with frequency, notably that it is infinite for the first and third stop bands, and null for the second. This is irrespective of the fact that the first stop band is due to acoustic regularity and the second and third stop bands are due to geometric periodicity. To the author's knowledge this is a new observation, at least within the realm of musical acoustics, but analogous systems may exist for electronic or crystalline structures.

In contrast with the tonehole lattice cutoff frequency f_{c}, the second stop band is due to the geometric periodicity of the resonator. This has an interesting consequence for wave propagation in this type of waveguide: it is possible to independently vary the two stop bands. The resonators used in this dissertation have $f_{\mathrm{B}} > f_{\mathrm{c}}$, and the input impedance is characterized by a stop band for low frequencies up to f_{c}, followed by a pass band that is punctuated by several hundred Hz stop bands at integer multiples of f_{B}. This is characteristic of 'clarinet-proportioned' geometrically regular resonators. With more exotic choices of geometry it is possible to design resonators where $f_{\mathrm{B}} < f_{\mathrm{c}}$ or $f_{\mathrm{B}} = f_{\mathrm{c}}$. To the author's knowledge this is also a new observation.

Although this second type of stop band is interesting, it is not commonly discussed and is probably irrelevant in musical acoustics. The toneholes in the lower range of a clarinet are approximately 0.02 [m] apart, corresponding to $f_{\mathrm{B}} \approx 8.5$ [kHz]. An additional stop band at these high frequencies is unlikely to have a strong effect on the sound production or radiation of an instrument. Furthermore, this stop band relies on geometric regularity, which is not the case for most musical instruments. Therefore, the stop band centered at f_{B} is not treated any more in this dissertation, even though it is an interesting property of this type of waveguide.

There are also stop bands relating to non-planar modes in the resonator. The 'sloshing mode' is the lowest non-planar mode, and has a cut on at $f_{\mathrm{sloshing}} = 1.84c/a$ for speed of sound c, radius a, and the coefficient 1.84 is calculated from the Bessel function [50]. For a characteristic radius of the clarinet $a = 0.0075$ [m], this corresponds to a cut on at approximately 13 [kHz], considerably higher in frequency than any of the following analysis. Therefore, stop bands due to non-planar modes are ignored for the remainder of the manuscript.

[6] A spatially periodic medium may exhibit a stop band for wavelengths that are twice (and integer related wavelengths) the length of the periodic structure. This phenomena exists in many areas of physics.

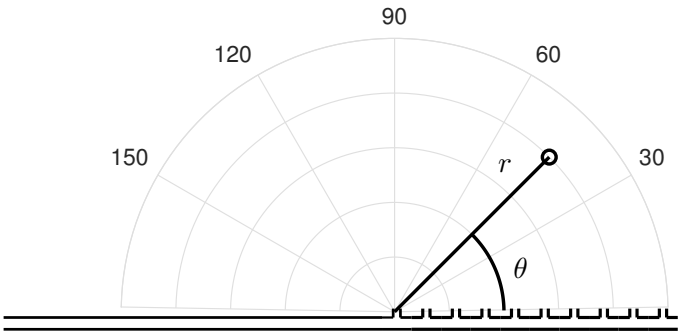

Figure 2.6: The resonator orientation in polar coordinates with the origin at the location of the first open tonehole (also see Figure 2.2). This coordinate system is the reference used in Figures 2.8, 2.9, 2.10, 2.13, and Eq. (2.34). Simulated directivity patterns assume rotational symmetry about the axis of the resonator (implicit in the monopole radiation hypothesis), which is not the general case for the measurements in Figure 2.13.

2.4 Implications of the cutoff frequency

Some general comments about the effect of the tonehole cutoff lattice frequency can be made following the development of the cutoff in Section 2.2. This section returns to the analysis of finite resonators, but the analysis and definition in Eq. (2.29) for an infinite lattice is assumed valid provided there are at least several open toneholes. Consider an academic resonator with a length of duct followed by a lattice of 10 identical cells as shown to scale in Figure 2.6. The toneholes with inter-hole spacing $2\ell = 2 \cdot 0.0163$ [m] have dimensions $b = 0.004$ [m], $h = 0.0098$ [m], and the main duct with radius $a = 0.0065$ [m] has a length $L = 0.398$ [m] before the first cell of the lattice. This resonator, designed following the equations provided in Chapter 3 [29] and Chapter 4 [51] is used to demonstrate typical cutoff behavior the remainder of this section as well as Section 2.5.

2.4.1 Academic resonator: the effect of the cutoff on internal variables

To demonstrate the effect of a lattice on internal variables, the input impedance of a simple cylinder terminating in a radiation load is simulated along with that of the academic resonator, as seen in Figure 2.7. Below cutoff, a wave entering the lattice is evanescent, and either radiates from the first open tonehole or reflects back into the resonator. This is most clearly seen on the reflection coefficient, which has a value close to unity implying that energy at these frequencies largely remains in the upstream portion of duct. The consequence of this on internal variables is that the resonator appears to be truncated (approximately) at the first tonehole, and the input impedance of the resonator resembles that of a simple cylinder.

Above cutoff the wave propagates in the lattice and the input impedance is complicated due to successive reflections from subsequent toneholes and the termination of the resonator, and undergoes additional thermoviscous losses due to the longer propagation

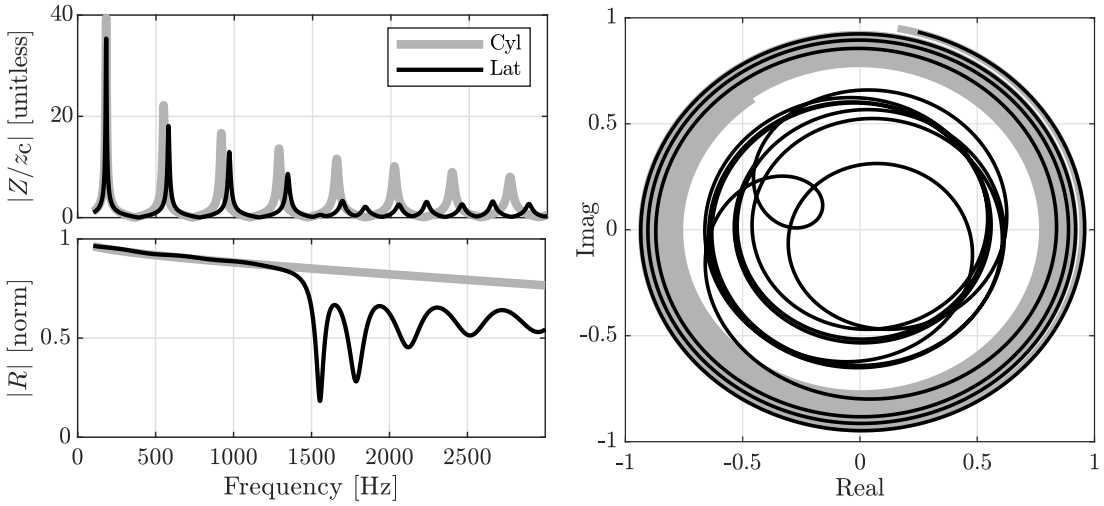

Figure 2.7: A resonator with a tonehole lattice is compared with a simple cylinder through TMMI simulation. Input impedance modulus and reflection coefficient modulus on left, and a Nyquist (100-3000 [Hz]) representation on right. All three demonstrate a change due to the tonehole lattice cutoff, explicitly identified as 1500 [Hz] on the two left panels.

path. The decreased values of the reflection coefficient above cutoff indicates that a much smaller amount of energy is reflected back into the resonator compared with below cutoff. This prevents the formation of strong impedance peaks, which explains the decreased amplitudes of the input impedance peaks above cutoff. The Nyquist plot demonstrates how the resonances of the cylinder remain orderly with increasing frequency while slowly loosing energy to radiation and thermoviscous losses, compared with the academic resonator, which resembles the cylinder below cutoff but traces a complicated path above cutoff.

2.4.2 Academic resonator: the effect of the cutoff on external pressure

The radiation properties of a lattice for frequencies above cutoff are considerably more complicated than for below cutoff. Above cutoff there is ongoing wave propagation within the lattice which results in radiation from all of the apertures. Therefore the resonator appears as a collection of discrete sources (toneholes and termination) each with a distinct frequency dependent amplitude and phase. This implies that the directivity of this lattice is a complicated function of frequency above the cutoff, and may be compared with collections of simple sources that have known solutions [52].

2.4.2.1 Transfer function from internal variables to external variables

One way to observe the effect of the cutoff on radiation is to observe its effect on the transfer function between internal and external acoustic variables. Figure 2.8 shows the TMMI simulated transfer function between internal acoustic flow at the input of the resonator and the pressure at three external observation points, normalized by the maximum

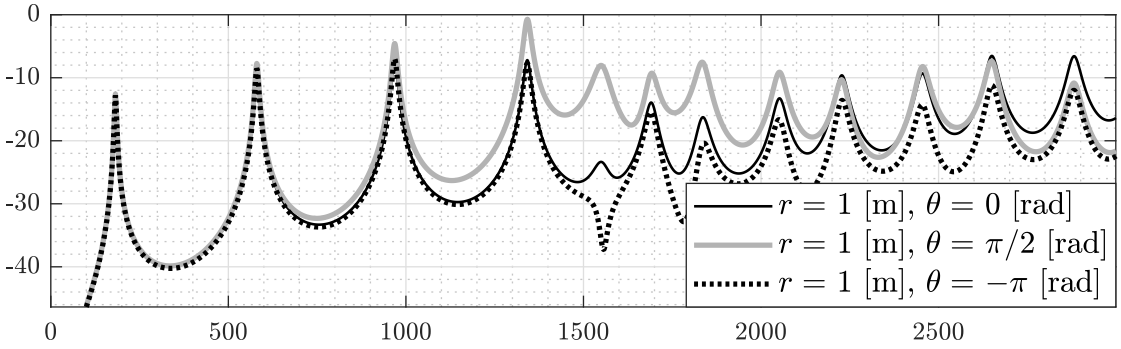

Figure 2.8: Transfer function (TMMI simulated) between external pressure and (internal) flow at the input of the resonator for observation angles $0, \pi/2, \pi$ [rad] and distance $r = 1$ [m], following the reference coordinates in Figure 2.6. The monopole radiation below the cutoff and an indication of the directivity at and above the cutoff are evident. Compare this figure to Figures 2.9, 2.10 and 2.13.

value. These simulations agree qualitatively to analytic calculations [15] and measurements [16]. However, the comparison is not exact for several reasons: the geometry of the resonators used in those two studies are different from each other and different from the one shown here, so necessarily the results will not be identical. Additionally, the exact observation location is not specified in those two studies, so they can not be compared directly with the two specific observation locations chosen here. Regardless, the general trends are consistent between all three studies.

The transfer functions demonstrate some basic results regarding the influence of the cutoff on radiation. The strong directivity at cutoff (and somewhat weaker above) is seen as a nearly 30 dB difference between the observation locations. This leads to further analysis of the directivity using the same simulation methods with a finer angular spatial discretization.

2.4.2.2 Directivity based on TMMI simulations

The farfield directivity of the resonator in Figure 2.6 is simulated following the principles in Section 2.2.5. The details of the simulation are omitted here because the goal is to demonstrate general radiation characteristics of the resonator, not present the methodology of the radiation model which is provided in Chapter 4. The orientation is as shown in Figure 2.6, with the origin at the left most tonehole. The directivity is simulated at $f = [250, 1587, 2520]$ [Hz] in order to compare with measurements of a real clarinet in Section 2.5.2 that were not performed by the current author [53], see Section 2.5.2.2.

These plots demonstrate the three main directivity patterns associated with this type of lattice. Below the cutoff there is low frequency monopole radiation from the first tonehole which deforms to produce strong directivity lobes perpendicular to the lattice at cutoff, with a slight bias towards the termination of the resonator [3, 54]. The transition from monopole to perpendicular lobes is relatively smooth, which has been verified by tracing the plots of intermediate frequencies. For frequencies well above cutoff, the direc-

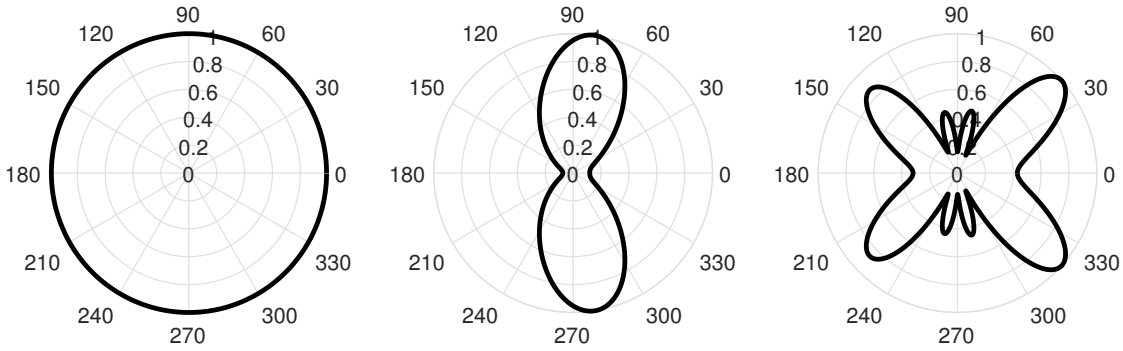

Figure 2.9: Farfield directivity (normalized to the maximum value at each frequency) of the resonator ($f_c \approx 1500$ [Hz]) depicted in Figure 2.6 and for (from left to right) $f = [250, 1587, 2520]$ [Hz] simulated using TMMI with a simplified radiation model. The plots demonstrate characteristic radiation patterns below, equal to, and above the cutoff.

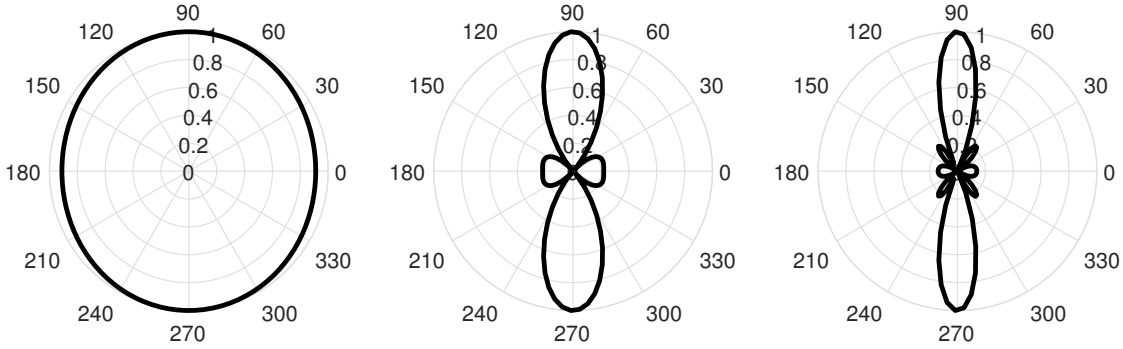

Figure 2.10: Directivity of a equal amplitude, in phase monopole antenna with 10 elements spaced $2 \cdot 0.0163$ [m] apart for (from left to right) $f = [250, 1587, 2520]$ [Hz]. This represents the simplified antenna model of the academic resonator depicted in Figures 2.6.

tivity is characterized by a complicated lobe pattern that evolves quickly with frequency, but maintains the general shape (mostly forward pointing but also strong backward pointing lobes) as the pattern for 2520 [Hz].

A similar resonator with a different cutoff has the same type of directivity lobes, which transition at the cutoff as shown in Figure 2.9 (this has been verified through simulation). This radiation pattern has practical use for real woodwind instruments such as the clarinet: more or less high frequency content can be captured by choosing a suitable microphone location. This is discussed by Benade for both musical [8] and scientific [55, 56] considerations.

2.4.2.3 Directivity of an equivalent antenna

A crude approximation of the directivity may be found using antenna theory, treating each tonehole as an identical monopole source and ignoring the termination of the instru-

ment. Consider an antenna with $N = 10$ equal amplitude and in phase sources separated by a distance 2ℓ.[7] The farfield pressure of such an antenna aligned along the horizontal axis is

$$P(k, \theta) \propto \frac{\sin(10k\ell\cos(\theta))}{\sin(k\ell\cos(\theta))}, \tag{2.34}$$

where $k = \omega/c$ is the wave number, and the source strength, spherical spreading, and other constants are ignored [23, 57]. As for the simulations in Figure 2.9, the normalized directivity of an antenna with $\ell = 0.0163$ [m] is plotted for $f = [250, 1587, 2520]$ [Hz] in Figure 2.10.

The antenna simulation results in Figure 2.10 resemble the TMMI simulation results in Figure 2.9 for frequencies up to the cutoff. However, some care must be taken in this analysis. Here, the monopole-type radiation at $f = 250$ [Hz] is contingent on the condition $kG \ll 1$ for a characteristic length G. A reasonable value for G might be 0.15 [m], or about half the length of the antenna. At $f = 250$ [Hz] $kG = 0.69$, which explains the slight contraction of the directivity at angles $\theta = 0$ and π [rad]: the radiating apertures are too far apart relative to the wavelength to be considered a simple source. In the TMMI model, the radiation is monopole-like because the first tonehole is the predominant flow source of the resonator, with very minor contributions from the remaining apertures of the lattice. So, although these two methods produce similar results at low frequencies, the interpretation is different.

At cutoff the TMMI simulation and simplified antenna model match very well. This is physical: at cutoff, the phase velocity (see Eq. (2.33)) in the resonator is very high and the ten holes are of nearly equal amplitude and phase, matching the hypothesis of the antenna. The slight deformation of the TMMI simulated directivity in the direction $\theta = 0$ [rad] is due to slight variations between toneholes in amplitude and phase, in addition to the radiation from the termination of the resonator, both of which are ignored in the antenna model. At frequencies well above the cutoff the two models diverge. This is because the radiating apertures of the lattice no longer have equal amplitudes and phases, which is a key assumption in Eq. (2.34). Furthermore, for frequencies well above cutoff, the radiation is predominantly from the termination of the resonator, which is not included in the antenna model [23, p. 819].

This exercise is informative because it demonstrates the strengths and limitations of treating the tonehole lattice as an antenna of monopoles and applying classic directivity equations. The low frequency results are misleading because they appear correct but do not capture the correct physics of the radiation of the resonator. The use of antenna theory is valid at cutoff, and fails at high frequencies. This particular interpretation of the physical validity of antenna theory to describe a lattice of toneholes is, to the best knowledge of the author, has not been previously published.

2.5 The clarinet as an acoustically periodic waveguide

The tonehole lattice cutoff frequency theory presented in Section 2.3 begins with the assumption of an infinite lattice of geometrically identical cells, is generalized to an

[7] A more complicated antenna could be implemented by allowing for differences in monopole amplitude and phase, but it is still informative to demonstrate the simplest case.

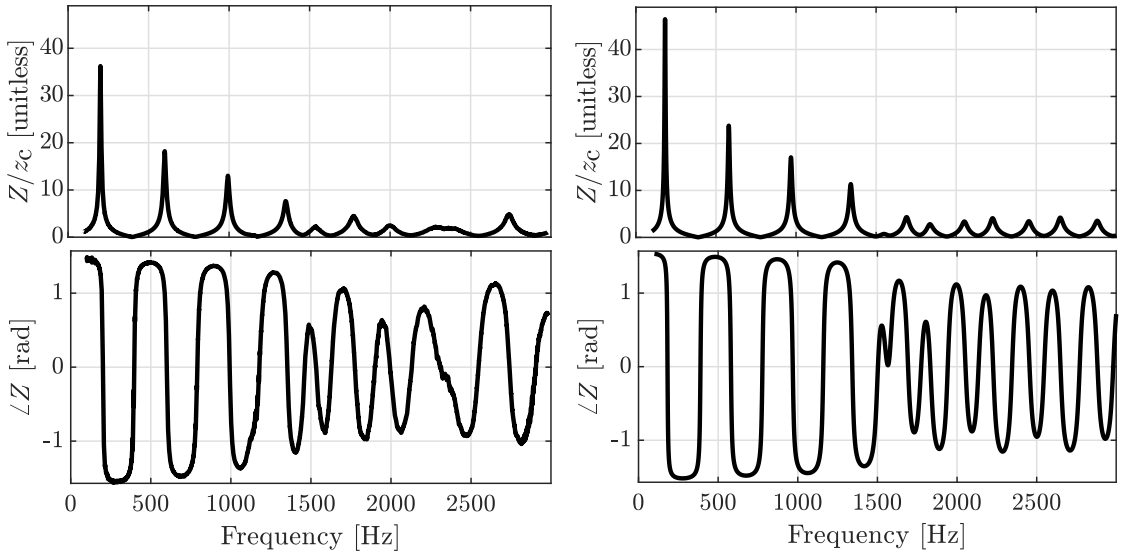

Figure 2.11: Measured input impedance of a B♭ clarinet with 5 open toneholes (written A, 196 [Hz] on left) and TMMI simulated input impedance of a simplified resonator ($f_1 = 182, f_c = 1500$ [Hz]) with 10 open toneholes on right.

infinite lattice of acoustically regular cells, and then shown to remain approximately valid for finite lattices. These last two steps are the basis for applying the theory of wave propagation in periodic media to real woodwind resonators which are neither perfectly periodic nor infinite.

Woodwind instruments were developed over many years, and the geometry of the tonehole lattice evolved empirically to achieve a desired intonation, timbre, and ease of playing. *Designing the lattice as a periodic waveguide with a well-formed tonehole lattice cutoff frequency was not likely a conscious design objective for historic instrument manufacturers, although the cutoff frequency may have been accounted for indirectly due to its effect on timbre. This particular behavior of periodic waveguides was observed in acoustical measurements of real instruments, and only then were the resonators interpreted within the context of wave propagation in periodic media* [1]. In this section, some of the ways in which cutoff may be observed in real instruments are explored and compared with the academic resonators and theory that were analyzed in detail in Section 2.4.

2.5.1 The cutoff frequency influence on internal variables of a clarinet

The cutoff of real woodwind instruments is typically observed on internal acoustic variables. A classic method [3] is to search for a perturbation of the modulus and argument of the input impedance, which may be measured or simulated, and attribute this to the cutoff of the tonehole lattice. Figure 2.11 shows the modulus and argument of a clarinet (measured) and the academic resonator from Section 2.4 (simulated) that has a first impedance peak frequency and cutoff similar to the clarinet. This facilitates a comparison between a resonator that is suspected of having a tonehole lattice cutoff (the clarinet) and

one that has been specifically designed to have a cutoff. The measured input impedance of the clarinet has a lower peak amplitude compared with the simulated academic resonator, possible due to losses in the adapter piece between the clarinet and measurement device or the constant z_c used to normalize the input impedance. Regardless of the amplitude difference, the similarity between the curves is reasonable.

The cutoff of the academic resonator at $f_c = 1500$ [Hz] is evident, seen as the point where the modulus peaks diminish in amplitude and spacing. It is more apparent in the argument, which responds dramatically at the cutoff.[8] This demonstrates a common mistake: identifying a cutoff from only the modulus of the input impedance is not advisable because it is only accurate to within the inter-peak spacing, and the natural decrease in peak amplitude with frequency can also obscure the effect.

The clarinet presents similar behavior around 1400 [Hz], a reasonable candidate for the cutoff of this fingering. There is an additional 'blip' of unknown provenance around 1100-1200 [Hz]. This demonstrates the difficulty of developing useful objective metrics for identifying the cutoff of real resonators. The academic resonator has regularly spaced peaks above cutoff, interpreted as the resonances associated with the total length of the waveguide [17]. The clarinet has irregularly spaced peaks above the cutoff, likely due to deviation from acoustic regularity of the lattice in addition to the frequency dependent effective acoustical length of the bell.

These observations regarding the cutoff for a real instrument represent a 'best case' scenario. The effect of the cutoff on this fingering, measured on this instrument, is particularly clear. It is often less clear for forked fingerings and lower notes for which only a few holes are open. As noted earlier, the clarinet is more acoustically regular than most woodwinds, and its cylindrical bore avoids many of the complications that arise from conical bores [58]. Therefore, the discussion of Figure 2.11 is taken as a reference for how a cutoff can look for a real instrument, with most subsequent comparisons failing to achieve this clarity, a topic treated at length in Chapter 5.

2.5.2 The cutoff frequency influence on external variables of a clarinet

The effect of the lattice cutoff on radiation is considerably more complex for a real instrument than it is for the academic resonator. One reason for this, as for internal variables, is that real resonators are generally not strictly acoustically regular, and may not have a strong cutoff. Even an acoustically regular (but not geometrically regular) lattice with a very strong cutoff on internal variables may still exhibit complicated external characteristics due to irregular spacing of the toneholes. Furthermore, toneholes of different sizes may not radiate uniformly [59], which may impact external characteristics such as the directivity. Because real instruments have complicated, irregular geometries, it is not simple to make general comments about the effect of cutoff on radiation.

2.5.2.1 Transfer function from internal variables to external variables

As for the academic resonator in Section 2.4, one way to view the impact of cutoff on radiation is to study the transfer function between external and internal acoustic

[8] For the case of an infinite, lossless lattice, the argument has a discontinuity at cutoff.

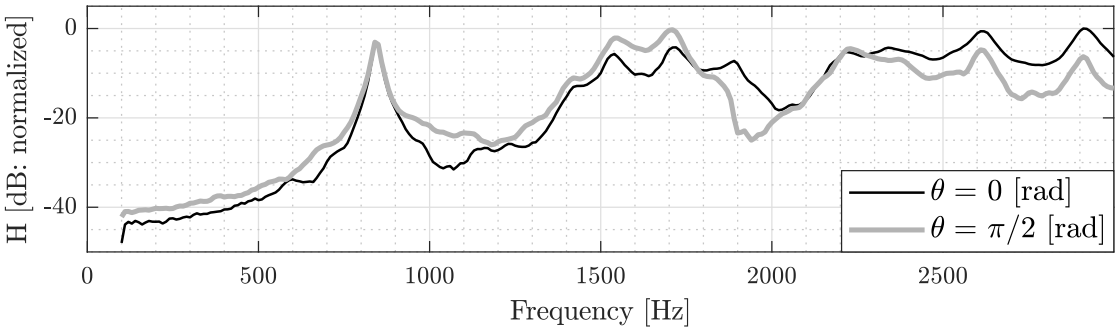

Figure 2.12: Transfer function (measurement in anechoic conditions) between external and internal pressure of a B♭ clarinet in neutral (unpressed keys) position. Two observation points at $r = 0.67$ [m] and angles $0, \pi/2$ [rad]. Note that this is a transfer function between pressure and pressure, not pressure and flow as in Figure 2.8. General trends remain true: monopole radiation at low frequencies, and strong on-axis directivity at high frequencies.

variables. Figure 2.12 shows the measured transfer function between external and internal pressure for a clarinet.[9] The internal pressure is measured near the location of the mouthpiece and the clarinet is in an neutral position with no keys depressed. Note that in the simulations shown in Figure 2.8, the transfer function is between external pressure and internal flow, whereas the measurements were made with microphones so the transfer function is between external and internal pressure (see Appendix A). At low frequencies and assuming monopole radiation, a high external pressure corresponds to a maximum of flow through the first tonehole.[10] Therefore, the peaks of the simulations are at frequencies for which there is a maximum flow through the first tonehole divided by a minimum flow at the input, similar to the input impedance. In contrast, the peaks of the measurements are formed by a maximum flow through the first hole divided by a minimum in pressure in the mouthpiece, which does not occur at the input impedance peak frequencies. This does not pose a problem, it simply must be understood when interpreting the data.

Some of the characteristic features of the cutoff demonstrated in Figure 2.8 are also observed in Figure 2.12. At low frequencies the two measurement points equidistant from the first tonehole have nearly the same amplitude, suggesting monopole type radiation. Figure 2.13 confirms that this is not a coincidence due to sparse spatial sampling. The higher pressures (about 5 [dB]) measured off-axis between 1500 [Hz] and 1700 [Hz] resembles that due to the cutoff at 1500 [Hz] in Figure 2.8. Lastly, above 2500 [Hz], the on-axis microphone is a consistent five [dB] stronger than the off-axis microphone, suggesting a strong directivity, likely due to both the tonehole lattice and the bell. While none of these characteristics are as clear as for the academic resonator, results obtained for resonators with strong cutoffs help identify the effects of the cutoff in the more ambiguous case of

[9] These measurements were performed with the help of Romane Rosser during a 10 week internship at LMA. Protocol details are provided in Appendix A.

[10] At low frequencies, the farfield pressure radiated from a monopole may be approximated by the time derivative of the acoustic flow [30, p. 184].

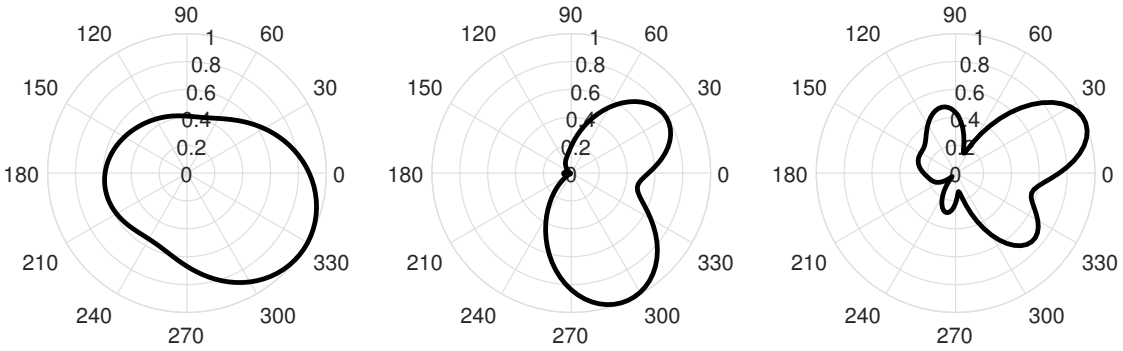

Figure 2.13: Directivity of a B♭ clarinet for third octave bands centered at $f = [250, 1587, 2520]$ [Hz], measured under playing conditions in an anechoic environment [53]. Reference plane is the same as for the simulations in Figures 2.9 and 2.10.

the clarinet.

2.5.2.2 Directivity based on measurements

It is also possible to compare the directivity of a clarinet with the academic resonator either through simulation or measurement, although simulation is cumbersome due to the increased geometric complexity. The measured directivity of a B♭ clarinet, taken from a publicly available data base [53], is shown in Figure 2.13 at third octave bands centered at $f = [250, 1587, 2520]$ [Hz]. The clarinet was played by a musician under a canopy of microphones in anechoic conditions. Note that this is the only data presented in this chapter under playing conditions, everything else has been about the passive response of the resonator. Here, these third octave frequency bands are chosen to represent directivity well below, comparable to, and well above the nominal cutoff of a clarinet at 1500 [Hz]. This figure may be compared with the directivity of an academic resonator in Figure 2.9, for which there are many similarities. A notable difference is the asymmetry along the axis of the resonator that exists for the measurements but not the simulations. This could be due to several factors, such as the presence of a musician in the anechoic chamber, asymmetry of the instrument, key pads covering the instrument, or a limitation of the monopole radiation assumption in the simulations. As with the transfer functions, a qualitative comparison between the directivity of the clarinet and the academic resonator is suggestive of a link between the cutoff frequency and radiation, demonstrating the utility of first studying the phenomena on simplified resonators.

2.5.3 The bell as a surrogate tonehole lattice

Another geometric difference between a real clarinet and the academic resonator is the flaring bell at the end of the instrument. Due to its changing cross section, the bell affects the acoustic response of the instrument in several ways [60]. A common explanation is that the bell serves to smoothly match the impedance between the constrained interior of the waveguide and the open environment, facilitating radiation [41, 42]. This is partially

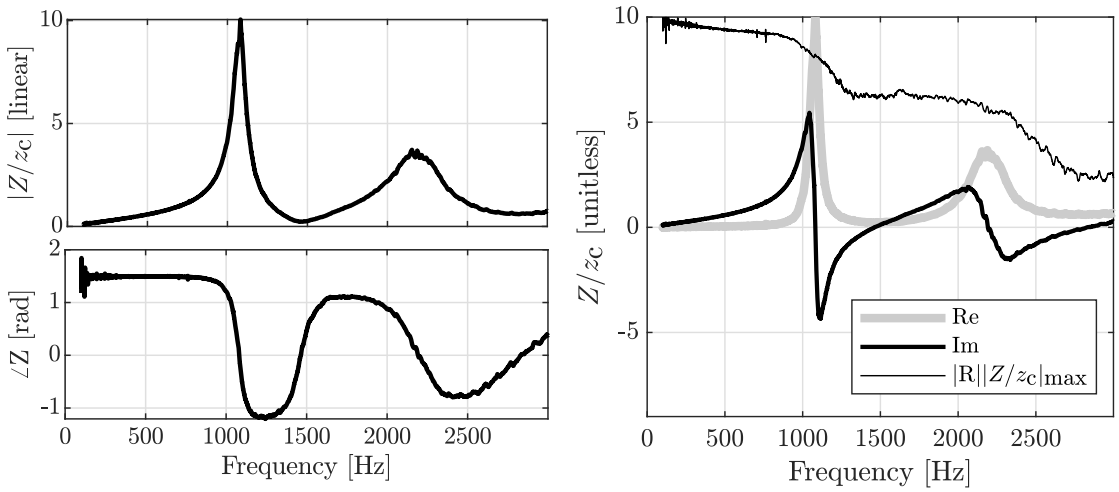

Figure 2.14: Measured input impedance of a B♭ clarinet bell modulus and argument (left) and real and imaginary components (right). Also on right, reflection coefficient modulus multiplied by input impedance modulus maximum for readability. The acts as a high pass filter by facilitating radiation above 1000 [Hz]. This figure may be compared to the infinite lattice in Figure 2.3.

true, but primarily at high frequencies. It is generally not true for frequencies with wavelengths that are long relative to the characteristic size of the bell G, determined by the condition $kG \ll 1$. At these low frequencies, the bell does not act as an impedance matcher, so the bell appears as a length extension to the main portion of the resonator. It should be mentioned that this discussion is mainly relevant for the lowest fingerings of the instrument, for which there are very few open toneholes. The frequencies that are too low to be efficiently radiated by the bell are generally in the stop band of the tonehole lattice, and will therefore not reach the bell if there are open toneholes.

Another effect of the bell is to serve as a surrogate tonehole lattice for the lowest couple fingerings on the instrument, for which there are not sufficiently many open toneholes to create a lattice cutoff [61]. As described above, the bell acts as a high pass filter, much like the tonehole lattice. Figure 2.14 shows the measured input impedance of a B♭ clarinet bell. The impedance imposed by the bell is mainly reactive below 1100 [Hz], suggesting that the energy at these wavelengths are largely reflected back into the instrument. This behavior is comparable to that of the 'infinite' lattice shown in Figure 2.3, with the exception that bell is finite so there are additional resonances above its cutoff.

Figure 2.15 shows the input impedance and reflection coefficient for the lowest note (all holes closed) of a B♭ clarinet with the bell and with the bell removed. Removing the bell shortens the effective acoustic length and shifts the first impedance peak up by about 55 cents. The bell also decreases the amplitude of the first peak, presumably because the long wavelength condition $kG = 0.35$ is not entirely satisfied assuming a characteristic length $G = 0.1$ [m], so the radiation at this frequency is increased by the bell. The bell does provide a satisfactory cutoff type behavior, nominally around 1000 [Hz], seen

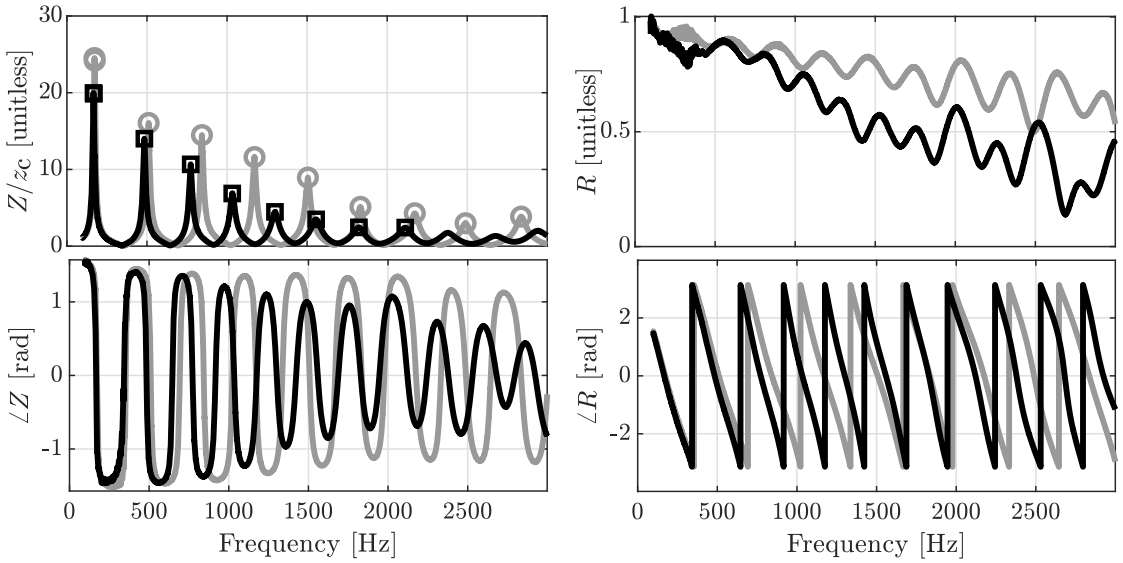

Figure 2.15: Measured input impedance and reflection coefficient of a clarinet (E3 written, 147 [Hz], no open toneholes) with the bell (black) and without the bell (grey). The internal acoustic variables are impacted as if there was a tonehole lattice, exhibiting a cutoff type behavior around 1000 [Hz].

mostly clearly in the input impedance argument and the reflection coefficient modulus. It is generally assumed that this improves the homogeneity between the lowest notes of the instrument and the rest of the register [62].[11] While this is likely a good thing from a perceptual perspective, the similar effects of the bell and lattice cutoff frequency complicates the study the cutoff on its own.

One way in which the effect of the bell is very different than the lattice cutoff is its frequency dependent radiation pattern. The bell may have some directivity that varies with frequency, but it is not likely to have the strong side lobes characteristic to a lattice at cutoff, as demonstrated in Section 2.4.2. Therefore, the argument that the bell acts as a surrogate lattice is largely reasonable for internal variables, but remains to be demonstrated for the radiated sound field.

2.6 Discussion

The main goal of this chapter, as stated earlier, is to orient the reader to the tonehole lattice cutoff frequency. The focus on the cutoff frequency, at the cost of discussing other topics, is intentional: the treatment of woodwinds as periodic structures has been studied only intermittently over the last several decades, and it is reasonable to assume that some of its established implications may have been forgotten. However, the details provided in the previous sections do not consider how the resonator might behave differently under playing conditions. The following discussion is meant to demonstrate the role of the resonator within the broader context of a woodwind instrument, in preparation for the

[11] Although the discussion of homogeneity of sound is subjective, and there are differing opinions [63].

following chapters.

The theory and results developed in this chapter, with the exception of Figure 2.13, are developed under the assumption that the resonator is passive and linear. This is a reasonable assumption when the sound pressure level inside the resonator remains small compared to atmospheric pressure [64]. However, under playing conditions the sound pressure levels inside a woodwind can reach 170 [dB], which at about 6% of atmospheric pressure is non-negligible, and can lead to nonlinear losses at the toneholes [65, 39, 66, 67]. This may be mitigated by undercutting the toneholes to prevent the generation of turbulence [66, 68]. Note that, as seen in Figures 2.8 and 2.12, this high internal sound pressure does not present a danger to the listener because woodwinds are inefficient acoustic radiators and only transmit a small fraction of this energy to the external sound field. One way in which nonlinear effects may impact the current work is that the transfer function between internal and external acoustic variables under playing conditions may be somewhat different than the transfer functions shown in Figures 2.8 and 2.12, which were simulated and measured under passive and linear conditions.[12] The formation of shocks due to high sound pressure is not expected due to the relatively short length of waveguide [70, 71].

A fully assembled (reed) woodwind instrument has, in addition to the resonator, a mouthpiece and reed ensemble that is used to play the instrument. With the exception of rarely used extended techniques, playing conditions imply that the reed is in a state of auto-oscillation. In the case of a woodwind instrument, there are three main components: the (quasi-) static energy source (pressure in musicians mouth), a passive resonator (the body of the instrument), and a nonlinear valve (the reed) [7, 72]. Auto-oscillation is the transformation of the (quasi-) static source energy into periodic acoustic energy [26]. For a reed instrument, the pressure in the musicians mouth injects energy into the system, and the vibration of the reed is regulated by the reflections of traveling waves in the body of the instrument, vibrating preferentially at frequencies near the input impedance peaks [73]. In addition to being well represented in literature, the study of this dynamic system is an ongoing topic of research and an important description of sound production for many types of instruments.

The resonator is considered passive because it does not contribute energy as the instrument is played, and only modifies the response of the dynamic system by fixed operations such as opening and closing keys [74]. This is why it is reasonable to model it with static descriptors such as the input impedance and transfer functions: they are immutable characteristics of the instrument.[13] In contrast, the injection of energy and the dynamic response of the reed is constantly evolving under playing conditions due to deliberate and undeliberate actions of the musician, as well as changes in the environment [75, 76]. Variables such as static mouth pressure, lip position, temperature, humidity, and reed response can all influence characteristics of the produced sound such as pitch, spectral content, and slowly varying (compared to the fundamental frequency) temporal features [77, 78]. Therefore, the internal spectrum is determined by both the variable control parameters of the reed/human system and the static characteristics of the resonator sampled at the harmonics of the produced sound. The external spectrum

[12] Although one study found that playing dynamics does not affect the directivity [69].

[13] Without invasive procedures!

is the internal spectrum filtered by transfer functions of the type shown in Figures 2.8 and 2.12.

The dual role of the resonator introduces a competition between sound production and radiation. Energy at harmonics that are weakly transmitted to the external soundfield largely remains inside the resonator, leading to a reinforcement of reed vibration at these frequencies. These harmonics will be strong in the internal spectrum, but less efficiently radiated by the resonator. In contrast, energy at harmonics that are efficiently radiated contribute less to reinforcing the reed vibration, and are therefore weaker in the internal sound. However, these efficiently radiated harmonics are not necessarily strong in the external sound because they do not reinforce themselves in the internal spectrum, *due to their efficient radiation.* This competition is mentioned in the literature [8],[14] but few quantitative studies exist [4, 5]. A central goal of the manuscript is to study the role of the cutoff frequency on this competition between sound production and radiation of woodwind instruments.

[14]This particularly entertaining account is provided by Benade in the proceedings of a 1979 seminar at the Royal Swedish Academy of Music: "Because of the weak radiation of the fundamental component of the tone, it is strongly reflected and comes back to give the reed vigorous instructions on how to breed more of its kind. The second harmonic returns less strongly, and so breeds its replacement less successfully at the reed. Continuing this line of thought shows that any components that happen to be produced by the reed above the tone-hole cutoff frequency simply run down the bore and escape! They do not return to breed, and so to strengthen their tribe."

Chapter 3

The effect of the cutoff frequency on sound production of a clarinet-like instrument

PREFACE

There are many different possible approaches to studying the cutoff of a lattice. One option is to design digital versions of 'resonators' that have the desired cutoff behavior. A hypothetical resonator with a cutoff could, for example, be modeled by the reflection coefficient as an equivalent filter that has a large modulus at low frequencies and which rolls off to a small modulus at high frequencies, corresponding to the stop and pass bands of the lattice, respectively.[1] Another option is to construct an artificial input impedance using modal analysis, retaining only modes below the cutoff frequency [79, p. 269-297.]. While both of these approaches could be used to evaluate the effect of the cutoff using, for example, digital synthesis [80, 81], they could lead to numerical problems such as a non-causal impulse response. Additionally, because the position and geometry of the radiating toneholes and termination of the resonator are not specified, the results are limited because they are not easily adapted to studying the radiation. For the same reason, this type of methodology is limited to simulation because the cutoff frequency is artificially imposed, rather than the response of a physically realizable resonator. Lastly, the generalization of results found through this type of inquiry to real instruments is not evident. Therefore, although this approach has some merits, it is abandoned due to these restrictive limitations.

Once this perspective is understood, it becomes clear that it is necessary to develop an analytic model of an acoustically regular lattice for which it is possible to fix a desired cutoff frequency directly from the geometry. With a few exceptions, previous studies deduced the cutoff of a lattice from a given geometry or acoustical response of a resonator, rather than the guiding design criteria by which the geometry is then determined [12, 3, 61]. The basis for this was previously developed [23, 383], but it is necessary to complete the model so that, in addition to the cutoff, the first impedance peak frequency can be chosen by the correct length of leading duct. The results in this chapter provide the formula for designing physically realizable resonators with independently variable first impedance peak and cutoff frequency [29].

[1] For a discussion regarding the vocabulary conventions adopted for stop and pass bands, see 2.3.4.

These analytically designed, simplified resonators can then be used to evaluate the effect of the cutoff frequency on sound production and radiation of woodwind-like instruments, while limiting the complications that arise when using real instruments. The set of possible first impedance peak frequency and cutoff frequency combinations is enormous, but luckily the topic of the dissertation informs the decision, narrowing the values to the range observed with existing instruments. In part because the resonators are cylindrical, and in part because the clarinet is relatively well studied, frequencies similar to the clarinet are prioritized: fundamentals at approximately 200 Hz and cutoff frequencies between 1000 Hz and 2000 Hz [23, 383]. Because these resonators have been designed analytically using simple manipulations of the resonator geometry, the characteristics of the resonators (such as input impedance and reflection coefficient) can be simulated using the simple and efficient transfer matrix method, and physical prototypes can be constructed using 3D printing or drilling through existing cylindrical ducts. These simplified resonators may be used to evaluate the effect of the cutoff frequency on sound production and radiation by simulation and experiment.

The effect on sound production could be examined using an artificial blowing machine, instrumented mouthpiece, or digital synthesis [82, 83]. These different options all have positive and negative attributes, and are more or less informative depending on the goal of the study. Experimental methods are useful because the radiated soundfield can be directly measured, while the internal mouthpiece waveforms could be measured with an instrumented mouthpiece, with either the control of an artificial blowing machine or a skilled musician. However, it proves impractical to mount an experimental investigation as the first step because to study many different combinations of first impedance peak and cutoff frequencies would require constructing a large number of resonators, and there is no basis to guide the choice of a subset of representative resonators. Therefore, the goal of the first study is to use digital synthesis with a wide range of resonators, and quantify the effect on sound production by comparing the synthesized internal pressure and flow waveforms. Because there are many results that can be determined from the internal waveforms alone, the effect on radiation is largely ignored at this point and addressed in Chapter 4 [51].

The digital synthesis codes are based on solving a physics based model in the discrete time domain [10, 84], rather than a frequency domain model such as the harmonic balance method [85]. Therefore, the effect of the cutoff frequency can be analyzed in terms of both frequency domain characteristics as well as transitory temporal characteristics. This allows a more complete description of the effect of cutoff on sound production by including characteristics that may be related to the 'ease of playing' such as attack time, in addition to intonation and timbre descriptors that can be extracted from the steady portion of a produced tone. Although this study is not exhaustive, it provides a quantitative link between the cutoff and sound production, and acts as a preliminary response to part of the guiding question of this dissertation.

Additional comments

This remainder of this chapter is a reproduction the published article:

E. Petersen, P. Guillemain, J. Kergomard, and T. Colinot. The effect of the cutoff frequency on the sound production of a clarinet-like instrument. *J. Acoust. Soc. Am.*, 145(6):3784–3794, 2019

Comments:

- Original abstract has been omitted.
- The term tonehole lattice cutoff frequency varies between chapters due to evolving requirements of the research. Because this chapter treats only the case of academic resonators, ambiguities regarding the cutoff of real instruments are ignored. The cutoff is defined by acoustic regularity of an infinite, loss-less lattice (Chapter 2 Eq. (2.29), and Chapter 3 Eq. (3.3)) and assumed to be valid for the finite, lossy lattices used in the current chapter. For a more complete discussion of cutoff definitions, see Chapter 5.

3.1 Introduction

Reed instruments are typically characterized by two main components: the reed and flow rate as a nonlinear excitation mechanism and the main bore of the instrument as a passive acoustic resonator that responds to and influences the excitation mechanism. Under normal playing conditions the resonator responds to an injection of acoustical energy from the exciter by radiating sound, but also facilitates the self-sustained oscillation of the exciter [3]. The input impedance, determined by the specific geometry of the bore and tonehole network, is a standard way to characterize the acoustic behavior of the resonator. A resonator with a series of open toneholes exhibits a well-known behavior called the tonehole lattice cutoff frequency, below which a lattice wave sampled at discrete points is evanescent, while above, a lattice wave can propagate further into the bore [2, 1, 19]. Below the cutoff frequency the resonator has an effective length that is approximately the length between the input and the first open tonehole. In the case of a cylindrical bore, due to constructive interference of the reflected waves, the input impedance is characterized by well-defined, nearly harmonically spaced maxima expected of a quarter-wave resonator. Above the cutoff frequency, the effective length of the resonator is a complicated function of frequency, so there is less organized constructive and destructive interference, and the impedance is characterized by attenuated peaks that are not harmonically related to the first impedance peak.

It is often assumed that the cutoff frequency behavior is related to the perceptual characteristics of the sound produced by an instrument [3, 24]. However, it is not known precisely in what way the cutoff frequency affects the production and radiation of sound. Therefore, it is worth investigating how the frequency at which cutoff occurs, and the severity of the cutoff behavior on the input impedance, could impact the self-sustained oscillation and the temporal and spectral characteristics of the produced sound. Similarly, the cutoff frequency may impact characteristics of sound radiation such as directivity and total radiated power with respect to frequency. The complicated behavior associated with sound production and radiation are linked to one another through the competition between the acoustical energy that is retained within the resonator, which facilitates production, and that which is radiated into the surrounding environment.

The goal of this article is to evaluate how the cutoff frequency impacts different aspects of sound production and timbre features. To reduce the number of parameters that influence the acoustical behavior of a real instrument, the current work (except Section 3.3.3) considers resonators composed of a cylindrical main bore terminated by a lattice of geometrically regularly spaced toneholes. This simplified version of a clarinet resonator allows direct analysis of the effects of the cutoff frequency without added complications such as irregular tonehole lattices, conical segments, and undercut toneholes, as is the case for actual woodwind instruments.

Section 3.2 contains a review of the Transfer Matrix Method (TMM) [86, 87, 17] for simulating the input impedance of a pipe, including the related Transfer Matrix Method with external Interactions (TMMI) [28], which accounts for mutual radiation impedance when there are more than a single radiating aperture (toneholes and open termination of the main bore). Section 3.3 details the design and experimental verification of a cylinder and tonehole lattice resonator for which it is possible to specify both the frequency of the

first impedance peak and the cutoff frequency. The effects on sound production, for three different resonators, are compared using digital synthesis in Section 3.4. The main focus of this section is to characterize the internal sound field, as well as the transfer function between internal and radiated time averaged intensity. Examples of synthesized pressure and velocity waveforms are furnished as supplementary materials online. Conclusions and proposals for future work are covered in Section 5.4.

3.2 Input impedance calculations via the Transfer Matrix Method and the Transfer Matrix Method with external Interactions

While the TMM is elegant, simple, and efficient, it ignores the effects of external interactions due to toneholes radiating simultaneously into the same space. A variant of the TMM is the Transfer Matrix Method with external Interactions (TMMI) [28, 23]. This method accounts for propagation within the main bore while also accounting for the mutual impedance between apertures (N toneholes and the bore end) that are assumed to radiate into the same space, and therefore have a mutual influence.

The TMMI allows the calculation of the acoustic pressure vector P and the acoustic flow vector U through each aperture of the resonator. They are related to the source term by

$$\begin{aligned} U &= [\mathbb{I} + \mathbb{Y}(\mathbb{Z} + \mathbb{B})]^{-1} U^{\mathrm{s}} \\ P &= \mathbb{Y}^{-1}(U^{\mathrm{s}} - U), \end{aligned} \tag{3.1}$$

where U^{s} is the source vector, of dimension $N+1$ and with only one non zero element: $U^{\mathrm{s}}_n = \delta_{n,1}$. $\mathbb{I}$ is the identity matrix, and $\mathbb{Y}$ is a tri-diagonal admittance matrix, derived from the 2x2 transfer matrices of the main bore between toneholes. A cylinder is added to account for the section of pipe separating the mouthpiece from the first open tonehole of a real instrument. $\mathbb{B}$ is the impedance matrix for the acoustic mass of each tonehole: the definition includes many equations, and can be found in the appendix of Lefebvre *et al* [28]. $\mathbb{Z}$ is the radiation impedance matrix. Along the diagonal, it accounts for the classical self radiation impedance of each aperture, and for the mutual radiation impedance between two apertures, it is assumed that they radiate as a monopole in an half infinite space [45, 28, 88]. The input impedance is calculated from the knowledge of the quantities P_1 and U_1.

At low frequencies the monopoles can be assumed to radiate into a full space, however, the uncertainty of the mutual loading approximation is greater than the factor of two between half space and full space radiation.

The TMMI impedance calculation yields subtly different results when compared with that of the standard TMM, as seen in Figure 3.4. The two methods are in good agreement at low frequencies. At higher frequencies, the TMMI reduces the height of the resonances and reduces the depth of the anti-resonances, which can be interpreted as a reduction in the standing wave ratio of the resonator and an increase of the radiation losses in the system. Knowing P and U at the location of the toneholes allows for the calculation of external values such as directivity and the pressure waveform at a given external location, topics that are outside the scope of this paper but useful for future work.

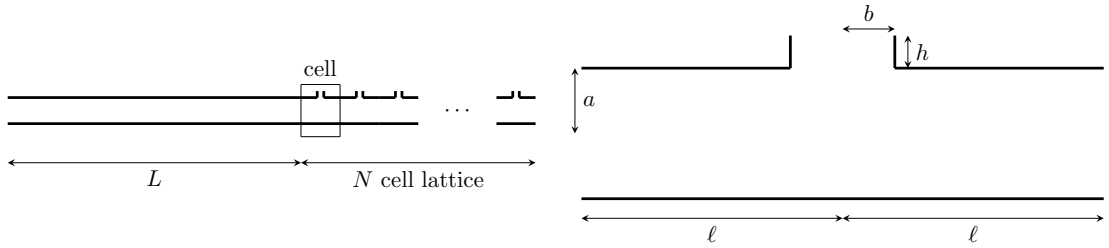

Figure 3.1: Pipe and lattice resonator (a) constructed from identical cells (b).

3.3 Resonator design

3.3.1 Periodic lattice of holes and resulting cutoff frequency

The basic resonator considered in the current work is designed to have a desired first impedance resonance frequency at f_1 and desired cutoff frequency at f_c that can be manipulated independently from one another by varying the geometry. This is achieved by concatenating a cylinder of length L, which largely determines f_1, to a lattice of geometrically regular toneholes that imposes the cutoff behavior at f_c, as shown in Figure 3.1(b). This is similar to the resonator design in the dissertation by Worman [12]. While not explained in great detail, it is important to note that simple geometric calculations must include low frequency length corrections, defined in Section 3.3.2, due to the lattice of toneholes as well as the more familiar radiation length correction at each open tonehole.

The analytic formulations used in this method allow only for the frequencies f_1 and f_c to be independently determined (see Eq. (3.2) and (3.4)). The second impedance peak of two resonators with different cutoff frequencies occur at nearly the same frequency because there is very low inharmonicity due to the cylindrical portion of the resonator, and the use of identical toneholes. Dimensions and acoustic features of sample resonators are provided in Appendix 3.5.

3.3.2 Geometrically regular lattice

A geometrically (and therefore also acoustically) regular lattice is constructed by repeating the basic cell shown in Figure 3.1 (b) to create the lattice shown in Figure 3.1 (a). If the cells are all identical and their number infinite, the global cutoff frequency, which can be estimated from impedance measurements or simulations, will be equal to the local cutoff frequency. The local cutoff frequency is approximated by the Helmholtz resonance of a single cell whose main bore is closed at the extremities,

$$\omega_c = 2\pi f_c \approx \frac{c}{\ell}\frac{1}{\sqrt{\left(\frac{c}{\ell}\right)^2 m_h C_a + 1/3}}, \tag{3.2}$$

where $C_a = 2\ell\pi a^2/\rho c^2$ is the acoustic compliance of the main pipe, $m_h = \rho h/\pi b^2$ is the acoustic mass of the tonehole, and a, ℓ, b and h are the geometric dimensions of the cell shown in Figure 3.1 (b) [22].

The exact local cutoff frequency for a cell in an infinite lattice can be calculated from

$$\frac{\ell}{c}\cot(k\ell) = \omega m_h C_a, \tag{3.3}$$

which is derived by solving the pressure and flow transfer matrix equations assuming either Dirichlet or Neumann boundary conditions within the main bore [23, 380]. This exact form differs by less than 1% from the approximate form given in Eq. (3.2) for an equivalent Helmholtz resonator of dimensions used in the current article.

To impose a desired local cutoff frequency it is sufficient to find a combination of dimensions a, ℓ, b, and h, accounting for the length corrections due to the inertial effect of adjacent fluid and the radiation impedance of the tonehole, that result in the desired resonance. Therefore, it is possible to design a lattice to have a desired global cutoff frequency by manipulating the dimensions of the constituent cells to have the same local cutoff frequency. To impose the frequency of the first impedance peak f_1, a cylinder of length L is concatenated to the lattice and treated like a quarter-wave resonator,

$$f_1 = \frac{c}{4L_a}, \tag{3.4}$$

where $L_a = L + \Delta\ell$ is an effective acoustic length that accounts for the presence of a lattice of open toneholes. The lattice modifies the radiation impedance of the cylinder as a mass-like term, and is treated as a length correction

$$\Delta\ell = \ell\sqrt{1 + \frac{\ell^2}{c^2} C_a m_h}, \tag{3.5}$$

which must be included in addition to the physical length of the main cylinder when determining the appropriate length that results in the desired frequency f_1 [3]. A strong cutoff frequency behavior is observed with as few as three open toneholes, however, the frequency at which cutoff occurs tends to be somewhat higher than that calculated in Eq. (3.2) when the lattice is comprised of a small number of holes, see Fig 3.2. Lattices with 10 toneholes exhibit a very strong cutoff behavior at the desired frequency. Three resonators, all with first resonance frequencies $f_1 = 170$ Hz and with cutoff frequencies $f_c = 1000$, 1500, and 2000 Hz, are used frequently in the current paper and will therefore be referred to as resonators $\mathcal{R}_{1.0}$, $\mathcal{R}_{1.5}$ and $\mathcal{R}_{2.0}$. All three have ten toneholes in addition to the open termination of the pipe. The input impedance of all three were simulated and two ($\mathcal{R}_{1.0}$, $\mathcal{R}_{2.0}$) were constructed physically (dimensions provided in Appendix 3.5) and compared with simulation in Section 3.3.4.

3.3.3 Acoustic regularity

Although the analysis based on digital synthesis in Section 3.4.1 is limited to a tonehole network composed of geometrically regular cells, Moers and Kergomard [22] show that it is possible to define an acoustic regularity for which each constituent cell has the same Helmholtz resonance, but not necessarily the same geometry. In that article, they consider the inverse problem of determining the division of an acoustically regular lattice that results in the expected global cutoff frequency. In the present paper, the problem is

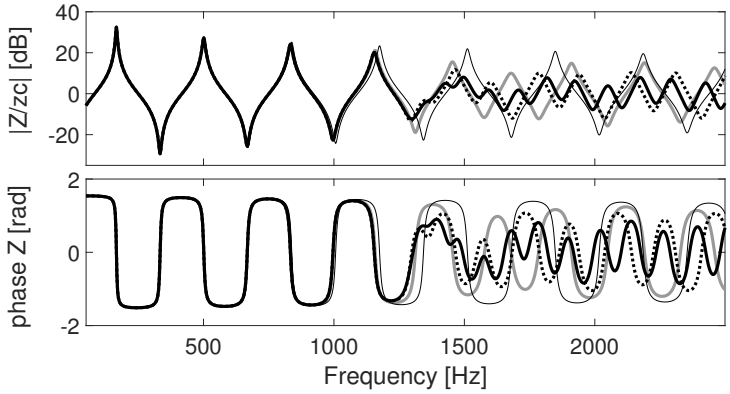

Figure 3.2: Simulated impedance curves of resonators with $f_1 = 170$ Hz, $f_c = 1350$ Hz, and varying number of toneholes (thin solid black: cylinder; thick solid grey: 4 holes; thick dashed black: 10 holes; thick solid black: 20 holes). The cutoff frequency $f_c = 1350$ Hz was chosen to occur at an impedance minimum so that the effect on the next maximum can be more easily distinguished. Lattices with 10 holes exhibit very strong cutoff behavior.

solved directly by designing each cell to be geometrically different, except the bore radius, but have a common Helmholtz resonance, and therefore have an acoustic regularity that results in the desired global cutoff frequency. The individual cells have identical main bore internal radii a, and the tonehole radii and heights b, h taken from the clarinet dimensions provided in Appendix A1 of Moers and Kergomard [22]. Once a desired cutoff frequency is set, the length of pipe ℓ on each side of the symmetric cells is deduced by Eq. (3.2). This acoustically regular lattice can then be constructed with a leading pipe to create the desired first resonance peak described in Section 3.3.2. Figure 3.3 shows that a global cutoff frequency is attained using an acoustically (but not geometrically) regular lattice. As with a geometrically regular lattice, the low frequency behavior of the acoustically regular lattice is largely unchanged between resonators with different cutoff frequencies. Specifically, the height and frequency of the first two impedance peaks are negligibly different for different resonators. This similarity between geometrically and acoustically regular resonators suggests that the choice to use geometrically regular resonators in this work is a reasonable simplification of real instruments, which exhibit substantial acoustic regularity. Next, the effect of the order of acoustically regular cells is examined by calculating the input impedance for randomized permutations of the cell locations. Figure 3.3 demonstrates that the order of the cells in the lattice does not greatly influence the frequency at which cutoff occurs and, as above, has a negligible influence on the height and frequency of the first two impedance peaks. This is a result of work by Fürstenberg [89] demonstrating exceptions to the nonexistence of pass bands in an infinite one-dimensional random medium [90, 22]. It is worth noting that, above the cutoff frequency and up to approximately 2000 Hz, the impedance of each resonator, regardless of the cell order, follows similar and slowly diverging paths. This is unexpected

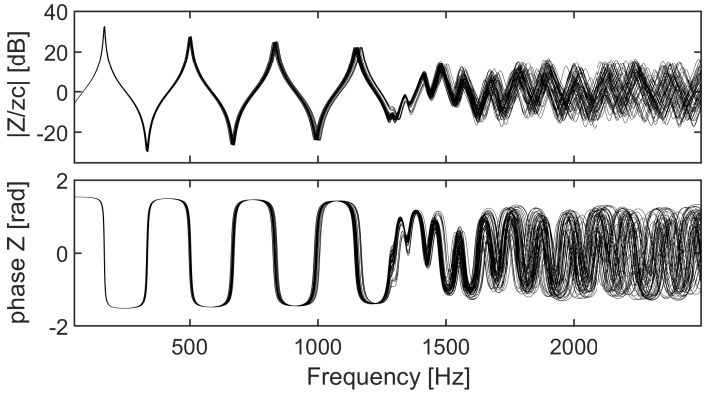

Figure 3.3: Multiple simulated input impedances for resonators with acoustically regular lattices and random cell orders (50 permutations). The target frequencies are $f_1 = 170$ Hz and $f_c = 1350$ Hz.

and suggests that, for frequencies just above cutoff, the input impedance behavior is determined by global features of the lattice. This is curious, but less relevant to the case of real clarinets, which typically have a fairly regular progression from small, closely spaced holes near the top of the instrument, to large and distantly spaced holes near the bell.

3.3.4 Experimental results of a simple resonator

The simplified pipe-lattice resonator described in the previous section was tested experimentally by measuring the input impedance of two polyamide 6 tubes where the lengths L and tonehole network geometries are designed to have first impedance resonances at 170 Hz and cutoff frequencies at 1000 Hz and 2000 Hz ($\mathcal{R}_{1.0}$, $\mathcal{R}_{2.0}$), according to Eq. (3.2) and (3.4). The dimensions are summarized in Appendix 3.5. The input impedance was measured using an impedance measurement device developed at CTTM [91]. Figure 3.4 shows that the target first impedance resonance and cutoff frequencies are attained by both simulation and measurements. This demonstrates the relevance of the model and accuracy of the measurement methodology. The better agreement between simulation and measurement for the $f_c = 1000$ Hz resonator is a consequence of the greater distance between holes, and not a general trend related to the cutoff frequency of a resonator. A second stop band in the impedance of $\mathcal{R}_{1.0}$ is visible around 2500 Hz both in the simulation and measurement. The discrepancy between simulation and measurements at high frequencies may be due to slight imprecision of the physical geometries of the experimental pipes, inaccuracies of the measurement hardware, or higher order phenomena not included in the simulation. These differences do not affect the conclusions, which are based on the location of the cutoff frequency and not the precise high frequency behavior.

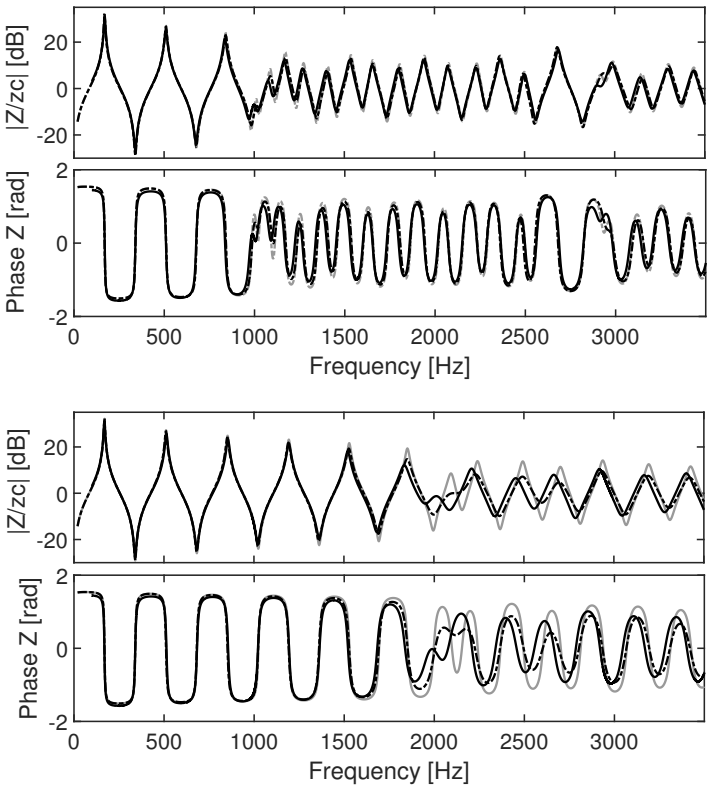

Figure 3.4: Input impedance of $\mathcal{R}_{1.0}$ (a) and $\mathcal{R}_{2.0}$ (b). Grey: TMM simulation; dashed black: TMMI simulation; solid black: experimental.

3.4 Effects of cutoff frequency using digital synthesis

Digital sound synthesis is a convenient method to evaluate the playing characteristics of a real or hypothetical resonator, and to compare two or more different resonators, because it can synthesize time domain acoustic pressure and volume velocity waveforms inside the mouthpiece for a wide range of control parameters. One can then compute descriptors of the waveform that are used to quantify playing characteristics, with respect to the control parameters, such as playing frequency, spectral centroid, and attack time. These playing descriptors are functions of the dimensionless control parameters excitation pressure γ, and embouchure ζ (defined below), but also are dependent on the reed parameters and input impedance of the resonator [92, 93]. It is assumed that γ and ζ control timbre features of a given instrument, and are therefore useful parameters to evaluate the connection between sound production and sound descriptors. It is important to note that synthesized waveforms do not necessarily match those of a real instrument because the values of physical parameters, particularly regarding the reed dynamics, are not precisely known. However, digital synthesis is a reasonable tool to compare the behavior of different resonators. The following sections are based on synthesis for resonators $\mathcal{R}_{1.0}$, $\mathcal{R}_{1.5}$ and $\mathcal{R}_{2.0}$ as defined in Section 3.3.2.

3.4.1 Digital synthesis model

The digital synthesis model used in this work combines the discretization scheme of Guillemain [92], with the use of the reflection function to model the response of the resonator [94, 95]. Its purpose is to solve, in the domain of time sampled signals, a system of three equations and three unknowns giving the values at sample number n as functions of the past known values of the three variables. For that purpose, we start with the continuous time model describing the resonator, the reed dynamics, and the nonlinear relationship between pressure and flow in the mouthpiece.

3.4.1.1 Continuous time model

The continuous time reed instrument model used in this work is comprised of three main equations (Eq. (3.7), (3.9), and (3.10)). The three variables are the dimensionless pressure, flow rate, and reed displacement, respectively

$$\begin{cases} \tilde{p}(t) &= p(t)/p_M \\ \tilde{u}(t) &= Z_c u(t)/p_M, \\ \tilde{x}(t) &= x(t)/H, \end{cases} \tag{3.6}$$

where Z_c is the characteristic impedance, p_M is the pressure difference needed to close the reed completely in a static situation, and H is the distance between the tip of the reed and the mouthpiece lay at equilibrium. The value $\tilde{x} = -1$ corresponds to the closure of the reed. The first equation corresponds to the movement of the reed which consists of a damped spring-mass driven by the pressure differential between the mouth of the musician and the mouthpiece

$$\begin{cases} \frac{1}{\omega_r^2}\frac{d^2\tilde{x}(t)}{dt^2} + \frac{q_r}{\omega_r}\frac{d\tilde{x}(t)}{dt} + \tilde{x}(t) = \tilde{p}(t) - \gamma \text{ if } \tilde{x} > -1, \\ \frac{d\tilde{x}(t)}{dt} = 0 \text{ if } \tilde{x} < -1, \end{cases} \tag{3.7}$$

where ω_r is the resonance angular frequency of the reed, q_r is the damping coefficient, and the parameter $\gamma = p_m/p_M$ is the dimensionless pressure in the mouth of the musician. Following values similar to other articles [93], the synthesis results presented in this paper assume $\omega_r = 2\pi f_r = 2\pi 1500$ (rad/s) and $q_r = 0.4$ (dimensionless). The second line of Eq. (3.7) corresponds to the limitation of the reed displacement by the mouthpiece lay. There exist more refined models of the reed that include dynamical behavior and the collision of the reed and the lay [96, 97, 98]. These models, however, are unnecessary for the current work which aims to efficiently compare the response of different resonators, not predict absolute behavior. The nonlinear relationship relating the input flow $u(t)$ as a function of the pressure differential and the reed position is

$$\tilde{u}(t) = u_b(t) + u_r(t), \tag{3.8}$$

where

$$\begin{cases} u_b(t) &= \zeta(1 + x(t))\text{sign}(\gamma - \tilde{p}(t))\sqrt{|\gamma - \tilde{p}(t)|}, \\ u_r(t) &= \lambda_c \frac{dx(t)}{dt}. \end{cases} \tag{3.9}$$

The variable $\zeta = Z_c w H \sqrt{2/\rho p_M}$ is the dimensionless embouchure parameter, depending on the width w and height H of the reed channel cross section when the reed is at rest, and is proportional to the square root of H because p_M is a function of H. The total flow rate is the sum of the flow computed from the stationary Bernoulli equation u_b and the flow due to the movement of the reed u_r, depending on the speed of the reed and a parameter λ_c that characterizes the effective vibrating surface of the reed [99].

The third principle equation represents the passive role of the resonator and is expressed by its input impedance. Following McIntyre [26] and Gazengel [94], a straightforward change of variables in the Fourier domain, using wave variables rather than Kirchhoff variables, leads to the expression of the backward pressure wave at time t in the temporal domain

$$p^-(t) = (r * p^+)(t), \tag{3.10}$$

where $p^-(t) = (\tilde{p}(t) - \tilde{u}(t))/2$ and $p^+(t) = (\tilde{p}(t) + \tilde{u}(t))/2$ are the backward and forward pressure waves in the resonator. The operator $*$ represents continuous time convolution and r is the reflection function of the resonator, obtained from the input impedance by

$$r = \mathcal{F}^{-1}\left(\frac{Z(\omega) - Z_c}{Z(\omega) + Z_c}\right), \tag{3.11}$$

where $\mathcal{F}^{-1}$ is the inverse Fourier transform. The advantage of using the reflection function rather than the impulse response is that it is assumed to decrease much faster in time, and can therefore be truncated to save computation time.

3.4.1.2 Discrete model

The continuous time model of the complete instrument is discretized so that temporal synthesis can be simulated by a computer. Therefore, a strictly causal formulation must be found so that every variable at a given time sample can be computed from the previous values of all variables. Equation (3.7) is discretized using the finite difference scheme [95], such that

$$x[n] = b_{1r} p[n-1] + a_{1r} x[n-1] + a_{2r} x[n-2], \tag{3.12}$$

where the tilde notation is omitted for dimensionless variables in the discrete formulation ($p[n]$ is the n^{th} sample of the dimensionless pressure signal). The coefficients b_{1r}, a_{1r} and a_{2r} are given in Guillemain et al [95]. In order to ensure the limitation of the reed displacement, the following condition is added

$$\text{if } x[n] < -1, \text{ then } x[n] = x[n-1]. \tag{3.13}$$

Once the position of the reed at sample n is known, the reed flow is computed using the finite difference scheme

$$u_r[n] = \lambda(x[n] - x[n-1]). \tag{3.14}$$

The parameter $\lambda = \lambda_c f_s$ is fixed at the value -0.7 as in Coyle et al. [93] based on the measurements available in the literature [99, 26, 100, 101]. The third equation involving the reflection function can be reformulated using the discrete convolution product

$$(r * p^+)[n] = \sum_{i=0}^{\infty} r[i]p^+[n-i], \tag{3.15}$$

where r is the discrete version of the reflection function, which is causal. For the numerical application, the reflection function is deduced from the computed input impedance, which is windowed down to the characteristic impendance by 8 kHz, well below the first nonplanar mode and following recommendations from Gazengel [94]. Above this frequency the impedance is completed by the characteristic impedance until the Nyquist frequency, before computing the reflection function by inverse Fourier transform. Only the first $D = 3000$ elements of the reflection function are kept for the synthesis, chosen to be long enough so that it does not disturb the low frequency content of the resonator's response. Specifically, the impulse response is a sum of exponentially damped sinusoids and this choice of D ensures that the time response of the lower mode, with the highest quality factor, is not truncated. The backward pressure wave corresponds is written as

$$p^-[n] = \sum_{i=0}^{D} r[i]p^+[n-i]. \tag{3.16}$$

Separating this equation into a strictly causal and an instantaneous part and substituting for p and u, $p^-[n]$ becomes

$$\frac{1}{2}\left(p[n] - u[n]\right) = \frac{1}{2}r[0]\left(p[n] + u[n]\right) + \frac{1}{2}\sum_{i=1}^{D} r[i](p[n-i] + u[n-i]), \tag{3.17}$$

where $r[0]$ is the first sample of the discrete reflection function. This yields $p[n]$ as a function of $u[n]$ and the past of p and u

$$p[n]\left(1 - r[0]\right) = u[n](1 + r[0]) + \sum_{i=1}^{D} r[i](p[n-i] + u[n-i]), \tag{3.18}$$

The final pressure expression is as follows:

$$p[n] = \frac{1 + r[0]}{1 - r[0]}u[n] + \frac{1}{1 - r[0]}\sum_{i=1}^{D} r[i](p[n-i] + u[n-i]). \tag{3.19}$$

Using Eq. (3.19), it is possible to implement the temporal synthesis scheme described in Guillemain et al. [95], because it is in the form $p[n] = b_{c_o}u[n] + V$ where V is a known quantity at sample n.

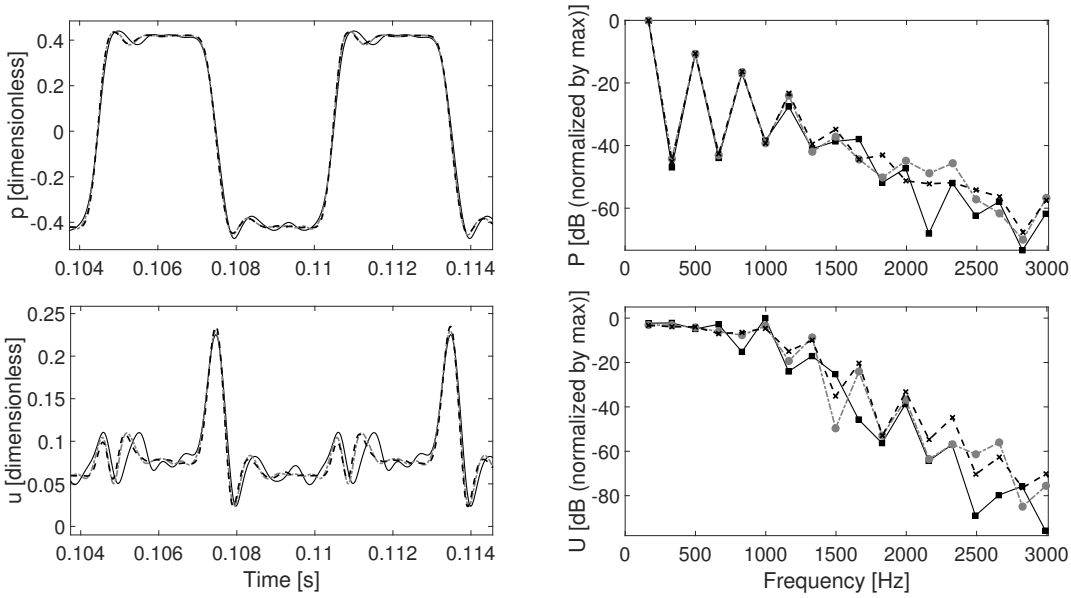

Figure 3.5: Synthesized (dimensionless) pressure (top) and flow (bottom) inside mouthpiece for resonators $\mathcal{R}_{1.0}$ (solid black), $\mathcal{R}_{1.5}$ (dash-dot gray), and $\mathcal{R}_{2.0}$ (dashed black) in the time (left) and frequency (right) domains. Control parameters are $\gamma = \zeta = 0.45$, and reed resonance $f_r = 1500$ Hz.

3.4.2 Results

Synthesized time and frequency domain waveforms of the internal pressure and flow for resonators $\mathcal{R}_{1.0}$, $\mathcal{R}_{1.5}$, and $\mathcal{R}_{2.0}$ are shown in Figure 3.5, and available to listen to online [102]. The waveforms are taken from the periodic and steady state region of the synthesis, which is calculated with control parameters $\gamma = 0.45$, $\zeta = 0.45$. In this representation the signals from the three resonators have been arbitrarily shifted in time by less than one cycle, so that they overlay one another, facilitating visual comparison. The timing difference of the pressure and flow signals is small, and may result from a small change in playing frequency. There is a subtle difference between both the pressure and volume velocity for resonators $\mathcal{R}_{1.0}$, $\mathcal{R}_{1.5}$, and $\mathcal{R}_{2.0}$. The biggest visual difference is in the volume velocity waveform, in which resonator $\mathcal{R}_{1.0}$ has larger amplitude and lower frequency rippling when compared with resonators $\mathcal{R}_{1.5}$ and $\mathcal{R}_{2.0}$. A simple interpretation, examined in Section 3.4.2.1, is that there is more energy in the high frequency harmonics in the waveforms computed from resonators with higher cutoff frequencies. The height of the peaks that are the main feature in the velocity waveform, corresponding to the closing of the reed, also changes between the different resonators.

3.4.2.1 Frequency domain characteristics

Frequency domain characteristics are computed directly from the steady state portion of the synthesized waveforms p and u inside the mouthpiece, discarding the attack transient. The playing frequency, f_p, of resonators $\mathcal{R}_{1.0}$, $\mathcal{R}_{1.5}$, and $\mathcal{R}_{2.0}$, as a function of γ with

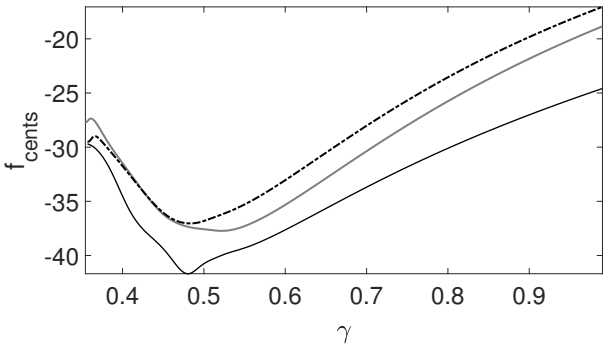

Figure 3.6: Synthesized playing frequency in cents, normalized by the first impedance peak frequency, for resonators $\mathcal{R}_{1.0}$, $\mathcal{R}_{1.5}$, and $\mathcal{R}_{2.0}$ with solid black, solid grey, dashed black lines, respectively.

constant $\zeta = 0.45$, are displayed in Figure 3.6. The values are presented in cents, relative to the frequency of the first impedance peak, such that

$$f_{\text{cents}} = 1200\log_2\left(\frac{f_\text{p}}{f_1}\right). \tag{3.20}$$

It is seen that resonators with higher cutoff frequencies also have playing frequencies that are higher by a few cents. In the beating reed regime, approximately $\gamma > 0.5$, the difference between resonators $\mathcal{R}_{1.0}$ and $\mathcal{R}_{2.0}$ is greater than five cents, therefore possible large enough to be perceived by a human [103]. This is not due only to the difference in inharmonicity between the first and second peaks, verified through analytical formulations [93], in which the inharmonicity of these resonators results in a maximum of 2.5 cents difference between resonators $\mathcal{R}_{1.0}$ and $\mathcal{R}_{2.0}$. However, the tonehole lattice also changes the inharmonicity of higher resonances of the input impedance below the cutoff frequency. This could influence the playing frequency, particularly at high values of γ and ζ.

To define a single value descriptor, the spectral centroid [104], is calculated as

$$\text{centroid} = \frac{\sum_{m=1}^{M} f(m)G(m)}{\sum_{m=1}^{M} G(m)}, \tag{3.21}$$

where $G(m)$ is the single sided power spectrum corresponding to the Fast Fourier Transform frequency bins $f(m)$ up to $f(M) = 8$ kHz, at which point the assumptions made in the impedance simulation regarding thermo-viscous losses and radiation are no longer valid. This definition results in a single number for a given spectrum with units of Hz, which follows the 'center of mass' interpretation of the spectral content. The spectral centroid values, normalized by the playing frequency at each combination of control parameter and for each resonator, are shown in Figure 3.7. The spectral centroid is higher

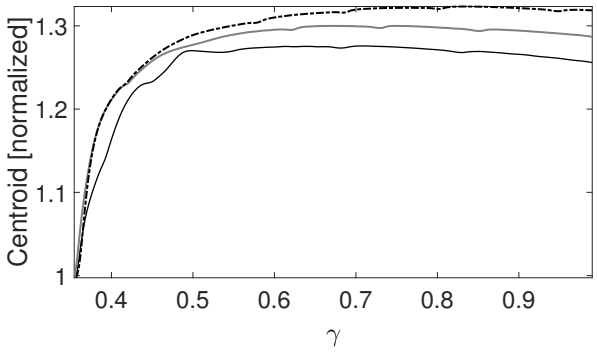

Figure 3.7: Synthesized spectral centroid, normalized by the playing frequency, for resonators $\mathcal{R}_{1.0}$, $\mathcal{R}_{1.5}$, and $\mathcal{R}_{2.0}$ with solid black, solid grey, dashed black lines, respectively.

for resonators with higher cutoff frequencies, even after adjusting for the playing frequency.

To evaluate the influence on the distribution of harmonics in synthesized signals, the input impedance was simulated for a wide range of resonators with fundamental frequencies of 20 consecutive semitones ranging from 110 to 330 Hz for all three cutoff frequencies 1000, 1500, and 2000 Hz. This results in 60 simulated resonators: 20 of each type $\mathcal{R}_{1.0}, \mathcal{R}_{1.5}$ and $\mathcal{R}_{2.0}$. The first impedance peak frequency is manipulated by changing the length of the cylinder between the mouthpiece and the first open tonehole, leaving the lattice of 10 open toneholes unchanged. Digital sound synthesis was then calculated for the 60 resonators, using a beating regime value $\zeta = 0.45$, $\gamma = 0.55$ in order to generate more even harmonics. A peak detection scheme was applied to the spectra of the internal pressure where the square and circular data markers correspond to the odd and even harmonics. The results are plotted in Figure 3.8 for resonators of type $\mathcal{R}_{1.0}, \mathcal{R}_{1.5}$ and $\mathcal{R}_{2.0}$ in top, middle, and bottom, respectively, and vertical lines denote the cutoff frequency of the resonators used in each figure.

For all resonators shown here, regardless of their cutoff frequency, the odd harmonics that are below the cutoff frequency have approximately the same amplitude climbing the semitone scale. Around and above the cutoff frequency the amplitudes of the odd harmonics decreases, and the strong organization disappears as also seen in Figure 3.5, which implies that the complicated input impedance above cutoff frequency has a randomizing effect on the production of odd harmonics. This can be interpreted as the system no longer behaving as a quarter-wave resonator at these frequencies. Additionally, the even harmonics generally grow in amplitude as a function of frequency, and display a marked increase in amplitude for frequencies higher than the cutoff frequency. This implies that below the cutoff frequency, the spectral content of the waveforms produced by resonators with different cutoff frequencies is relatively similar, but that the high frequency spectra, and hence the perceived sound, can be quite different above the cutoff frequency. Specifically, the plots show more energy in even harmonics above the cutoff frequency.

The same 60 resonators are compared in terms of the time averaged intensity at

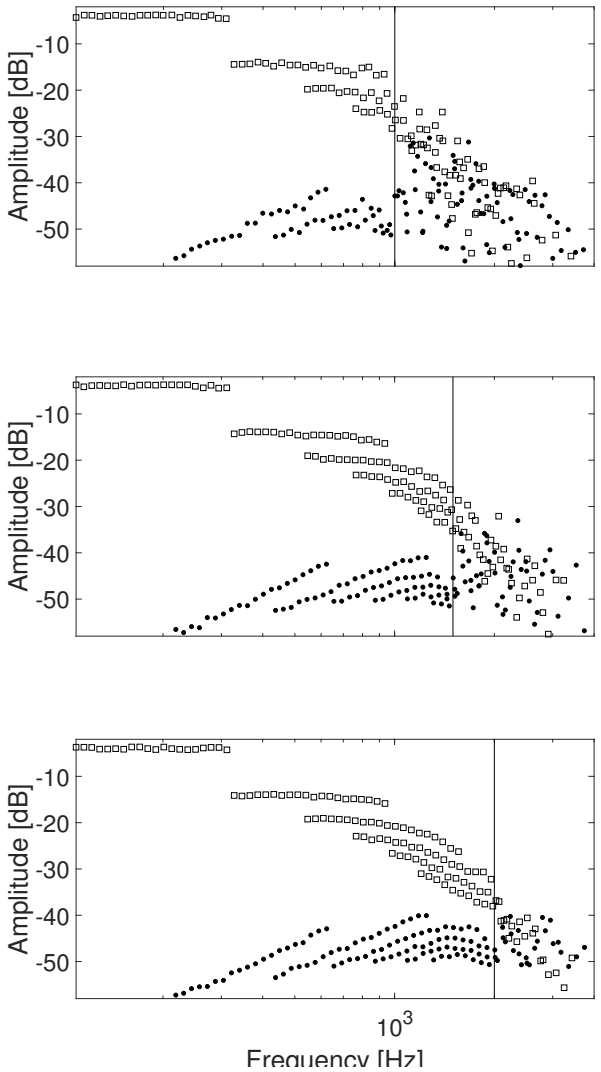

Figure 3.8: Synthesized ($\zeta = 0.45$, $\gamma = 0.55$) spectra of the mouthpiece pressure for resonators $\mathcal{R}_{1.0}, \mathcal{R}_{1.5}$, and $\mathcal{R}_{2.0}$ for 20 fundamental frequencies ranging chromatically from 110 Hz to 330 Hz. Odd and even harmonics denoted by squares and circles, respectively.

input of the resonators and the the time averaged intensity summed over each radiating aperture, shown in Figure 3.9. The time averaged intensity is defined as

$$< I_{\text{in}} > = \frac{1}{2}\text{Re}[P_0 U_0^*], \tag{3.22}$$

$$< I_{\text{rad}} > = \sum_{n=1}^{M} \frac{1}{2}\text{Re}\left[P_n U_n^*\right], \tag{3.23}$$

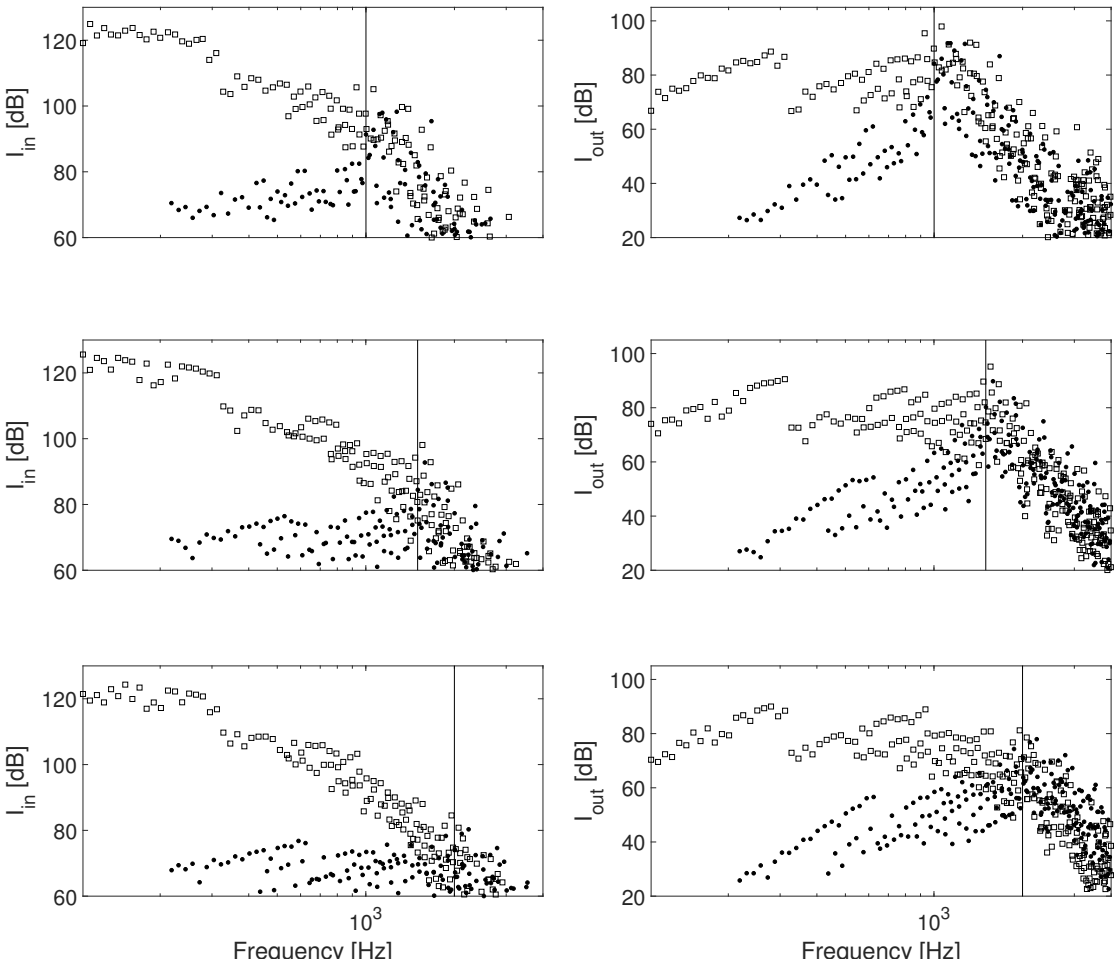

Figure 3.9: Time averaged intensity passing through the entrance of the resonator (left) and the summed over ten toneholes and exit of resonator (right). Resonators and synthesis control parameters are the same as in Figure 3.8. The cutoff frequency for each set of resonators is marked by a vertical line.

where $M = N + 1$ is the number of toneholes N plus the open end of the resonator. This provides a direct comparison between the energy that remains inside the resonator and contributes to the auto-oscillation and the total energy that exits the resonator. A comparison of the left and right panels shows that the time averaged intensity of the fundamental frequency at the input is on the order of 40 dB higher than the output, suggesting that the resonators are inefficient sound sources, regardless of cutoff frequency. Note that the level of the fundamental frequency input intensity is not horizontal as it is for pressure in the mouthpiece. The output intensity of the fundamental frequency increases proportional to ω^2. This is consistent with known monopole radiation efficiency and bolsters the claim that, below the cutoff frequency, the main radiating source can

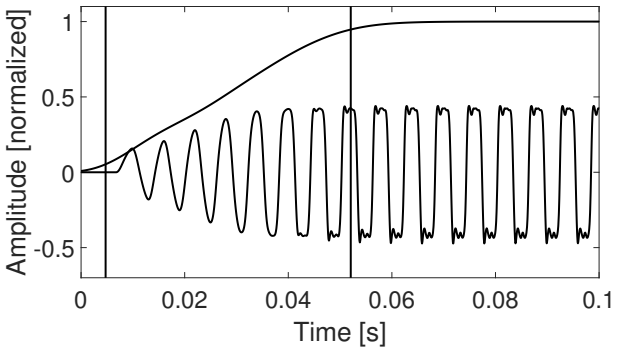

Figure 3.10: Synthesized pressure waveform and sum of time evolving harmonics for resonator $\mathcal{R}_{1.0}$ with 5% and 95% thresholds marked.

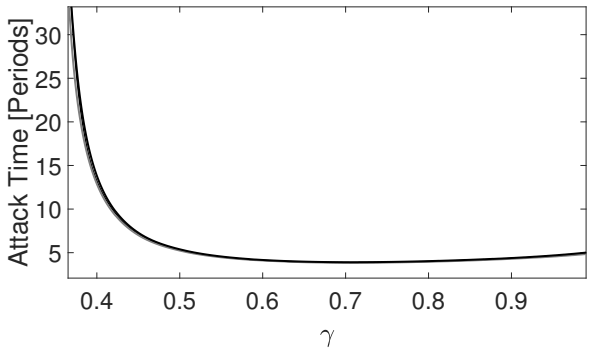

Figure 3.11: Synthesized attack time normalized by period of playing frequency for resonators $\mathcal{R}_{1.0}$, $\mathcal{R}_{1.5}$ and $\mathcal{R}_{2.0}$ with solid black, solid grey, dashed black lines, respectively. Variation in attack times due to cutoff frequency is generally less than 10%.

be treated as a monopole at the location of the first open tonehole. Above the cutoff frequency the time averaged intensity is approximately the same for the input and output. This implies that the resonators are more efficient sources above the cutoff frequency.

It is concluded that the cutoff frequency affects the spectral content of waveforms within the mouthpiece by both demarcating the frequency at which even harmonics develop, as well as shifting the spectral centroid higher for resonators with higher cutoff frequencies.

3.4.2.2 Attack time

To evaluate the influence of the cutoff frequency on the transient portion of the waveform, the time evolution of the waveform as the musician increases the blowing pressure from atmospheric pressure ($\gamma = 0$) to the steady state value of γ is simulated. To avoid discontinuities in the onset pressure, the transition from $\gamma = 0$ to the steady state value follows the curve of the first half of a Hann window. In the current work the duration of

the transition is 201 samples, corresponding to about five milliseconds for a sampling rate of 44100 samples per second. To define the attack time, the time domain pressure signal is decomposed into its constituent harmonics, each of which evolves as a function of time. To include frequencies above the cutoff frequency of all resonators, 16 harmonics are considered. The harmonics are calculated by an inverse Fourier transform on windowed versions of the spectrum around each harmonic. This estimates the instantaneous amplitude and frequency of each harmonic for the duration of the signal, including during the attack transient. The sum of the squared amplitude of these bands is proportional to the total energy in the signal at a given instant, and the energy in the steady state portion of the signal can be determined by choosing this value well into the steady state portion of the signal. The beginning of the attack is determined when the signal first passes a threshold that is a specific, arbitrary fraction of the final value, and the end of the signal attack is defined as the last time that the sum is outside a threshold from the steady state value. Onset threshold values of 5 and 10 percent, and ending threshold values of 90 and 95 percent have been investigated. Figure 3.10 shows a typical pressure waveform onset (in this case for $\mathcal{R}_{1.0}$), with the sum of the first 16 harmonics, normalized to have a maximum value of unity, superimposed. The threshold at 5% and 95% are marked in bold lines. It is found in this work that the attack time is linearly related to the choice of threshold, and therefore any of these four choices (5-90, 5-95, 10-90, 10-95) is reasonable for comparing the attack time of different resonators. Figure 3.11 shows the attack time normalized by the period of the playing frequency as a function of γ with constant $\zeta = 0.45$. Thresholds of 5% and 95% are used to define the onset and saturation of the waveform. The attack time of resonators $\mathcal{R}_{1.0}$, $\mathcal{R}_{1.5}$, and $\mathcal{R}_{2.0}$ are sufficiently similar as to be difficult to discern. The difference between attack times of different resonators is less than 10% of a period for $\gamma > 0.5$, and up to 2.5 periods for $\gamma < 0.5$. However, for low blowing pressures the attack time is of the order of tens of periods, so the difference of 2.5 periods is still a small percentage of the total attack time. It is concluded that the cutoff frequency does not strongly impact the attack time of a given resonator which, in a musical context, may be related to the ease of playing.

3.5 Conclusion

The acoustic resonators developed in this work are adapted for studying the effect of the cutoff frequency on sound production and, potentially, radiation. The simple nature of these resonators, for which it is possible to independently vary the frequencies of both the first impedance peak and the cutoff frequency, is particularly useful because the low frequency behavior (below cutoff) is largely the same for resonators with very different high frequency behavior. The data resulting from either digital sound synthesis or experimental measurements can then be used to directly assess the effect of the cutoff frequency on the sound production and resulting external sound field.

It is found that the cutoff frequency does affect the synthesized waveform within the mouthpiece, particularly the spectral characteristics. Resonators with a higher cutoff frequency have higher playing frequencies, and higher spectral centroids, when compared with resonators with lower cutoff frequencies. Furthermore, even harmonics tend to be excited above the cutoff frequency of a given resonator. However, the differences between

internal waveforms in resonators with different cutoff frequencies is subtle. Furthermore, the cutoff frequency of a resonator is not found to have a significant influence on the attack time, showing that one measure of the "playability" of a clarinet-like instrument relies more on the low frequency response of the resonator. This implies that an instrument maker may be able to make modifications to the geometry of an instrument that results in a different cutoff frequency, without the risk of greatly changing the sound production qualities of the instrument.

In contrast to the relatively small effect of the cutoff frequency on sound production, the cutoff frequency has a larger impact on the high frequency spectral characteristics and radiation. The radiation efficiency, calculated as the ratio of the time averaged intensity at the input of the instrument with that summed over the radiating apertures, is higher above the cutoff frequency than below. Above the cutoff frequency the resonators produce more even harmonics and radiate more efficiently, implying that the cutoff frequency could have a substantial impact on the perceived timbre of different instruments, or different notes on the same instrument. This, along with the small impact on sound production, indicates that the cutoff frequency may be used to change the timbre characteristics of an instrument without altering its sound production qualities.

Future work includes extending the synthesis analysis to the external sound field to evaluate the effect of the cutoff frequency on radiated sound, for which Figure 3.9 provides an initial answer. This includes directivity of the source due to multiple radiating apertures. A characterization of the external sound field can then be compared with the internal sound field to evaluate the competition between sound production and radiation of clarinet-like musical instruments.

Appendix

Two resonators were realized to experimentally verify the feasibility of designing resonators with independently chosen first input impedance peaks and cutoff frequencies. The resonators were made by drilling holes in polyamide 6 tubes, the dimensions of which are summarized in Table 3.1. The input impedance was then measured using the impedance measurement device developed at CTTM in hemi-anechoic conditions [91]. Table 3.2 summarizes the first two impedance peak frequencies of resonators $\mathcal{R}_{1.0}$, $\mathcal{R}_{1.5}$, and $\mathcal{R}_{2.0}$ used for the digital synthesis. The inharmonicity, in cents, is defined as

$$\text{inharmonicity} = 1200\log_2\left(\frac{f_2}{3f_1}\right). \tag{3.24}$$

Table 3.1: Dimensions for two prototype resonators with the first impedance peak f_1 at 170 Hz and cutoff frequencies f_c at 1000 Hz and 2000 Hz. Simulated and measured input impedance are provided in Figure 3.4.

Resonator	L [mm]	a [mm]	ℓ [mm]	b [mm]	h [mm]
$\mathcal{R}_{1.0}$	436.7	7.0	32.8	4.0	8.4
$\mathcal{R}_{2.0}$	470.1	7.0	8.9	4.0	8.4

Table 3.2: Frequencies of the first two impedance peaks and inharmonicity of resonators $\mathcal{R}_{1.0}$, $\mathcal{R}_{1.5}$, and $\mathcal{R}_{2.0}$.

Resonator	f_c [Hz]	f_1 [Hz]	f_2 [Hz]	inharm [cents]
$\mathcal{R}_{1.0}$	1000	170	511.6	5.4
$\mathcal{R}_{1.5}$	1500	170	513.0	10.2
$\mathcal{R}_{2.0}$	2000	170	513.1	10.5

Chapter 4

The link between the tonehole lattice cutoff frequency and clarinet sound radiation: a quantitative study

PREFACE

Chapter 3 demonstrates the effect of the cutoff frequency on sound production of clarinet-like instruments. However, the main results are demonstrated for internal variables, and radiation is considered only in terms of time averaged intensity of the radiating toneholes. This limits the scope of the study to conclusions about how the cutoff frequency does or does not impact the sound production and internal spectral characteristics, while ignoring the equally important aspect of how the cutoff impacts external, and therefore perceived, characteristics of a clarinet-like instrument. The connection between the internal variables and their external counterparts is an important continuation and complement to the results in the previous chapter.

The effect of the cutoff frequency on the relationship between internal and external variables can be assessed under two, not obviously related conditions: one where the resonator is excited by a forcing source, such as a loudspeaker, that is not dependent on the resonator feedback to maintain oscillation, and 'playing' conditions where a reed is in a state of auto-oscillation due to the feedback from the resonator[1]. Both methods come with a host of potential difficulties. Additionally, the choice of method emphasizes different aspects of the link between internal and external variables, so the desired results should be well defined in order to choose the proper methodology.

The first option could be implemented using a flow source such as a compression chamber and measuring or simulating the transfer function between the pressure or flow inside the resonator and the radiated pressure at external points in the room [15]. This method provides considerable information about the resonator as a radiating sound source. One advantage is that the transfer functions can be easily determined across a broad range of frequencies, not only the playing frequency (and its harmonics) present during playing conditions. The full band response (not just sampled by harmonics) provides a much more detailed description of the resonators behavior. In particular, it resolves the peak spacing above cutoff that are due to resonances that are proportional to the total length of the resonator, including the lattice. Another advantage of this method is that a low

[1] The first case naively treats the loudspeaker as an ideal source and hybrid methods exist [105].

internal sound pressure level can be maintained, eliminating concerns about the introduction of nonlinear phenomena provided the use of suitable post-processing methods. This makes it easier to interpret the results, particularly when compared with linear models of the transfer functions. The main disadvantage of using an independent source to excite the resonator is that it is hard to interpret the results in terms of a musically realistic situation, for which a clarinet is almost always played with a reed. A secondary disadvantage is that additional components must be manufactured to connect a compression chamber to the resonator, and ideally the measurements would be made in an anechoic environment which can prolong the experiment.

The external response of the resonator under playing conditions could be studied using an artificial blowing machine, human musician, or through simulation by coupling a synthesis model and radiation model [16, 106]. The advantage of this approach is that the instrument is operating under conditions for how woodwinds are usually heard: played with a mouthpiece and reed. Therefore, the results obtained through this method may be more easily related to musically relevant characteristics, such as timbre. However, measurements under playing conditions can be hard to interpret because there are many more variables to consider compared with a passive response measurement. One major limitation is that the reed and resonator are coupled during playing conditions, which can make it complicated to isolate the effect of the cutoff frequency from properties (such as natural resonance frequency) of the reed. Furthermore, the sound pressure levels inside the resonator can be very high during loud notes, which could introduce nonlinear effects at the toneholes that are not captured by a simple radiation model [107]. The excitation source also matters: an artificial mouth is convenient for reproducibility, but may not 'play' the instrument in a musically informed manner, which diminishes the value of this method. A live musician may play the resonator more musically, but not necessarily reproducibly. The external environment must also be accounted for: an anechoic chamber is not likely a good decision due to the strong directivity of the resonators, while the laboratory spaces that often house artificial blowing machines may be problematic due to small volumes and ventilation noise. A good option for measurements of a musician playing *in situ* may well be a musically appropriate room such as a small recital or lecture hall [55].

As detailed above, both of these options can provide insight into the effect of the cutoff on the radiated soundfield. The types of conclusions that can be made in both cases depends on the method of study. Generally, the first option examines how the complicated internal soundfield transmits to the exterior soundfield, while clearly demonstrating the high frequency modes in the lattice. The second method hides much of the complicated internal behavior, and instead demonstrates how the cutoff can be viewed as a filter between an internal complex harmonic signal and the exterior waveform. The two are directly related, but can be more or less easily seen in the data depending on the chosen method.

Therefore, the work in the preceding chapter, which focuses on digitally synthesized signals under playing conditions, is better complemented by a study of the instrument under playing conditions rather than a passive response measurement. One way to extend the previous work would be to perform measurements internal to the resonator using an artificial blowing machine and comparing it with the simulated waveforms. This is of

limited scope, however, because an accompanying external soundfield measurement using the artificial blowing machine is complicated due to the room acoustics of a laboratory space and, more importantly, is very sensitive to microphone location due to the directivity of the resonators. Instead, the effect of the cutoff on sound radiation is evaluated *in situ* under playing conditions by a live musician in a musically appropriate, medium sized lecture hall, and supported by simulation [55, 4, 5]. This choice of methodology, excitement mechanism, and environment allows confidence that the results correspond to a musically meaningful characterization of the cutoff frequency on sound radiation. The results obtained through this type of study are likely applicable to other woodwind instruments and may also apply to groups of woodwinds, such as in an orchestra.

Additional comments

This remainder of this chapter is a reproduction the article:

Petersen, Erik Alan, Colinot, Tom, Guillemain, Philippe, and Kergomard, Jean. The link between the tonehole lattice cutoff frequency and clarinet sound radiation: a quantitative study. *Acta Acust.*, 4(5):18, 2020

Comments:

- Original abstract has been omitted.
- The term tonehole lattice cutoff frequency varies between chapters due to evolving requirements of the research. Because this chapter treats only the case of academic resonators, ambiguities regarding the cutoff of real instruments are ignored. The cutoff is defined by acoustic regularity of an infinite, loss-less lattice (Chapter 2 Eq. (2.29), and Chapter 3 Eq. (3.3)) and assumed to be valid for the finite, lossy lattices used in the current chapter. For a more complete discussion of cutoff definitions, see Chapter 5.

4.1 Introduction

Woodwind instruments are complex objects with geometries that have evolved through empirical experimentation over centuries. The resonator bore can be predominantly cylindrical or conical, and many instruments terminate in a bell that has yet another cross section profile. The position and size of the toneholes are chosen to balance intonation and timbre, and each hole affects the influence of the others. While these geometrical variations are often subtle, they may have a strong influence on the sound of an instrument.

The playing frequency of a woodwind instrument is largely determined by the distance between the reed and the first open tonehole, and to a first approximation the downstream toneholes are ignored. However, in many instruments this 'unused' lattice of toneholes acts as an acoustic high pass filter, thereby modifying the response of the resonator and, eventually, the radiated sound [3]. The low frequency first hole approximation and the high frequency lattice filtering are separated by the tonehole lattice cutoff frequency f_c, and is due to the pass and stop bands of waves propagation in periodic media [2, p. vii-viii]. The existence of a cutoff frequency is a communality among many different woodwinds including the clarinet, saxophone, bassoon, and tárogató [3]. Some instruments, such as the Kaval [108], even have additional toneholes that are never closed during normal playing, which may have been introduced to serve as a lattice for the lowest notes of the instrument.

The cutoff frequency is generally assumed to influence the sound that an instrument makes, possibly even mapping to certain adjectives used by musicians to describe the 'character' of a given instrument. However, there are few quantitative links between the cutoff and radiated sound [24, 60]. In his final article [5], Benade published a study connecting room-averaged external spectra across the first register of the saxophone, demonstrating a frequency band with increased radiation centered at what he calls the 'break frequency.' For the saxophone, he asserts that the break frequency in the spectra of the radiated sound is related to the tonehole lattice cutoff. This interpretation is complicated, however, because there is no rigorous definition of the cutoff frequency of a real instrument. Furthermore, a recent article demonstrates that, in contrast to the clarinet, the cutoff frequency of the saxophone varies considerably over the range of the first register [6].

Attempts to study the tonehole lattice cutoff of real instruments generally fall either into empirical or analytic methods, both of which have flaws. One empirical approach is to define the cutoff frequency from an input impedance measurement by identifying a perturbation in the modulus or argument of the input impedance or reflection coefficient. This is often done by human judgment, although it is also possible to apply arbitrary thresholds, and both methods have merits and drawbacks. Analytic approaches can be adapted from the theory of wave propagation in periodic media [1], although the finite and nature of the resonators complicates the analogy. Furthermore, the lattices of real instruments are not typically periodic, so it is necessary to extend the theory in one of several ways by considering, for example, pairs of adjacent toneholes [16]. One form of analysis may be more appropriate than another for a specific family of instruments. An instrument with a high degree of acoustical regularity, such as the

clarinet [22], seems more suitable for the analytic approach than an instrument that is highly irregular, such as the bassoon. Furthermore, some instruments have cutoffs that evolve in conjunction with the changing notes of a chromatic scale, such as the saxophone. In this case an empirical approach may be more appropriate because the lattice is less periodic (geometrically and acoustically) than a clarinet.

In order to avoid the inherent ambiguity surrounding the cutoff frequency of real instruments, the current work starts with simplified resonators that have been analytically designed with constant chosen cutoffs. This has the advantage that external spectral characteristics are expected to be directly linked to the cutoff frequency of the resonators. However, because the cutoffs of the resonators used in these experiments are strong and unambiguous, care must be taken when extrapolating to real instruments, which may have ambiguous or diffuse cutoffs as well as other competing behavior due to the conicity, the bell, and additional geometric differences. Because it is difficult to design and impractical to construct conical resonators with strong cutoffs, the simplified resonators used in this study are cylindrical, and the results are mainly applicable to instruments in the clarinet family.

The basic theory of tonehole lattice cutoff frequencies is reviewed in Section 4.2, and applied towards the design of simplified resonators with known cutoffs. Experimental results of external sound field measurements using the simplified resonators are discussed in Section 4.3, with complementary simulations in Section 4.4. Application to a clarinet recorded in anechoic conditions is treated in Section 4.5, followed by concluding remarks in Section 5.4.

4.2 Basic theory

4.2.1 The tonehole lattice cutoff frequency

The cutoff frequency is determined by the geometry of a constituent cell of the lattice, depending on the radius of the main bore, the tonehole radius, chimney height, and inter-hole spacing, shown in Figure 4.1. The geometry of a lattice can be designed to have a desired cutoff frequency [22, 23, 29]. While a true cutoff exists only for infinite, lossless lattices [2, p. vii-viii], a strong cutoff behavior can exist for finite resonators with at least two or three open toneholes. Furthermore, the theory is developed for geometrically regular lattices consisting of repeating, identical cells, which is in contrast with the geometric irregularity of real instruments. However, it has been shown that an acoustic regularity may be achieved even for geometrically irregular lattices with no adverse impact of the cutoff of the lattice, which reinforces the application of cutoff theory to real instruments.[2] It is convenient, though not necessary, to design the acoustically regular lattice to also be geometrically regular. In this case, the cutoff frequency of the lattice is achieved if the constituent cell is designed according to

$$f_c = \frac{c}{2\pi}\sqrt{\frac{s}{2\ell h S}}, \tag{4.1}$$

[2] A geometrically regular lattice has geometrically identical cells to form a periodic structure. An acoustically regular lattice is formed by cells that all have the same acoustical response, but that are not necessarily geometrically identical. Geometric regularity is a subset of acoustic regularity.

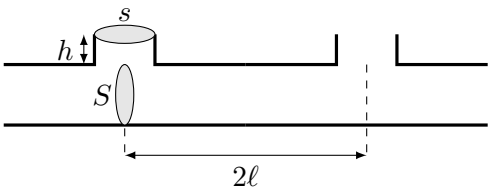

Figure 4.1: Geometrical dimensions of a tonehole pair. When repeated, this element forms a regular lattice with a cutoff frequency provided by Eq. (4.1).

where c is the speed of sound in air, $s = \pi b^2$ is the cross section of the tonehole, $S = \pi a^2$ that of the main bore, h the height of the hole, and 2ℓ the distance between two subsequent holes. Equation (4.1) corresponds to the eigenfrequency of the cell assuming rigid conditions at the extremities of the main bore [23, 383]. Variations of this formula can be derived for more complicated geometries, including conical resonators [6].

For the purposes of this study, a lattice with at least five open toneholes designed following Eq. (4.1) is considered to have a tonehole lattice cutoff, even though the theory is derived under the assumption of an infinite, lossless lattice. The resonators presented in Section 4.2.2 and analyzed in Sections 4.3 and 4.4 follow this definition and are said to have a strong cutoff, which can be clearly identified to reasonable precision on measurable characteristics such as the input impedance or reflection coefficient. Real instruments, however, do not generally respect Eq. (4.1), and may only exhibit a weak or diffuse cutoff whose precise determination is not obvious from measurement or theory, but still recognizable as an effect of the lattice.

4.2.2 Resonators designed to have cutoffs at chosen frequencies

Four resonators are designed and produced for this study. The resonators are built using stiff, cylindrical plastic tubing, three of which are pierced with toneholes, resembling the geometry of a clarinet. The fourth resonator is a simple cylinder without toneholes. A clarinet mouthpiece can be inserted at the upstream end of the resonators. As for a real instrument, the portion of the duct upstream from the lattice determines the playing frequency of the highest note, and the lattice toneholes can be consecutively closed to achieve lower notes. In contrast with a real clarinet, the size and location of the toneholes are not designed to produce the notes of a specific musical scale, but rather to present an acoustically periodic lattice that alters the high frequency response of the resonator.

All four resonators are designed to have the first impedance peak at approximately 185 Hz when all toneholes are open, and the three resonators with tonehole lattices have cutoffs at 1.0, 1.5, and 2.0 kHz [29]. Each resonator, except the simple cylinder, has 10 toneholes. The input impedance and geometries of the resonators are shown in Figure 4.2 and Table 4.1, respectively. The cutoff is evident for the three resonators with lattices, seen as a change in spacing and height of the impedance peaks. The regularly spaced peaks characteristic of a quarter wavelength resonator are seen for the simple cylinder.

In order to maintain a strong cutoff for different fingerings, at least five consecutive, downstream toneholes remain open for all measurements. This results in six possible notes per resonator with fundamentals ranging from 114 Hz to 154 Hz under playing

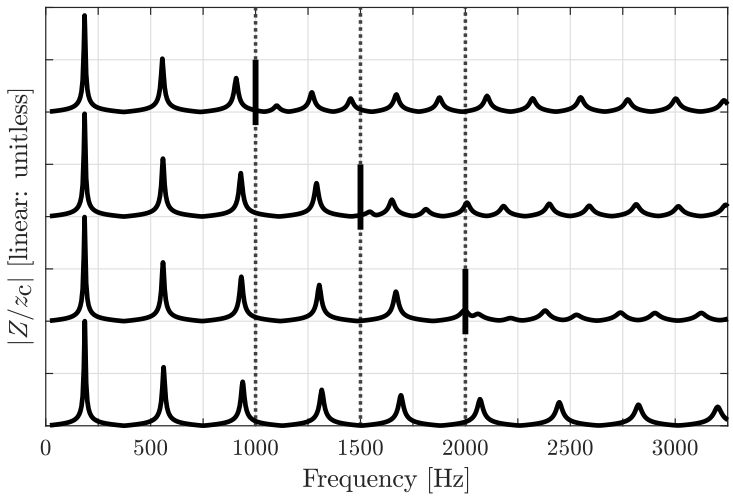

Figure 4.2: Simulated input impedance modulus for (top to bottom) resonators with $f_c = 1.0$, 1.5, 2.0 kHz, and a cylinder with no tonehole lattice, vertical offset for clarity. Normalized by characteristic impedance z_c of the duct.

Table 4.1: Geometrical dimensions of three resonators with the same first impedance peak f_1 and different cutoff frequencies f_c. First peak and cutoff frequencies in Hz, all other quantities in mm. The first hole is located at $L + \ell$. Consider $\ell = 0$ for the cylinder.

$\mathcal{R}$	f_1	f_c	L	h	a	b	ℓ
$\mathcal{R}_{1.0}$	185	1000	398.8	9.8	6.5	2.5	16.3
$\mathcal{R}_{1.5}$	185	1500	417.0	9.8	6.5	4.0	16.3
$\mathcal{R}_{2.0}$	185	2000	426.0	9.8	6.5	5.8	16.3
$\mathcal{R}_{\text{cyl}}$	185	—	450.0	—	6.5	—	0.0

conditions. Because the lattices are acoustically regular, each of these six notes has a nearly identical cutoff.

4.2.3 Radiation characteristics above and below the tonehole lattice cutoff frequency

The radiation of a resonator with a tonehole lattice has significant differences for frequencies below and above the cutoff. Below the cutoff, the wave does not propagate into the lattice, so the resonator predominantly radiates as a monopole source from the first open tonehole. Above the cutoff, the wave does propagate into the lattice and radiates from subsequent toneholes and the termination of the resonator. The wave also reflects back into the resonator from the termination of the lattice [17, 23]. Above the cutoff, the contributions from multiple radiating apertures create complicated radiation properties, which can affect the directivity and efficiency of the resonator.

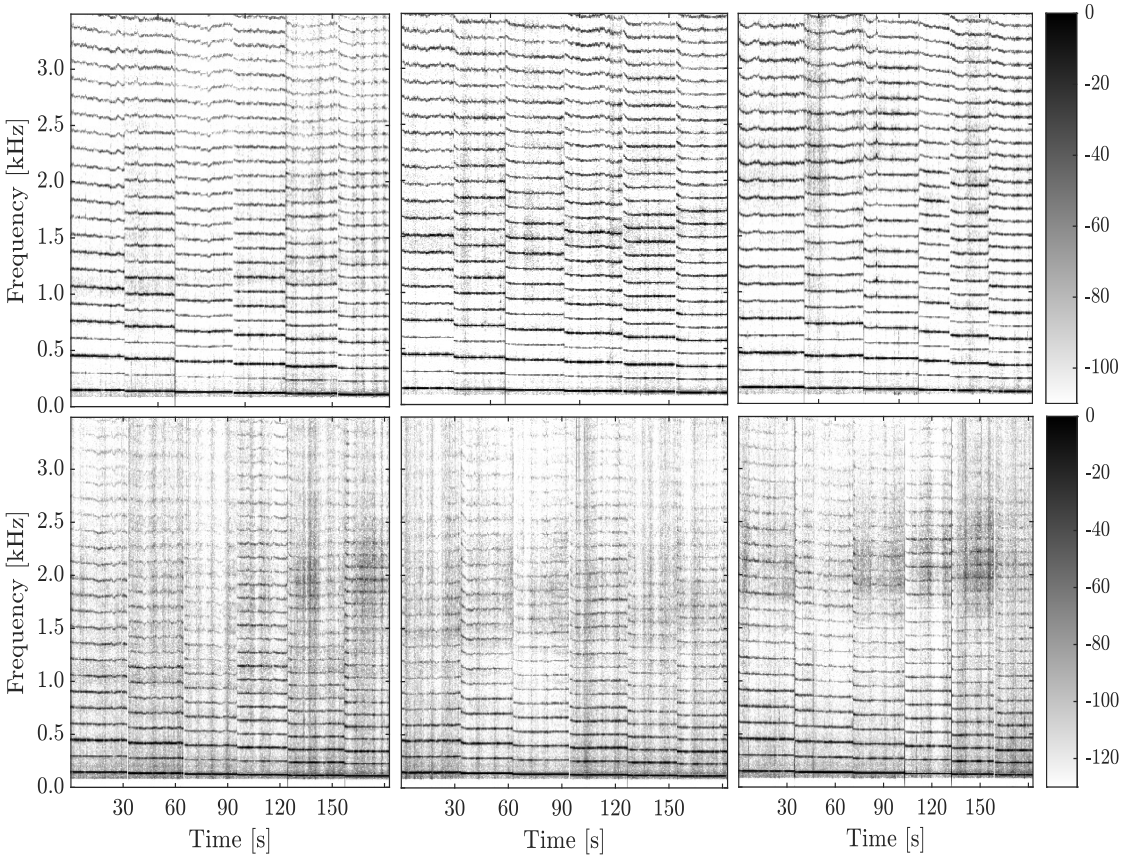

Figure 4.3: Spectrograms of six notes played in a descending scale using a clarinet mouthpiece. Top panels at *forte* and bottom panels at *piano* playing levels for resonators with, from left to right, f_c = 1.0, 1.5, 2.0 kHz. The analysis is performed on composite signals from the Neumann U87 and two Neumann KM 184. Color map in decibels.

At the cutoff, the phase speed within the resonator is very high and the flow through the toneholes is nearly in phase, creating a strong directivity lobe perpendicular to the lattice. Above the cutoff, the flow through the toneholes is no longer in phase and the radiation is characterized by complicated directivity lobes. Frequencies well above cutoff propagate in the lattice and only weakly radiate from the toneholes, mainly reflecting and radiating from the termination of the resonator. For the simplified resonators, the cutoff frequency is at a rapid transition between these two frequency band behaviors, while the distinction is more complicated for real instruments for which the inter-hole spacing is not uniform and the different tonehole radii influence the radiation efficiency of each source.

4.3 External sound field measurements of simplified resonators

4.3.1 Basis for measurement protocol

The methodology follows the protocol developed by Benade to measure the radiated sound fields of woodwind instruments, notably for the clarinet and saxophone [4, 5]. In contrast with most acoustical measurement requirements, Benade realized that it is informative to measure the spectral radiation characteristics of instruments in musically appropriate environments. The defining sound features of an instrument family are easily identified by experienced listeners regardless of the room in which they are played. Benade concludes that the spectral characteristics that are relevant to human perception could also be measured in 'normal' rooms, i.e. not under anechoic conditions, and that the results describe the instrument under the same conditions for which an audience typically consumes music. To avoid complications due to the strong directivity of many instruments, the instrument and microphone should be placed far apart, and both should be slowly moving to introduce a type of 'room averaging.' The protocol and its implications are detailed in several documents [56, 55].

4.3.2 Details of measurements

The simplified resonators are outfitted with a clarinet mouthpiece and a Plasticover (RICO-RP05BCL200) strength 2 B♭ clarinet reed in order to be played by a musician. The room is a medium sized lecture hall with 122 seats on a steep incline and an approximate volume of 730 cubic meters. This room is chosen because it has light acoustic treatment and is a reasonable example of a musically appropriate environment. This is desirable because the purpose of the study is to identify global spectral characteristics of the resonators in realistic playing conditions.

Each of the six notes with fundamentals ranging from 114 to 154 is played for approximately 20 s for both *forte* and *piano* dynamics, subjectively determined by the musician. In order to avoid inconsistencies due to strong directivity lobes of the resonator, the musician slowly sways the instrument back and forth with a period of about four seconds. Four microphones are used to record the signal in the room: a DPA-4099 instrument microphone attached to the resonator approximately 8 cm above the center of the lattice, two stationary Neumann KM 184 (cardioid) microphones at a distance 8 m and 12 m from the musician, and a Neumann U87 (cardioid operating mode) at a distance of approximately 4 m. The U87 is manually waved back and forth with an approximate period of four seconds to provide some spatial averaging in the room. Therefore, there are 152 distinct signals: 3 resonators with 6 notes each, plus the simple cylinder, each with two dynamics, measured by four microphones. The data from the DPA is not used in the analysis because, due to its position just above the lattice and in a directivity lobe at cutoff, its data suggest a greater effect than what is measured by the more distant microphones.

Preliminary results are shown as spectrograms in Figure 4.3. Resonators with $f_c = 1.0, 1.5$, and 2.0 kHz are displayed from left to right, with *forte* playing levels on top and *piano* playing levels on bottom. The measurements from the Neumann U87 and two Neumann KM 184 are combined into a composite signal. The steady state portions

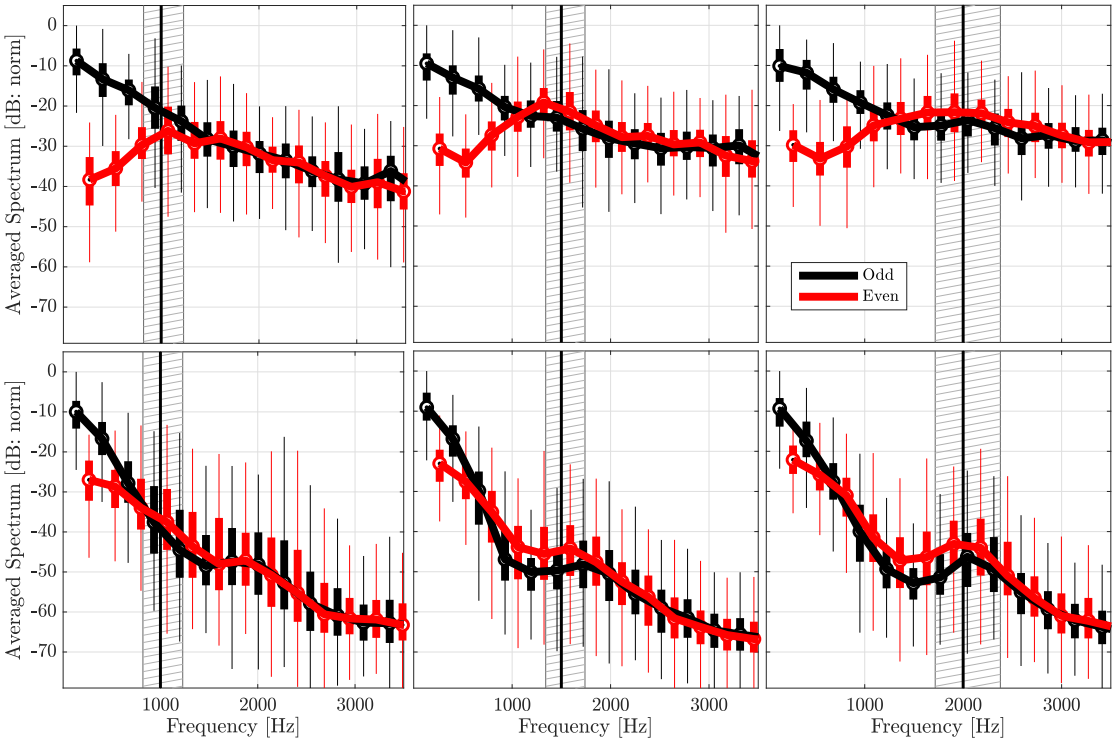

Figure 4.4: Measured external spectra, averaged over six notes played on each of three resonators with different cutoff frequencies. Top panels depict *forte* dynamics and bottom panels depict *piano* dynamics. Each box plot is computed from the n^{th} rank harmonic to present an averaged spectra that is characteristic to the resonator across different fingerings with fundamentals ranging from 114-154 Hz, and is positioned at the average frequency of the respective n^{th} rank harmonic. Data from manually waved microphone (Neumann U87 4 m distance). Black: odd harmonics, red: even harmonics, vertical line: cutoff frequency of the resonator. Box plots within hatched area have atleast one harmonic near cutoff. Solid black and red lines trace the median of each box plot. The median amplitude of the fundamentals are normalized to 0 dB in each panel. Boxes span from 25^{th}-75^{th} percentiles and thin lines show the span of the data ignoring outliers.

of each note are extracted from each microphone channel, highpass filtered at 100 Hz by the MATLAB highpass function, which uses a minimum-order filter with a Kaiser window resulting in a 60 dB stop band attenuation. The signals are then normalized by their root-mean-square value [3]. The power spectral density is calculated for successive Hann-windowed segments of 2^{13} samples using a 50 % overlap. The resulting spectra from the three microphones are summed, normalized by the maximum value at each time step, and plotted in decibel representation.

These spectrograms demonstrate room averaged characteristics of the sound field

[3] These signals will available online when the article is published.

radiated by individual notes of each resonator. The average spectral centroid for the resonators with $f_c = 1.0, 1.5$, and 2.0 kHz cutoffs is 0.55, 0.94, 1.12 kHz at *forte* playing levels, and 0.28, 0.22, 0.27 kHz at *piano* playing levels. This may be due to the appearance of additional energy around the cutoff of each resonator. This possible reinforced frequency region, particularly in this representation, may be partially hidden by the imparity between even and odd harmonics characteristic to cylindrical resonators. Nonetheless, these spectrograms are suggestive of an influence of the cutoff on radiation, although additional processing is needed to determine a quantitative link.

The data presented in Section 4.3.4 correspond to these three resonators. However, in deference to the measurement protocol proposed by Benade, only the Neumann U87 data is included in the following analysis.

4.3.3 Data processing

The same signal treatment is used for three different experiments in this study: *in situ* measurements of simplified resonators described in Section 4.3.2, the simulated replication of these measurements in Section 4.4, and anechoic recordings of a real clarinet in Section 4.5. Some preliminary steps are necessary for the simulations and anechoic recordings to reduce multiple channels of data into a single channel. These additional procedures are outlined in Sections 4.4.3 and 4.5. Once reduced, all the data are processed as follows.

The data of a given resonator consists of separate audio files, one for each note that is considered in the analysis. For each note, the signal is truncated to include only the steady-state portion of the tone to discard attack and decay transients. Furthermore, each signal has considerable variation in sound pressure level and timbre due to the directivity of the resonator, movement of the player, movement of the measurement microphone, and fluctuating control parameters. Therefore, the signal is analyzed in 0.5 s segments and treated with a Hann window of the same duration. The spectra is generated using the built-in MATLAB FFT, and handled to be proportional to units [Pa^2/Hz]. The harmonics in the spectra are then extracted using a peak detection scheme. Because the quantity of interest is the spectral envelope, an exact calibration is not necessary and results are depicted in normalized representations. This procedure is repeated for the remaining notes for the resonator.

The basic data set for each resonator is now the harmonic frequency and amplitude pairs at 0.5 s intervals for multiple fingerings. To demonstrate the global radiation characteristics of the resonator it is helpful to average the data. Several different approaches are used and described in the corresponding sections.

4.3.3.1 Measurement averaging

The signal from the Neumann U87 microphone used in Figure 4.4 is first treated following the protocol described in Section 4.3.3. This results in approximately 240 'instances' of the spectrum per resonator, calculated from six fingerings, each with 20 seconds of data divided into time frames of 0.5 s. In order to visualize the data, the statistical variation of each harmonic is depicted using box plots. Each box corresponds to the n^{th} rank harmonic from all the fingerings, excluding outliers. For example, the left-most black box in each

panel depicts the amplitude variation of the fundamental for all six fingerings, while the left-most red box depicts the first even harmonics of all six fingerings. The boxes are positioned at the average frequency of the n^{th} rank harmonic of the six fingerings. The lower and upper limits of the boxes mark the 25^{th} and 75^{th} percentiles. The median value of the odd and even harmonics are traced in black and red, respectively. Because this plot represents data with a large variation in amplitude, the upper contour of the whiskers tend to match a naive inspection of the raw data.

4.3.4 The reinforced spectrum region of the radiated sound field

The external spectra for all three resonator cutoff frequencies for both *forte* (top) and *piano* (bottom) dynamics are depicted in Figure 4.4. Below the cutoff of each resonator, the even harmonics are several decades weaker than the odd harmonics, as is expected of a quarter wave resonator. However, for the *forte* playing dynamic, the envelope of the even harmonics increases with frequency towards a maximum value near the cutoff of the resonator, above which the even and odd harmonics are equally strong. Although it is less obvious in this representation of the data, odd harmonics are also reinforced, seen here mainly by the envelope of the box plot whiskers. Figure 4.5, which uses the averaging scheme described in Section 4.4.4, shows more clearly that the reinforced spectrum region consists of both even and odd harmonics.

The lower panels of Figure 4.4 show that the effect of the cutoff is not as pronounced for *piano* playing dynamics, although the cutoff of the resonator does influence the shape of the spectral envelope. The slope of the envelope is much steeper than for the *forte* data because a softly played note is generally not as harmonically rich as one that is played loudly, and most of the energy is contained in the first several harmonics. Therefore, the reinforced spectrum region is weaker because it falls in a frequency range that does not have a lot of power in the internal waveform.

Repeating the same measurements with a simple cylinder (not depicted for brevity) demonstrates that the reed resonance f_r (see Section 4.4.2) may be a competing mechanism that can influence the spectral envelope. In particular, there is a convergence of even and odd harmonics at approximately 1.5 kHz, despite no tonehole lattice. Additional simulations suggest that this convergence is due to the reed resonance. This could be developed as a simple experimental method for coarsely estimating the resonance of a reed. For real clarinets, the cutoff and reed resonance occur at approximately the same frequency $f_c \approx f_r \approx 1.5$ kHz [109]. It is unclear how these parameters evolved towards the same value, and to what degree this is intentional. A future project could address how each parameter impacts the playability of an instrument.

4.4 External sound field simulations of simplified resonators

The external sound field of simplified resonators played with a clarinet mouthpiece measured in Section 4.3 is simulated by combining digital synthesis and a simplified radiation model. The external sound field simulations are implemented in two main stages. The first computes the characteristics of the passive, linear resonators, yielding the input impedance and transfer functions between the input of the resonator and each tonehole.

The input impedance is then used with a digital synthesis code to simulate the pressure and flow waveforms inside the mouthpiece. The transfer functions calculated in the first stage translate the flow waveform inside the mouthpiece to the corresponding flow through each tonehole, which radiate into the surrounding space.

4.4.1 From TMMI to external sound field simulations of passive resonator

The resonators are modeled as passive, linear waveguides that can be characterized independent of the source signal. As a first approximation, nonlinear effects due to high internal sound pressure levels as well as nonlinear effects in the toneholes are ignored. Although the simulation model ignores the nonlinear effects in the toneholes, the qualitative agreement between simulation and experiment is satisfactory. While accounting for these nonlinear aspects would likely improve the simulations, particularly at *forte* playing levels, it is outside the scope of this article to develop the nonlinear tonehole model, which is an open research topic.

First, the input impedance of the resonators is simulated using the Transfer Matrix with External Interactions (TMMI) [28], which is related to the transfer matrix method but accounts for external interactions of toneholes that radiate into the same space. Accounting for mutual radiation impedance improves the simulation of the input impedance, particularly above the cutoff.

In order to simulate the radiated sound field, the TMMI algorithm has been modified to compute the frequency domain pressure $P_n(\omega)$ and flow $U_n(\omega)$ at the n^{th} aperture (tonehole and termination of the resonator) resulting from an arbitrary source pressure $P^s(\omega)$ or flow $U^s(\omega)$ at the input. Therefore, the passive response of the resonator can be described by a set of transfer functions between the input of the resonator and all radiating apertures

$$H_n(\omega) = U_n(\omega)/U^s(\omega). \tag{4.2}$$

The far field external pressure at an observation point O is the superposition of the contribution of each source term $U_n(\omega)$

$$P_O(\omega) = \sum_{n=1}^{N} j\omega\rho \frac{H_n(\omega)U^s(\omega)}{4\pi r_n} e^{j(\omega t - kr_n)}, \tag{4.3}$$

where r_n is the distance between O and the n^{th} source, ω is the angular frequency, k the wave number, c and ρ the speed of sound and density of air. Each source term is treated as a monopole and diffraction due to the resonator is ignored. This development can be used to simulate the radiation properties of the resonators regardless of the driving source.

4.4.2 Digital sound synthesis

Digital synthesis is used to simulate the pressure and flow inside the mouthpiece in the discrete time domain. In this simulation, the action of the musician is represented by

Table 4.2: Digital sound synthesis parameters pertaining to reed dynamics. All unitless except f_r, in Hz.

Notation	f_r	q_r	K_c	β	η
Value	1500	0.4	100	5E-4	0.01

two dimensionless control parameters [77], defined by

$$\gamma = \frac{p_m}{p_M} \quad , \quad \zeta = wHz_c\sqrt{\frac{2}{\rho p_M}}, \tag{4.4}$$

where p_m is the pressure inside the mouth of the musician, p_M is the reference pressure necessary to close the reed channel completely, w and H are the width and height of the reed channel at rest, and z_c is the characteristic impedance of the resonator. The variables of the model discussed in this work are the reed displacement x and the acoustic pressure p^s and flow u^s at the input of the resonator, given in dimensionless form by

$$x = \frac{\hat{x}}{H} \quad , \quad p^s = \frac{\hat{p^s}}{p_M} \quad , \quad u^s = z_c\frac{\hat{u^s}}{p_M}, \tag{4.5}$$

where the hat notation signals the variable's physical value. The time-domain synthesis scheme follows previous work [93].

In order to accurately represent the high frequency behavior of the resonator, a reflection function formalism [94] is preferred over a truncated modal representation. The reflection function r links the reflected wave $p^- = (p^s - u^s)/2$ to the outgoing wave $p^+ = (p^s + u^s)/2$ through the relation

$$p^- = r * p^+, \tag{4.6}$$

where $*$ denotes the convolution product. Note that r is deduced from the input impedance as the inverse Fourier transform of the reflection coefficient. In the discrete form, it is truncated to the first 0.1 s, long enough to accurately represent low frequencies which have the longest response due to weak losses.

The reed is modeled by a damped single degree-of-freedom oscillator. Its dimensionless displacement from equilibrium follows the form

$$\frac{1}{(2\pi f_r)^2}\ddot{x} + \frac{q_r}{2\pi f_r}\dot{x} + x = p - \gamma + F_c(x), \tag{4.7}$$

where f_r is the reed eigenfrequency and q_r its damping coefficient. The force F_c, accounting for the contact with the mouthpiece lay [98], is defined by

$$F_c(x) = K_c\left(\frac{x + 1 - |x + 1|}{2}\right)^2(1 + \beta\dot{x}), \tag{4.8}$$

with nonlinear stiffness K_c and a damping coefficient β. The nonlinear characteristic

Table 4.3: Dimensionless control parameters used for digital synthesis following Eqs. (4.10) and (4.11).

dynamic	γ_c	γ_a	ζ_c	ζ_a
forte	0.70	0.05	0.40	0.05
piano	0.50	0.05	0.40	0.05

derived from Bernoulli's law that determines the flow through the reed channel is

$$u^s = \zeta \left(\frac{x + 1 + |x + 1|}{2} \right) \text{sign}(\gamma - p^s) \sqrt{|\gamma - p^s|}. \tag{4.9}$$

The nonsmooth functions in Eqs. (4.8) and (4.9) are regularized: the absolute values $|\cdot|$ are replaced by $\sqrt{\cdot^2 + \eta}$ [110]. The value of the parameters used to obtain the simulation are summarized in Table 4.2.

The control parameters, corresponding to pressure inside the mouth γ and musicians lips ζ, are slowly varied to approximate a real musician. A simultaneous variation of γ and ζ over a T = 10 s signal follows the form

$$\gamma(t) = \gamma_c + \gamma_a \text{sin}(2\pi \cdot t/T) \tag{4.10}$$

$$\zeta(t) = \zeta_c + \zeta_a \text{sin}(4\pi \cdot t/T), \tag{4.11}$$

where γ_c, γ_a, ζ_c, and ζ_a are constants, summarized in Table 4.3 for *forte* and *piano* playing levels [111, 112]. The static portion of the control parameters are chosen to create beating conditions for the *forte* playing level and to be near the threshold of oscillation for the *piano* playing level [113, 114]. The control parameters are varied slightly around static values using trigonometric functions because they are smooth, real valued, periodic, and well-known. This is intended to mimic the measurement conditions for which there was some variation in musician control due to the slow movement required by the measurement protocol.

4.4.3 Combining digital synthesis and radiation models

The external sound field of the instrument under playing conditions is simulated through the linear transformations of the waveforms inside the mouthpiece computed by digital synthesis. The acoustic flow $u^s(t)$ in the mouthpiece produced by digital synthesis is transformed to the frequency domain $U^s(\omega)$, and the resulting flow through each tonehole is calculated using $H_n(\omega)$. The pressure $p(t)$ at an observation point O is calculated as the inverse Fourier transform of $P_O(\omega)$, provided by Eq. (4.3).

Because each source term is treated as a monopole, the resonator is considered to radiate symmetrically about its axis. Therefore, the external sound field is simulated in two dimensions, with observation points O laying on a plane that includes the axis of the resonator. The first open tonehole defines the origin and 100 equally spaced observation points are defined along a circle with a 10 m radius centered at the origin.

This configuration is treated as an approximation of the sound power of the source in

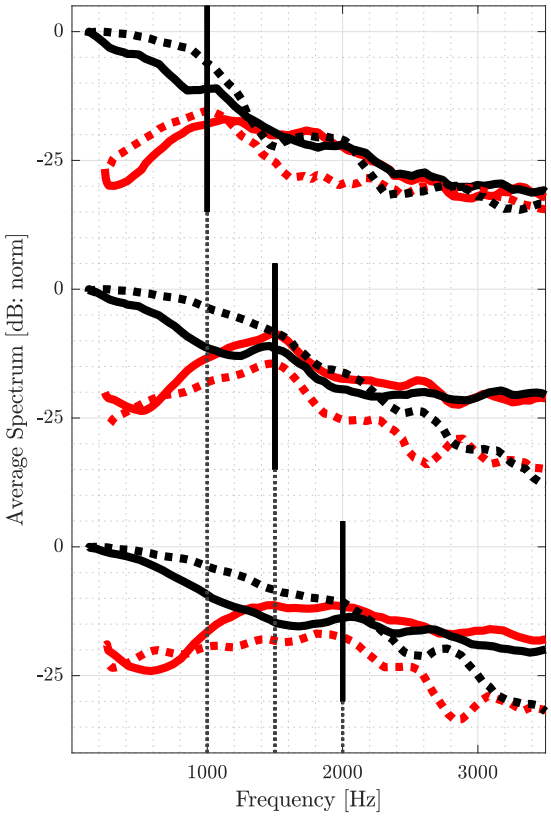

Figure 4.5: Comparison between measured (solid) and simulated (dashed) external spectra in a decibel representation for three resonators with cutoffs $f_c = 1.0, 1.5, 2.0$ kHz at *forte* playing conditions. Odd harmonics are depicted in black and even harmonics in red. Synthesis control parameters provided in Section 4.4.2.

an anechoic environment. The waveforms P_O as simulated at each position O are summed directly to produce a single composite waveform, which is processed as described in Section 4.3.3. This approximates the spatial averaging of the measurements, and helps avoid inadvertently favoring or neglecting frequency ranges that correspond to strong directivity lobes of the resonator.

4.4.4 Comparison between measurements and simulation

The simulation results for the three simplified resonators are presented in Figure 4.5, which also includes the measurements from Section 4.3. The simulated results use the synthesis parameters in Table 4.2 and musician control parameters corresponding to a *forte* dynamic in Table 4.3. The odd and even harmonics have been averaged using MATLAB function movmean with a five point window, and then smoothed. This averaging allows considerable structure of the spectrum to remain in the plots while suppressing the clutter of raw data points or box plots, making it easier to compare the four overlaying curves.

The most successful feature of the simulated curves is the increase in amplitude of the even harmonics as they approach the cutoff. The reinforced spectrum region is not evident in the simulated odd harmonics, although this could be due to the choice of control parameters. The odd and even harmonic parity above 3.0 kHz (and continuing off the graph), is accurately simulated, although the total energy at high frequencies is underpredicted compared to the measurements. This could be due to the model of mutual radiation impedance between neighboring holes, which is known to influence the total radiation of an acoustic source.

The simulations for the *piano* playing dynamic (not shown) do not correspond to the measurements as well, although this could be due to inaccurate choice of musician control parameters. However, the scope of this article is to investigate the effect of the cutoff frequency on radiated sound, which has a greater effect at *forte* playing levels. Therefore, the threshold for appropriate control parameters for a *piano* dynamic is not pursued.

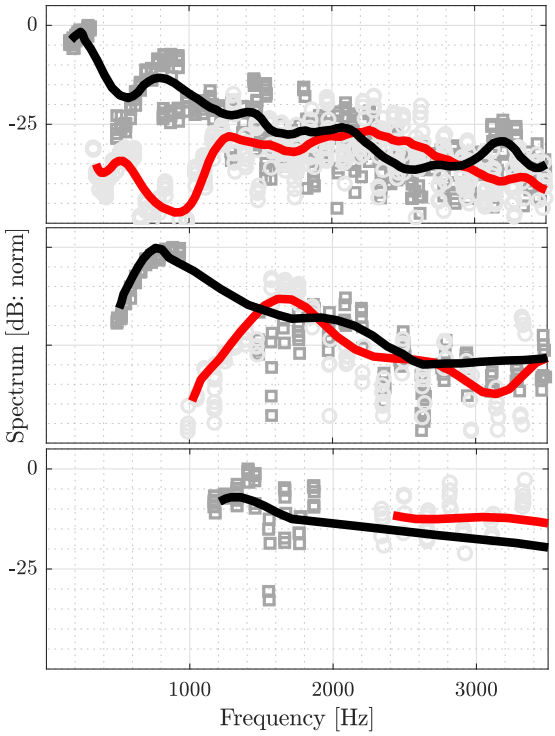

Figure 4.6: Radiated spectra of a real clarinet measured in anechoic conditions played at a *forte* level. Portions of the first (E3-E4), second (B4-A♯5), and third (D6-A♯6) registers are plotted from top to bottom. Raw data depicted by dark grey and light grey circles, plus their moving average by black and red lines, for odd and even harmonics, respectively. Data accessed through a publicly available data base [53].

4.5 Radiated spectra of a clarinet

To contextualize the academic results of Sections 4.3 and 4.4, a similar analysis is applied to a Herbert Wurlitzer Solistenmodell B♭ clarinet using measurements from a publicly available data base [53]. The data used in the current study consists of a 32 channel microphone array in an anechoic environment, with each note of the instrument held for approximately three seconds at a *forte* playing dynamic. As with the simulations in Section 4.4, the total radiation of the instrument of a given note is approximated by the sum of signals from different measurement locations, in this case 32 channels in a sphere around the clarinet. This composite signal of each note is processed following the procedure described in Section 4.3.3.

The results for portions of three registers of the clarinet are shown in Figure 4.6. The lowest notes of each register are neglected to ensure at least two open toneholes in the lattice. The notes included in the analysis are, from panels top to bottom, E3-E4 (165-330 Hz), B4-A♯5 (494-932 Hz), and D6-A♯6 (1175-1865 Hz).

Qualitatively, the trends pertaining to the simplified resonators are also present for the real clarinet for the first and second registers. The even harmonics increase towards a local maximum between 1.0 and 2.0 kHz, the nominal cutoff frequency of a clarinet. This appears more clearly in the second register, possibly because the reinforced spectrum region is produced by low ranking harmonics. The cutoff frequency is approximately the same for the first two registers because the sound is filtered by essentially the same lattice. For the third register, the notes have fundamental frequencies that are near the cutoff frequency of the lattice, so there is no consistent evolution towards a reinforced spectrum region at the cutoff frequency.

Although the results of the clarinet are generally similar to the simplified resonators, it is not appropriate to make a direct comparison because a clarinet is not an acoustically (or geometrically) regular resonator, so an exact lattice cutoff frequency does not exist. For example, unlike the simplified resonators, the even harmonics of the first register continue to increase after the nominal cutoff, to a maximum at approximately 2.3 kHz. This may be due to the bell of the clarinet, which has a resonance at 2.1 kHz and is not included on the simplified resonators.

The results from the real clarinet shown in Figure 4.6 are consistent with those reported by Benade (Figures 6-10) [4]. The coherence between these results demonstrates the robustness of his measurement protocol, which is considerably easier to implement compared with a multiple channel anechoic measurement. Furthermore, the reinforced spectrum region in the radiated sound field of the clarinet for both *in situ* and anechoic measurements provides justification for the anechoic simulation conditions in Section 4.4.

4.6 Conclusion

Simplified clarinet-like cylindrical resonators radiate with a reinforced spectrum region that appears near the cutoff frequency of the tonehole lattice. The reinforced spectrum emerges as the even harmonics grow in amplitude to become equally strong as the odd harmonics at the cutoff. This effect on the external sound field is a result of the geometry of the lattice, and provides a direct link between the tonehole lattice and spectral char-

acteristics of the radiated sound. The phenomenon is more pronounced at loud playing dynamics, but also affects the spectral envelope for soft dynamics. Digital synthesis coupled with a radiation model is sufficient to reproduce the measurement results through simulation. Results from a real clarinet, recorded in playing conditions in an anechoic chamber, demonstrate that a reinforced spectrum region also exists near the nominal cutoff of a real clarinet.

A similar evolution of even harmonics in the external sound field was demonstrated by Benade for the clarinet, along with the related break frequency for the saxophone. However, because the saxophone is an acoustically irregular lattice, the link between the tonehole lattice cutoff frequency and the region of reinforced spectrum is not conclusive. Furthermore, because the saxophone is conical, the reinforced spectrum appears as the odd and even harmonics both increase towards the approximate cutoff, in contrast with the current study of cylindrical resonators, for which the increase is primarily observed for the even harmonics. The effects of conical instruments on reinforced spectrum has also been studied for another conical instrument, the bassoon [115].

As suggested by Benade, the tonehole lattice cutoff frequency is generally assumed to influence the character of a woodwind instrument. This study provides one quantitative link between the cutoff and external spectral characteristics that are measurable in musically appropriate environments. While a musician can manipulate the timbre of a note by adjusting the blowing pressure and lip contact with the reed, the reinforced spectrum at cutoff is a consequence of the resonator's geometry, which is decided by the manufacturer. This allows the possibility of using the cutoff as a design parameter for new instruments. Future work could involve mapping the cutoff to perceptual descriptions of timbre.

Chapter 5

On the tonehole lattice cutoff frequency of conical resonators: applications to the saxophone

PREFACE

The articles in Chapters 3 and 4 are designed to complement one another by addressing two facets of the same question: how does the tonehole lattice cutoff frequency effect sound production and radiation? To probe this question, both articles use the same type of simplified resonators for which the first impedance peak frequency and cutoff frequency can be independently varied. The first article focuses on *interior* variables with the main result that the cutoff does not strongly impact sound production, demonstrated using digital synthesis. The second article focuses on *exterior* variables, in the form of measured and simulated room averaged pressure fields. The main results show that the spectral characteristics of the radiated sound is strongly affected by the tonehole lattice cutoff. Taken together, these articles form a quantitative link between the tonehole lattice cutoff frequency and the sound production and radiation of a clarinet-like instrument. A main conclusion is that the cutoff may be chosen by the manufacturer as a design parameter to achieve a desired sound characteristic, without degrading the playability of an instrument.

The current study addresses two major limitations of the preceding articles: they both use simplified, academic resonators to ensure a strong cutoff frequency behavior, and all of the resonators have cylindrical bores. Before, the use of academic resonators was justified because the goal was to quantify the effect of the cutoff on sound production and radiation, so a direct application to real instruments was not necessary. Furthermore, the instrument that most resembles the academic resonators used in those chapters is the clarinet, which is quite acoustically regular and has a cutoff behavior that matches reasonably well with the theory of simplified resonators [22]. Even simplified conical lattices are considerably more complex than their cylindrical counterparts, making it harder to extrapolate their behavior to conical instruments. This chapter addresses both of these limitations by extending the theory of acoustically regular cylindrical waveguides to conical lattices, and probing the limits of this theory when applied to non-academic, non-acoustically regular, conical resonators. This considerably widens the scope of the dissertation to include conical instruments such as the saxophone, oboe, and bassoon.

Conical lattices are difficult to analyze as a periodic medium because they cannot be

constructed by identical, repeating cells. Due to the changing cross section of the bore, successive cells will necessarily have different input radii. For the same reason, it is impossible to have symmetric cells, because the input radius on one side is strictly different than the output radius on the other side. A generalization to conical resonators forces the question [16]: can a conical lattice be considered a periodic waveguide when there is no possibility for geometric periodicity? It is tempting to assume that the notions of acoustical regularity, as detailed in Chapter 3 for cylindrical resonators, may be applied directly to a conical lattice. This is not an obvious solution because that derivation begins with the hypothesis of an infinite, geometrically regular lattice, and only arrives at the observation of acoustic regularity as an interesting interpretation of the final results [22]. In fact this interpretation is not essential in order to design a periodic cylindrical waveguide: one could use geometric periodicity without ever understanding the implications of acoustic periodicity. Here we show that, despite their inherent geometrical asymmetry, the interpretation of acoustic periodicity is possible for conical lattices.

Extending the theory to lattices that are inherently asymmetric opens the analysis to new ways of considering acoustic regularity. For example, because the unit T-cells of a conical guide cannot be symmetric even if the lengths on either side of the hole are the same, a logical development would be to break the symmetry even further and consider T-cells with different lengths of main duct on either side of the hole, as was done for the clarinet [22]. Another option is to divide a lattice not in T-cells, but rather in Π-cells, composed of two neighboring toneholes and the length of duct between them [16]. The analysis of an acoustically regular lattice as a series of Π-cells is essentially the same as with T-cells, and can also be applied to cylindrical lattices. Using Π-cells is particularly appealing because the division of the lattice is unambiguous, unlike the arbitrary division using T-cells. These extensions are the basis for a more comprehensive understanding of acoustically regular conical waveguides.

The second goal of this chapter is to determine how the theory of wave propagation in periodic media succeeds or fails when applied not to academic resonators, but rather to real instruments that are not necessarily acoustically regular. A measure of acoustic irregularity can be determined by how the eigenfrequencies of constituent cells (of whatever shape) vary across the length of the lattice. An acoustically irregular lattice does not have a true cutoff frequency, but can exhibit an empirically determined cutoff within the vicinity of the eigenfrequencies of multiple cells [16]. This can be viewed as a relaxation of the formalism of wave propagation in periodic media: recognizing that an approximate acoustic regularity is sufficient to impose a stop band in the lattice. The broader interpretation of a lattice as approximately acoustically regular is an important link between the simplified academic resonators and the complicated lattices of real instruments.

Lastly, the question arises of how to empirically determine a cutoff. Many real instruments, both cylindrical and conical, are not strictly acoustically regular, yet still exhibit a cutoff frequency [3]. It is reasonable to search for a definition of the cutoff that relies not on knowledge of the resonator geometry, but rather on measurable characteristics of its acoustic response. This type of analysis is a useful complement to the theoretical development of lattice cutoff frequencies because it corresponds to the behavior observed on real instruments and is also relatively easy to implement. Often the cutoff frequency is identified by human observation of the magnitude of the input impedance, a method that

is both approximate and vulnerable to human inconsistency. This provides an approximation of the cutoff or, perhaps more accurately, is a frequency at which the resonator behaves as if there is a tonehole lattice cutoff, even if there are other factors involved. However, cutoff-like behavior can manifest on the input impedance that is due to the presence of a bell, or the conicity of the resonator [41, 60]. Applying the formalism of periodic media, combined with empirically observed phenomena, provides a more robust description of the effect of the lattice. A comparison between empirically identified and theoretical cutoffs can help differentiate between the effects of various aspects of the resonator, such as the lattice, conicity, and bell, that can cause a cutoff behavior. Understanding these causes is an important aspect of studying the cutoff of both cylindrical and conical resonators, and a strategy to approach this problem is a key element of this chapter.

This chapter extends the topic of this dissertation both in terms of theory and application. The first is through the generalization of the tonehole lattice cutoff to conical resonators. This is an exercise in developing the theory of wave propagation in periodic media from one type of resonator to another, and remains mainly an academic subject. The second part attempts to analyze a real saxophone using the theoretical results, as well as empiric methods such as thresholds on the magnitude of the reflection coefficient. The analysis is largely coherent between the theoretical and empiric methods. It is an interesting result because the saxophone is quite acoustically irregular, but still exhibits strong cutoff behavior, which is well captured by the different forms of analysis. This result is another justification for applying the theory of wave propagation in periodic waveguides to musical instruments with highly irregular lattices.

Additional comments

This remainder of this chapter is a reproduction the published article:

E. Petersen, T. Colinot, J. Kergomard, and P. Guillemain. On the tonehole lattice cutoff frequency of conical resonators: applications to the saxophone. *Acta Acust.*, 4(4):13, 2020. doi: 10.1051/aacus/2020012

Comments:

- Original abstract has been omitted.

5.1 Introduction

Woodwind instruments such as the clarinet and saxophone have resonators that are composed of an acoustical duct for which the downstream section has a lattice of toneholes that can be opened and closed to change the playing frequency of the instrument. At low frequencies, the effective acoustical length of the resonator is defined by the distance between the mouthpiece and the first open tonehole because an acoustical wave, upon arrival at the tonehole, either radiates into the surrounding environment or reflects back into the main bore of the instrument. At higher frequencies, the wave is no longer evanescent and propagates into the remaining lattice of toneholes. For a real instrument of finite length, the (approximate) tonehole lattice cutoff frequency separates these two bands, although no definition is universally agreed upon and a precise definition does not exist because the toneholes do not constitute a perfectly periodic lattice.

The tonehole lattice cutoff frequency has been studied for various instruments, particularly the clarinet, but relatively little application to the saxophone exists in the literature [22, 60]. In fact, in his book, Benade provides the input impedance and discusses (approximate) cutoff frequencies for many instruments, including the clarinet, oboe, bassoon and tárogató, but not the saxophone [3]. The cutoff has also been studied for the flute [24]. It is generally assumed that the cutoff frequency has an impact on the timbre or perceived 'character' of a given instrument due to its influence on both sound production and radiation, and is therefore of interest to both instrument makers and musicians [3, 29].

A precise definition of the tonehole lattice cutoff frequency does not exist due to the finite and lossy nature of real instruments [2, p. vii-viii]. Therefore, only approximate definitions exist, which may be either empirical or analytic. A summary of the notation used in the current article is provided in Table 5.1. One way to define the cutoff frequency is to identify a disturbance in the measured or simulated input impedance or reflection coefficient, and set an arbitrary threshold to distinguish between the pass and stop bands. Often the disturbance is identified visually from the input impedance, which introduces questions about reproducibility, and the uncertainty can be on the order of the distance between impedance peaks. Regardless, this is the most common method for identifying the cutoff of woodwind instruments. A second empirical method to identify the cutoff frequency uses measurements external to the instrument during playing conditions across a large range of the instrument. From this, Benade defines a 'break frequency,' and related it to the cutoff frequency, which is at the intersection of the low frequency rise and high frequency roll-off of the spectrum envelope [5]. Both of these methods are prone to ambiguous results for certain fingerings and instruments. While empirically estimated cutoff frequencies are often assumed to be due to the tonehole lattice, it is not always a robust method because other components, such as the bell, can cause similar disturbances in the input impedance.

Analytically, the *global cutoff frequency* f_c^G can be developed following the theory of wave propagation in periodic media [2, p. 19], in which a cutoff frequency can be precisely defined for an infinite, lossless lattice. Here, local quantities corresponding to the unit cells of the lattice define the global cutoff frequency. In the case where the medium is a column of air punctuated by toneholes, the lattice is divided into discrete elements

Table 5.1: Summary of the different types of cutoff frequencies used in the current article.

	Eq.	Name and description
f_c^T	(5.13)	The *local cutoff frequency* is the natural frequency of a T-cell with one hole flanked by two lengths of bore that are closed at their extremities. The cell can be either symmetric (Eq. (5.13)) or asymmetric (Eq. (5.27)). Because this is a local quantity, it has a corresponding cell index n that is omitted to lighten the notation.
f_c^Π	(5.26)	The *characteristic frequency* is the natural frequency of a Π-cell consisting of two toneholes separated by a length of bore. Because this is a local quantity, it has a corresponding cell index n that is omitted to lighten the notation.
f_c^G	—	The *global cutoff frequency* is a global property of a lattice for which each element has exactly the same natural frequency, in which case $f_c^G = f_c^T = f_c^\Pi$. It is only strictly valid for an infinite, lossless lattice, but it is a good approximation for a tonehole network with at least three open toneholes and is used for finite lattices in this article.
f_t^R	(5.19)	The *transition band* is an approximation of the global cutoff derived from the reflection coefficient. It defines a frequency band over which the lattice appears to transition from below to above the cutoff frequency.
A lattice is *geometrically regular* if every cell is geometrically identical. In this case every cell has the same f_c^T (and f_c^Π) and the lattice has a global cutoff f_c^G. This is not possible for a conical lattice because no two cells can be identical due to the taper of the bore.		
A lattice is *acoustically regular* if every cell has the same local cutoff f_c^T (and f_c^Π), resulting in a global cutoff f_c^G. Conical bores can be acoustically regular because the cross-section and chimney height of a tonehole can be modified to account for the changing cross-section of the main bore.		

in the form of T-cells, a hole with flanking lengths of duct on either side, or as Π-cells with two neighboring (partial) holes and the length of duct between them. For either shape, an eigenfrequency can be calculated for each cell in the lattice, referred to as the *local cutoff frequency* f_c^T and *characteristic frequency* f_c^Π, respectively. If each cell in the lattice has the same eigenfrequency, then the lattice is considered an *acoustically regular* (periodic) medium, and the lattice formally has a global cutoff frequency that is equal to the common eigenfrequency of each constituent cell. Periodic cylindrical lattices are easily designed by concatenating identical unit cells to form *geometrically regular* lattices. For conical resonators, which cannot be geometrically regular due to the taper of the main bore's internal radius, a lattice can be periodic following the interpretation of acoustical periodicity. While these derivations are only strictly valid for an infinite, lossless lattice, the theory works well for lattices with as few as three toneholes.

The purpose of the current article is to generalize the theory of wave propagation

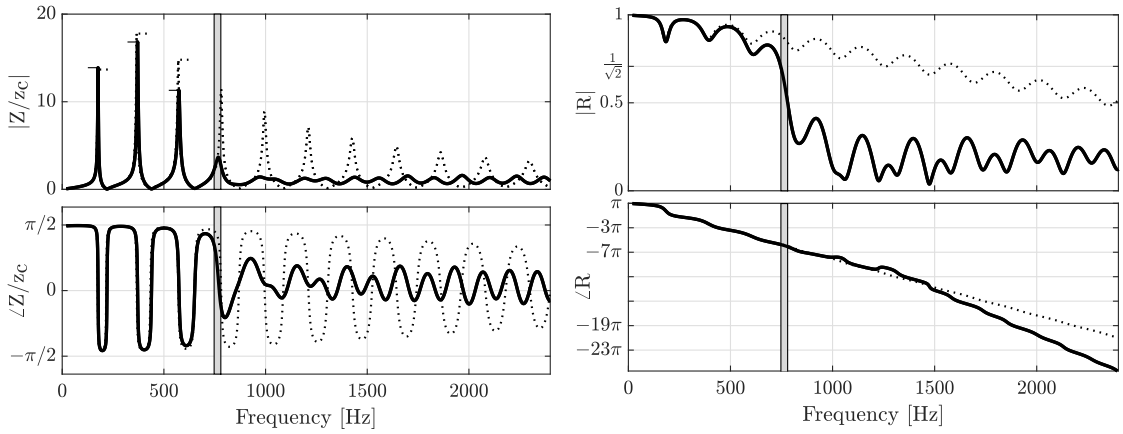

Figure 5.1: Input impedance (modulus and argument) and reflection coefficient (modulus and argument) of an acoustically regular conical resonator (solid black lines) with a first impedance peak at 177 [Hz] and a theoretical global tonehole lattice cutoff frequency at 750 [Hz]. A conical resonator (dotted lines) with the same first impedance peak frequency but no tonehole lattice is shown for comparison. The first three impedance modulus peaks are marked by a solid black line (resonator with a lattice) and dotted lines (simple cone). The cutoff transition band $f_{\mathrm{t}}^{\mathrm{R}}$ (defined in Section 5.2.4, Eq. (5.19)) is shown in shaded grey.

in periodic media from cylindrical to conical resonators. In a recent article, the current authors present an algorithm for designing cylindrical resonators with independently variable first impedance peak and global cutoff frequencies [29]. Analogous equations are derived for conical resonators in Section 5.2. Section 5.3 applies the analysis of a conical tonehole lattice to the geometry of a Buffet Crampon alto saxophone. This section also includes a comparison of the various cutoff frequency definitions and approximations as they apply to simplified resonators and the Buffet Crampon alto saxophone. Conclusions and perspectives are provided in Section 5.4.

5.2 Acoustically regular conical tonehole lattice

In this section a conical resonator is designed such that the frequency f_1 of the first impedance peak and the global tonehole lattice cutoff frequency $f_{\mathrm{c}}^{\mathrm{G}}$ can be independently varied. Inspired by the geometry of a saxophone resonator without a mouthpiece, this is achieved by using a length of cone that ends with a series of acoustically regular lattice cells. The input impedance peaks below the global cutoff frequency have relatively large magnitudes that are approximately harmonically related to the first peak. Above the global cutoff frequency the peaks and troughs are less pronounced and may not have the same organized spacing in frequency. This is also seen in the reflection coefficient, which has a value close to unity below the global cutoff frequency, and drops significantly at the cutoff. An example of a synthesized input impedance and reflection coefficient is shown in Figure 5.1 and discussed in greater detail in Section 5.2.4.

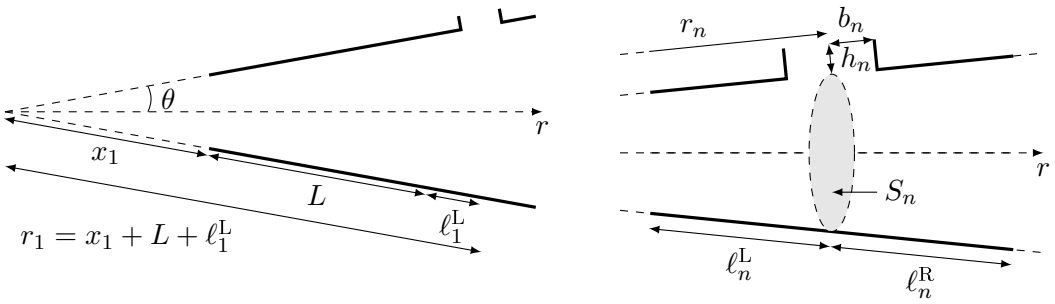

Figure 5.2: Schematic of a conical resonator with apex angle θ and a lattice of toneholes. There is a length of duct L before the first symmetric T-cell centered at r_1 (left panel). The missing length of the cone is x_1. The n^{th} T-cell, centered at r_n, is flanked by cones of length ℓ_n^{L} and ℓ_n^{R} on either side (right panel). The tonehole has cross-section $s_n = \pi b_n^2$ and chimney height h_n. The cross-section of the main bore under the tonehole is S_n.

In the following sections we derive the equations that describe the conditions for acoustic regularity of a conical waveguide. The derivation uses T-cells as the basic element of the lattice, although it is also possible to start with Π-cells.

5.2.1 Transfer matrix equations of a conical lattice

5.2.1.1 Basic equations

In the following derivation, a conical lattice is designed by concatenating n cells that have a tonehole at the center and truncated cones of length ℓ_n^{L} and ℓ_n^{R} to the left and right, as shown in Figure 5.2. The frequency domain Helmholtz equation for the acoustic pressure $P(r,k)$ is

$$\frac{\partial^2}{\partial r^2}\left[rP\left(r,k\right)\right] + k^2 rP(r,k) = 0, \tag{5.1}$$

where $k = \omega/c$ is the wavenumber with ω the angular frequency and c the speed of sound in air. Thermoviscous and radiation losses are ignored. The acoustic velocity $V(r,k)$ is derived from the Euler equation, $\partial_r P(r,k) = -j\rho ckV(r,k)$, where ρ is the density of air and j the imaginary unit.

A small angle approximation of the apex angle θ is applied for the following derivation. The approximation assumes that the difference between the spherical cap of a propagating wave and a flat surface cross-section of the main bore can be ignored. Similarly, the difference between a length along the axis r and its projection on the edge of the cone is ignored. For a typical apex angle $\theta = 0.028$ [rad] these approximations introduce less than 0.1 % error for the surface and less than 0.5 % error for the lengths. The advantage of this approximation is that it assumes planar waves, such that the pressure is constant across a flat surface cross-section of the main bore, allowing the use of a simple tonehole model.

5.2.1.2 Transfer matrix across a single cell

The relation between pressure and velocity across a section of the waveguide is written as a transfer matrix equation

$$\begin{pmatrix} r_1 P(r_1,k) \\ r_1 V(r_1,k) - \frac{P(r_1,k)}{jck\rho} \end{pmatrix} = M_{1,2}(k) \begin{pmatrix} r_2 P(r_2,k) \\ r_2 V(r_2,k) - \frac{P(r_2,k)}{jck\rho} \end{pmatrix}, \tag{5.2}$$

where the matrix $M_{1,2}(k)$ (written generically here, and with superscript labels and subscript indices when referring to specific sections) has elements $A(k), B(k), C(k)$, and $D(k)$ that correspond to the geometry of the waveguide sections. The transfer matrix relating pressure and velocity across the n^{th} cell (see Figure 5.2, right panel) centered at r_n is the product of the transfer matrices across the tonehole $M_n^{\text{h}}(k)$ and the left and right flanking conical sections $M_n^{\text{L}}(k)$ and $M_n^{\text{R}}(k)$,

$$M_n(k) = M_n^{\text{L}}(k) M_n^{\text{h}}(k) M_n^{\text{R}}(k). \tag{5.3}$$

It is convenient, although not necessary, to consider 'symmetric' cells (truly symmetric cells cannot exist due to the taper of the main bore) for which $\ell_n^{\text{L}} = \ell_n^{\text{R}} = \ell_n$

$$M_n(k) = M_n^{\ell}(k) M_n^{\text{h}}(k) M_n^{\ell}(k). \tag{5.4}$$

The remainder of this derivation assumes symmetric cells, and asymmetric cells are treated in Section 5.3.

The transfer across a truncated cone of length ℓ_n is

$$M_n^{\ell}(k) \;= \begin{pmatrix} \cos(k\ell_n) & j\rho c \sin(k\ell_n) \\ \frac{j}{\rho c}\sin(k\ell_n) & \cos(k\ell_n) \end{pmatrix}. \tag{5.5}$$

A tonehole is treated as a shunt acoustic mass: $m_n = \rho h_n / s_n$, where $s_n = \pi b_n^2$ is the cross-sectional area of the tonehole and the chimney height h_n includes the internal and radiation length corrections. The transfer matrix across the n^{th} tonehole is

$$M_n^{\text{h}}(k) \;= \begin{pmatrix} 1 & 0 \\ Y_n(k) & 1 \end{pmatrix}, \tag{5.6}$$

where $Y_n(k) = 1/(jckm_nS_n)$ is the specific admittance of the tonehole.

The transfer matrix equation relating $P(r,k)$ and $V(r,k)$ from $r_n - \ell_n$ to $r_n + \ell_n$ across the entire n^{th} symmetric cell centered at r_n is

$$\begin{pmatrix} (r_n-\ell_n)P(r_n-\ell_n,k) \\ (r_n-\ell_n)V(r_n-\ell_n,k) - \frac{P(r_n-\ell_n,k)}{jck\rho} \end{pmatrix} = M_n(k) \begin{pmatrix} (r_n+\ell_n)P(r_n+\ell_n,k) \\ (r_n+\ell_n)V(r_n+\ell_n,k) - \frac{P(r_n+\ell_n,k)}{jck\rho} \end{pmatrix}, \tag{5.7}$$

where $M_n(k)$ is determined by Eq. (5.4) using Eqs. (5.5) and (5.6), has elements classically

denoted $A_n(k), B_n(k), C_n(k), D_n(k)$ and its determinant is unity due to reciprocity.

5.2.1.3 From one cell to full lattice

The transfer matrix M for a lattice with N cells is the matrix product of the transfer matrix of each cell

$$M(k) = \prod_{n=1}^{N} M_n(k) = M_1(k)M_2(k)\cdots M_N(k). \tag{5.8}$$

The resulting matrix

$$M(k) = \begin{pmatrix} A(k) & B(k) \\ C(k) & D(k) \end{pmatrix}, \tag{5.9}$$

has coefficients $A(k), B(k), C(k), D(k)$ that can be used to calculate global features of the lattice such as the input impedance.

So far, the lattice modeled by $M(k)$ is not necessarily acoustically regular and may not have a global cutoff frequency. To create a lattice that is acoustically regular and exhibits a global cutoff it is necessary to impose conditions on the local elements accounted for by each cell $M_n(k)$.

5.2.2 The cutoff frequency of an acoustically regular lattice

For the pressure $P(r,k)$ defined at the input $r = r_n - \ell_n$ of the n^{th} cell, an acoustic periodicity implies

$$\begin{aligned} 2A_n(k)(r_n - \ell_n)P(r_n - \ell_n, k) = {} & (r_{n-1} - \ell_{n-1})P(r_{n-1} - \ell_{n-1}, k) \\ & + (r_{n+1} - \ell_{n+1})P(r_{n+1} - \ell_{n+1}, k), \end{aligned} \tag{5.10}$$

which is derived from Eq. (5.7). An explicit expression for $A_n(k)$ can be determined from the geometry of each cell, and the frequency $f = ck/(2\pi)$ that satisfies $A_n(k) = D_n(k) = \pm 1$ for a given cell is the local cutoff frequency f_{c}^{T}. When $A_n(k) = \pm 1$ occurs at the same frequency for every cell, then the lattice is acoustically regular and has a global cutoff frequency f_{c}^{G}, below which waves entering the lattice are evanescent [23, 381].

The transfer matrix elements $A_n(k)$ and $D_n(k)$ that define the local cutoff of a cell can be calculated directly from the geometry of the n^{th} cell. Therefore, it is possible to choose the cell geometry to achieve a desired local cutoff frequency. For a symmetric cell defined by Eqs. (5.4),(5.5),(5.6) and setting $A_n(k) = 1$, a transcendental equation defines the local cutoff in terms of cell geometry

$$\cot(k_{\text{c}}^{\text{T}}\ell_n) = 2k_{\text{c}}^{\text{T}}h_n S_n/s_n, \tag{5.11}$$

where $k_{\text{c}}^{\text{T}} = 2\pi f_{\text{c}}^{\text{T}}/c$. The local cutoff frequency is approximated using a Taylor expansion

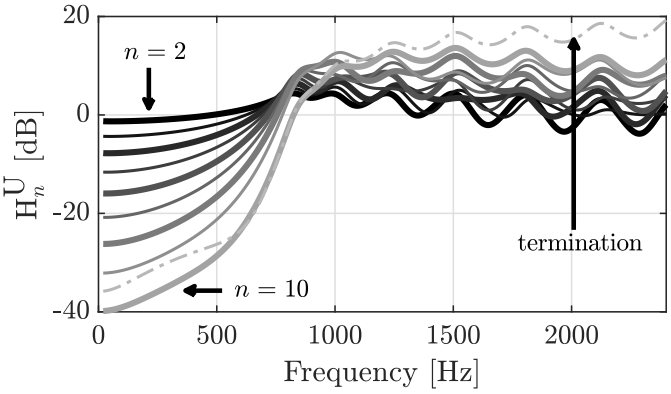

Figure 5.3: The transfer function between flow through the first tonehole and flow through the n^{th} (for $n = 2$ to 10) tonehole and open termination of a conical lattice with $f_{\mathrm{c}}^{\mathrm{G}} = 750$ [Hz]. The lattice geometry is Resonator 1 in Table 5.2, and is the same lattice used for Figure 5.1 and the bottom resonator in Figure 5.9.

of the cotangent in $k_{\mathrm{c}}^{\mathrm{T}}\ell_n$

$$f_{\mathrm{c}}^{\mathrm{T}} = \frac{c}{2\pi\ell_n}\left[\frac{1}{\sqrt{2(h_n/\ell_n)(S_n/s_n)+1/3}} + \mathcal{O}((k_{\mathrm{c}}^{\mathrm{T}}\ell_n)^3)\right], \tag{5.12}$$

$$f_{\mathrm{c}}^{\mathrm{T}} = \frac{c}{2\pi\ell_n}\left[\frac{1}{\sqrt{2(h_n/\ell_n)(S_n/s_n)}} + \mathcal{O}(k_{\mathrm{c}}^{\mathrm{T}}\ell_n)\right], \tag{5.13}$$

where the approximations correspond to expansions retaining two and one terms, respectively. Both of these expansions of the cotangent function are valid assuming $(k_{\mathrm{c}}^{\mathrm{T}}\ell_n)^2 \ll 1$, for which the half-spacing between holes is much smaller than the wavelength at the local cutoff, and the cell can be treated as a lumped element system. For a local cutoff at 900 [Hz] and a common inter-hole spacing $2\ell_n \approx 0.04$ [m], $(k_{\mathrm{c}}^{\mathrm{T}}\ell_n)^2 \approx 0.1$ and the condition is satisfied. As for the case of a cylindrical cell [22], the local cutoff frequency can be interpreted as the eigenfrequency of a single cell with Neumann boundary conditions satisfied at the left and right extremities of the main bore.

One way to quantify the tonehole lattice global cutoff frequency of an acoustically regular lattice is to examine the acoustic flow $U(\omega)$ through each radiating aperture, relative to the first tonehole. Figure 5.3 shows the transfer function $\mathrm{H}_n^{\mathrm{U}}(\omega) = 20\log_{10}(U_n(\omega)/U_1(\omega))$ for the acoustically regular lattice with geometry provided in Table 5.2, also depicted in Figure 5.1 and the left panel of Figure 5.9. These simulations follow the method outlined in Section 5.2.4. Below global cutoff, the flow is predominantly through the first tonehole, with an exponential decay of approximately 4.8 [dB] (at 50 [Hz]) for each subsequent tonehole. Above the global cutoff, the flow is predominantly through the termination of the lattice, with considerable contributions from multiple toneholes. This figure is the conical lattice counterpart to the results for measured [16, 17] and analytically studied

cylindrical lattices [15].

5.2.3 From lattice to a saxophone-type resonator

To better mimic the acoustical behavior of a real alto saxophone, the resonator is designed as a conical bore approximately 60 cm long that terminates in an acoustically regular lattice designed following the method proposed in Section 5.2.2 using Eq. (5.13). Dimensions of two possible examples are provided in Table 5.2. The upstream (closest to the mouthpiece) section of the cone determines the low frequency resonances of the resonator, and the lattice of open toneholes modifies the high frequency (above the global cutoff) resonances by changing the effective acoustical length. It is possible to design a resonator such that the frequency of the first impedance peak and the global cutoff frequency of the lossless tonehole lattice can be varied independently [29].

The length of a lattice-less frustum (cone truncated on both ends) with a desired first impedance resonance frequency f_1 is

$$L_{\text{eff}}(\lambda_1, x_1) = \lambda_1 \left(\frac{1}{2} - \frac{1}{2\pi} \arctan\left(\frac{2\pi x_1}{\lambda_1} \right) \right), \tag{5.14}$$

where $\lambda_1 = c/f_1$ is the wavelength corresponding to the first impedance peak frequency and x_1 the missing length between the apex and small end of the frustum. At low frequencies, a lattice of toneholes changes the terminal impedance of the cone by adding a mass-like term that can be expressed as a length correction $\Delta\ell_1$ [23, 382]. This length correction is a function of the first cell length ℓ_1^{L} and the wavelength λ_{c} at the local cutoff

$$\Delta\ell_1(\lambda_{\text{c}}, \ell_1^{\text{L}}) = \ell_1^{\text{L}} \sqrt{1 + \left(\frac{\lambda_{\text{c}}}{2\pi\ell_1^{\text{L}}} \right)^2}. \tag{5.15}$$

The end correction term implies that a conical resonator without a lattice (but same f_1) should be slightly longer than the length between the input and first hole of a resonator with a lattice. Therefore, the segment of the resonator before the lattice should have a length

$$L = L_{\text{eff}} - \ell_1^{\text{L}} - \Delta\ell_1, \tag{5.16}$$

depicted in the left panel of Figure 5.2.

These equations provide the basic algorithm for designing a resonator such that the first resonance frequency and the global tonehole lattice cutoff can be independently varied. It is possible to conceive different geometries that result in an acoustically regular tonehole lattice with the same global cutoff. In the current work, the geometries are inspired by, but not identical to, a Buffet Crampon alto saxophone.

5.2.4 Simulated impedance of acoustically regular lattice and equivalent truncated cone

The input impedance is simulated to demonstrate the validity of an acoustically regular conical lattice design. The simulations are based on the Transfer Matrix Method with ex-

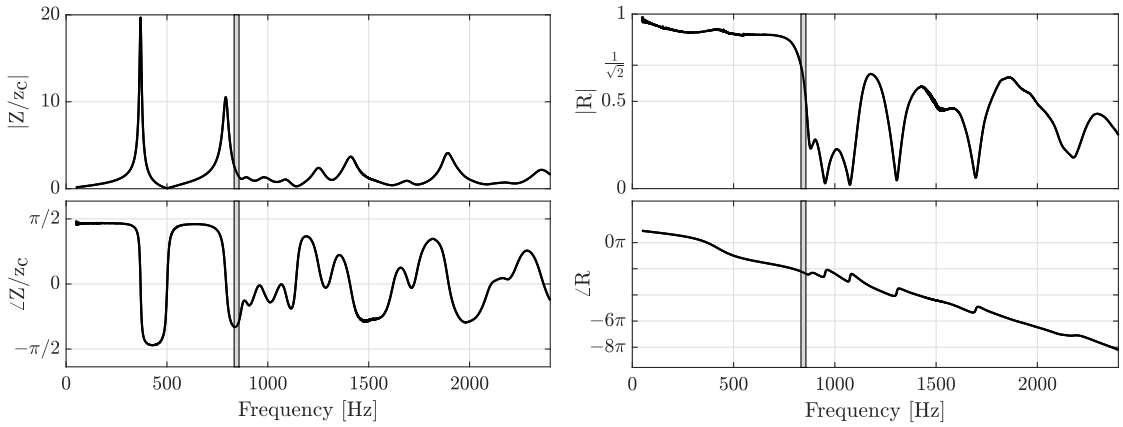

Figure 5.4: The input impedance (modulus and argument) and reflection coefficient (modulus and argument), measured for the high C fingering (written pitch, 311 [Hz]) of an alto saxophone. The cutoff transition band $f_{\mathrm{t}}^{\mathrm{R}}$ in grey.

ternal Interactions (TMMI), which is similar to the well-known Transfer Matrix Method, but includes the mutual impedance of toneholes that radiate into the same space [28]. In contrast with the previous theoretical development, the TMMI simulations include thermoviscous and radiation losses. The resonator has a first impedance peak at 177 [Hz] and a global cutoff at 750 [Hz]. The geometry of this academic resonator and another with a global cutoff at 1000 [Hz] is provided in Table 5.2.

Figure 5.1 shows the simulated input impedance

$$Z(\omega) = P(\omega)/U(\omega), \tag{5.17}$$

normalized by $\mathrm{z_c} = \rho c/(\pi a_{\mathrm{in}}^2)$ where $a_{\mathrm{in}} = x_1 \tan(\theta)$ is the radius of the entrance to the bore, and the corresponding reflection coefficient

$$R(\omega) = \frac{Z(\omega)/\mathrm{z_c} - 1}{Z(\omega)/\mathrm{z_c} + 1}. \tag{5.18}$$

The effect of the global cutoff frequency can be identified visually in the magnitude and argument of both the input impedance and reflection coefficient. The large and regularly spaced impedance peaks whose frequencies are determined by the upstream portion of the resonator are obliterated above the global cutoff because the wave propagates into the lattice and reflections back into the bore are weak. Furthermore, above the global cutoff the wave radiates from subsequent toneholes and experiences greater thermoviscous losses due to the increased propagation distance within the bore. These combined effects result in the disturbance seen in the input impedance and reflection coefficient.

Because the lattice is designed to have acoustically regular cells, the local (and therefore global) cutoff frequencies are, in principle, exactly 750 [Hz]. As noted before, it is not always sensible to define a precise, unambiguous definition of the cutoff from the input impedance and reflection coefficient. Therefore, a transition band $f_{\mathrm{t}}^{\mathrm{R}}$ shown in light grey

is defined by

$$f_{\min} \leq f_{\mathrm{t}}^{\mathrm{R}} \leq f_{\max}, \tag{5.19}$$

where the lower and upper bounds $f_{\min}$ and $f_{\max}$ correspond to the -3 and -6 [dB] roll off of the reflection coefficient. This is determined by the lowest frequencies that satisfy

$$|R(2\pi f_{\min})| = \frac{\sqrt{2}}{2} \tag{5.20}$$

$$|R(2\pi f_{\max})| = \frac{1}{2}. \tag{5.21}$$

Although the thresholds are arbitrary, this transition band serves as an objective empirical estimation of the global cutoff frequency for the remainder of this article. Note that it is distinct from a theoretically defined (global, local, or characteristic) cutoff, summarized in Table 5.1.

The dashed curve in Figure 5.1 shows the input impedance of a cone which terminates in a radiation load but no lattice. Its length is chosen so that the first impedance peak frequency is the same as that of the acoustically regular resonator that terminates with a lattice. This serves as a comparison to show which features of the input impedance are due to the tonehole lattice, and which arise solely from the conical geometry. As for the resonator with a tonehole lattice, the reflection coefficient of the simple cone also has regularly spaced dips. This behavior is due to the conical geometry of the waveguide, and is therefore seen in the simulations of both resonators, even below the global cutoff frequency of the resonator with a tonehole lattice.

For the readability of Figure 5.1, the cutoff transition band $f_{\mathrm{t}}^{\mathrm{R}}$ is not shown for the lattice-less cone. However, if the definition was applied, the threshold conditions are met for a range approximately 1250 to 2300 [Hz]. For this reason, the tonehole lattice cutoff frequency of a conical resonator is difficult to identify empirically in part because there are multiple phenomena that lead to similar measured behavior: the tonehole lattice, the conicity of the main bore, and the bell (not treated in the current article), can all cause perturbations of the input impedance and dips in the reflection coefficient. This may explain why there are comparatively few articles about the cutoff frequency of conical instruments such as the saxophone, and demonstrates the utility of using simplified resonators to study the phenomenon. In particular, the features that are evident in Figure 5.1 are helpful to guide the discussion for resonators that are not strictly acoustically regular.

5.3 Application to the saxophone: acoustically irregular lattices

Real saxophones do not have strictly acoustically regular tonehole lattices. However, cutoff frequency type behaviors are observed in the input impedance measurements for many fingerings of the saxophone, for which two examples are provided in Figures 5.4 and 5.5. In addition, the toneholes tend to increase in radius and inter-hole spacing progressively along the resonator, which suggests an approximate acoustic regularity of the type defined by Eq. (5.13). Therefore, it is still interesting to apply the theory of a

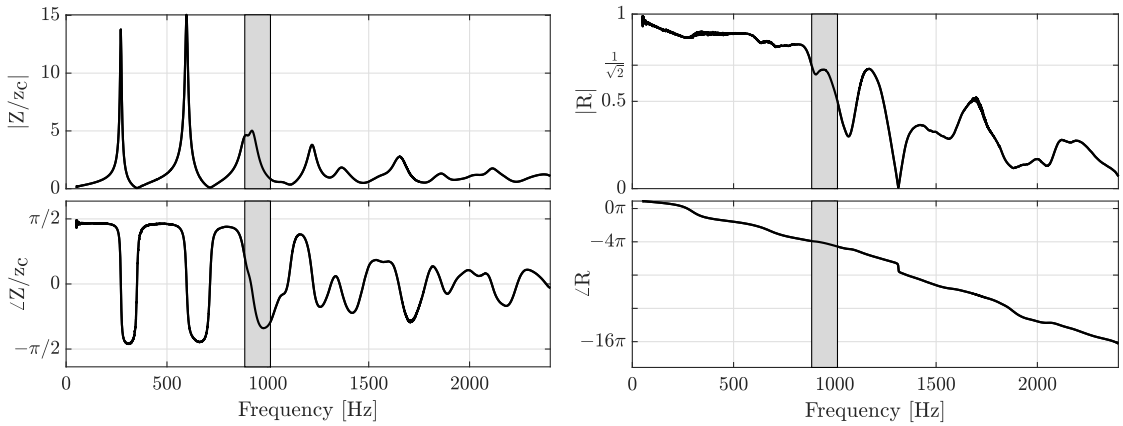

Figure 5.5: The input impedance (modulus and argument) and reflection coefficient (modulus and argument), measured for the G♯ fingering (written pitch, 246 [Hz].) of an alto saxophone. The cutoff transition band $f_{\mathrm{t}}^{\mathrm{R}}$ in grey.

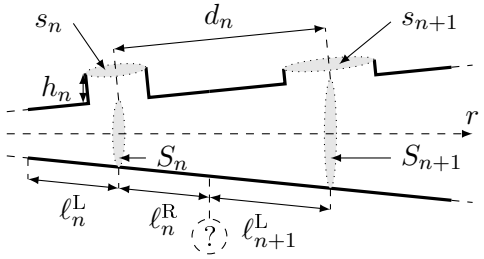

Figure 5.6: Schematic of a tonehole Π-cell. Inter-hole spacing $d_n = \ell_n^{\mathrm{R}} + \ell_{n+1}^{\mathrm{L}}$ is unambiguously defined.

tonehole lattice cutoff frequency to the saxophone.

A practical complication in assessing the acoustic regularity of a real instrument is precising the geometry of the tonehole cells because the lattice cannot, in general, be divided into symmetric T-cells. Can the geometry of a real saxophone be divided into cells such that local cutoff frequencies can be determined? This question is explored using Π-cells and asymmetric T-cells, and the methods are applied to the geometry of a Buffet Crampon alto saxophone [22].

5.3.1 Tonehole cell pairs

The first method to characterize the acoustic regularity of a lattice considers not the local eigenfrequencies of constituent T-cells, but rather defines the characteristic frequency f_{c}^{Π} (Eq. (5.25) and Table 5.1) of adjacent toneholes and the length of cone separating the pair, often referred to as a Π-cell. This way, the characteristic frequency of each tonehole pair in a lattice can be unambiguously calculated directly from the measured geometry of an instrument. As for a lattice of T-cells, if each Π-cell in a lattice has the same characteristic frequency then the lattice as a global cutoff $f_{\mathrm{c}}^{\mathrm{G}} = f_{\mathrm{c}}^{\Pi}$.

If the eigenfrequencies of adjacent symmetric T-cells are equal

$$f_{\mathrm{c}}^{\mathrm{T}} = \frac{c}{2\pi\ell_n}\left[\frac{1}{\sqrt{2(h_n/\ell_n)(S_n/s_n)}} + \mathcal{O}(k_{\mathrm{c}}^{\mathrm{T}}\ell_n)\right] \tag{5.22}$$

$$= \frac{c}{2\pi\ell_{n+1}}\left[\frac{1}{\sqrt{2(h_{n+1}/\ell_{n+1})(S_{n+1}/s_{n+1})}} + \mathcal{O}(k_{\mathrm{c}}^{\mathrm{T}}\ell_{n+1})\right] \tag{5.23}$$

then their geometries are related such that

$$\ell_n h_n \frac{S_n}{s_n} = \ell_{n+1} h_{n+1} \frac{S_{n+1}}{s_{n+1}} = \frac{c^2}{2(2\pi f_{\mathrm{c}}^{\mathrm{T}})^2}. \tag{5.24}$$

As shown in Figure 5.6, the spacing between the two holes is denoted $d_n = \ell_n^{\mathrm{R}} + \ell_{n+1}^{\mathrm{L}}$, where the assumption of symmetric T-cells is no longer necessary. Retaining one term of the Taylor expansion of Eq. (5.11) yields the characteristic frequency of a tonehole pair

$$f_{\mathrm{c}}^{\Pi} = \frac{c}{2\pi d_n}\left[\frac{1}{\sqrt{2\left(K_n + K_{n+1}^{'}\right)}} + \mathcal{O}(k_{\mathrm{c}}^{\mathrm{T}}\ell_n)\right], \tag{5.25}$$

where the dimensionless $K_n = \frac{h_n}{d_n}\frac{S_n}{s_n}$ and $K_{n+1}^{'} = \frac{h_{n+1}}{d_n}\frac{S_{n+1}}{s_{n+1}}$ are introduced for brevity. The subscript of d_n does not increment to d_{n+1} for $K_{n+1}^{'}$ because it is the *distance* between the n^{th} and $(n+1)^{\mathrm{th}}$ holes, which is a shared quantity. Retaining two terms of the Taylor expansion yields the characteristic frequency

$$f_{\mathrm{c}}^{\Pi} = \frac{c}{2\pi}\frac{2}{d_n\sqrt{3}}\left[\left(\frac{1}{3} + K_n + K_{n+1}^{'}\right)\Big/ \left[\left(\left(\frac{1}{3}\right)^2 + \frac{2}{3}\left(K_n + K_{n+1}^{'}\right) + 2K_nK_{n+1}^{'}\right)^2 - 4K_n^2K_{n+1}^{'2}\right]^{1/2} + \mathcal{O}\left((k_{\mathrm{c}}^{\mathrm{T}}\ell_n)^3\right)\right]. \tag{5.26}$$

If the lattice is acoustically regular then the characteristic frequency f_{c}^{Π} will be the same for each pair of adjacent toneholes. If the lattice is not acoustically regular, as is the case for a saxophone, then the variation of f_{c}^{Π} across the lattice can be treated as a measure of the degree of acoustical *irregularity* of a tonehole lattice. This is different from Keefe's interpretation, in which the local cutoff frequency is defined by the characteristic frequency f_{c}^{Π} of the first tonehole pair [16]. Here, all cells are considered and their variation throughout the lattice is interpreted as a deviation from perfect acoustic regularity.

Figure 5.7 shows the results of this theory applied to the geometry of an alto saxophone following a decreasing chromatic scale along the horizontal axis. For each fingering, the characteristic frequency f_{c}^{Π} of the first three pairs of open toneholes (when three are available, the lowest notes of scale have only one or two tonehole pairs available) are marked with circles and labeled in order with Roman numerals. The cutoff transition band $f_{\mathrm{t}}^{\mathrm{R}}$ is marked in light grey and asymmetric division (see Section 5.3.2) in dark grey.

There is considerable variation of f_{c}^{Π} from cell to cell, ranging from 500 [Hz] for cells

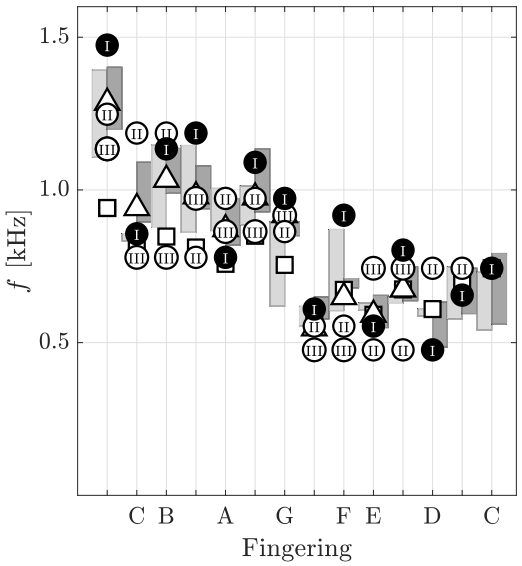

Figure 5.7: Estimation of the cutoff frequency for each fingering down to the low C (written, 156 [Hz]) of an alto saxophone. Data markers correspond to: the first three f_c^{Π} : Ⓘ Ⓘ Ⓘ; average of first three f_c^{Π} : △ ; average of all f_c^{Π} : □ ; asymmetric T-cells (see Section 5.3.2) : ■ ; transition band f_t^{R} : ■.

near the end of the lattice up to 1500 [Hz] for the highest cells. This indicates that the resonator cannot be considered acoustically regular. The variation is much greater than for the clarinet, which has cutoffs that typically range from 1150 [Hz] to 1450 [Hz] [22]. A visual inspection of the input impedance of all the fingerings (not shown) confirms that the cutoff increases substantially with increasing notes on the scale.

The characteristic frequencies for the first three open tonehole pairs follow the same downward trend as the measured global cutoff transition band for each fingering. This implies that an empirically observed cutoff on the input impedance or reflection coefficient is largely determined by the upstream (closest to the mouthpiece) open toneholes of the lattice for a given fingering. It is worth remarking that the (approximate) cutoff frequencies of the lowest notes in the scale are due to some combination of the conicity and flare of the bell, and can not be interpreted as the result of a tonehole lattice because there are not enough open toneholes to apply the theory of wave propagation in periodic media. This ambiguity is mentioned in Section 5.2.4, and demonstrates again why the tonehole lattice cutoff frequency is difficult to interpret for conical resonators.

5.3.2 Iterative cell division

The second method iteratively divides a tonehole lattice into acoustically regular asymmetric T-cells, as was done for the clarinet [22]. In contrast to Section 5.2, the tonehole is not necessarily located at the middle of the cell. This is permissible because the important acoustic components are the acoustic mass of the tonehole and acoustic compliance of the main bore, neither of which, at low frequencies, is impacted by the location of the

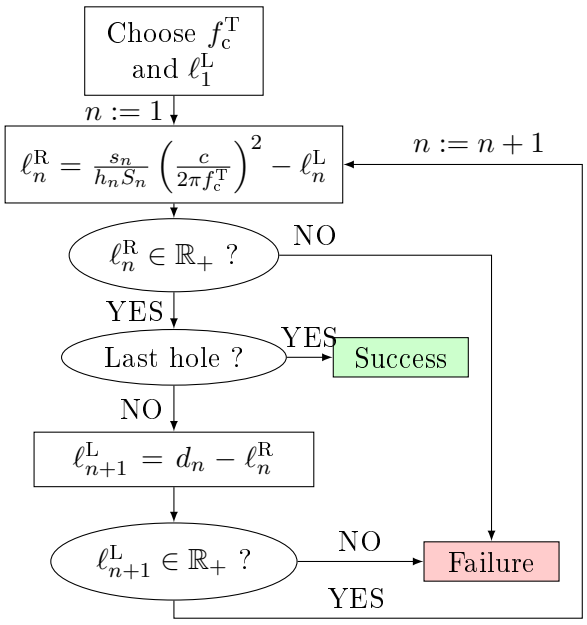

Figure 5.8: A flowchart of the asymmetric division algorithm described in Section 5.3.2 used to divide the acoustically regular lattices shown in Figure 5.9 and alto saxophone in Figure 5.10.

tonehole. The derivation follows the same steps as that of Eq. (5.13), except that in the asymmetric case the transfer matrix coefficient condition for the local cutoff frequency is $|A_n(k) + D_n(k)| = 2$ with $A_n(k) \neq D_n(k)$.

The n^{th} asymmetric cell with lengths ℓ_n^L and ℓ_n^R to the left and right of the tonehole has a local cutoff

$$f_c^T = \frac{c}{2\pi(\ell_n^L + \ell_n^R)}\left[\frac{1}{\sqrt{(h_n/(\ell_n^L + \ell_n^R))(S_n/s_n)}} + \mathcal{O}(k\ell)\right]. \tag{5.27}$$

As in Eq. (5.13), this is an approximate definition due to the number of terms retained in the Taylor expansion in $k\ell$ of the cotangent function.

A lattice can then be divided using iteration (see Figure 5.8) by choosing the initial length ℓ_1^L for the first cell and imposing a local cutoff frequency f_c^T. Because the tonehole dimensions are given, only ℓ_1^R can be varied to achieve the local cutoff frequency. The length of the right portion of the first cell ℓ_1^R, along with the distance to the next hole d_1, determines the left section of the next hole ℓ_2^L, and so forth for the entire lattice, see Figure 5.6. A division of the lattice is attempted for a wide range of initial lengths and eigenfrequencies: $\ell_1^L \in [0,\ d_1]$ [m] and $f_c^T \in [0.1,\ 3]$ [kHz]. Although it is mathematically possible for ℓ_n^L and ℓ_n^R to be complex, a lattice is only considered successfully divided if all ℓ_n^L and ℓ_n^R are real and positive, ensuring a physically realizable lattice. A successful division means that each cell of the lattice has the same local cutoff f_c^T, so the lattice is acoustically regular with a global cutoff f_c^G at this frequency. Because the constituent cells are allowed to be asymmetric, a single lattice can have a continuum of successful

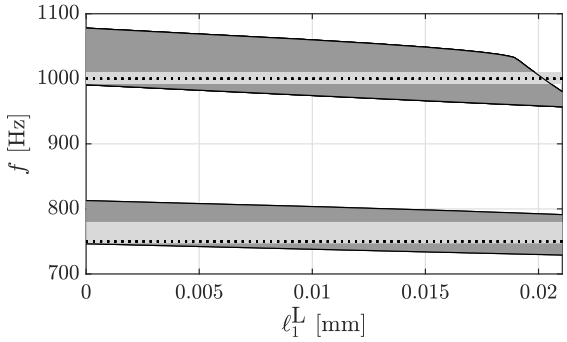

Figure 5.9: Cutoff frequencies found using asymmetric division (dark grey region) of acoustically regular conical lattices with global cutoff frequencies at 750 [Hz] (bottom) and 1000 [Hz] (top) for different initial cell length ℓ_1^{L}. The characteristic frequencies $f_{\mathrm{c}}^{\Pi} = f_{\mathrm{c}}^{\mathrm{T}}$ are marked by a dashed line, and the cutoff transition band $f_{\mathrm{t}}^{\mathrm{R}}$ by light shaded grey.

divisions, and the span of this continuum is interpreted as the breadth of admissible frequencies for which the resonator can be considered acoustically regular.

The asymmetric division algorithm is applied to two acoustically regular lattices designed following the criteria in Section 5.2.4 with global cutoff frequencies at 0.75 and 1.0 [kHz]. The dark grey region in Figure 5.9 depicts the continuum of successful asymmetric divisions of the two lattices. Additionally, the tonehole pair characteristic frequencies f_{c}^{Π}, marked as a dashed line, are all equal because the lattices are acoustically regular so $f_{\mathrm{c}}^{\mathrm{T}} = f_{\mathrm{c}}^{\Pi}$ for all cells. The cutoff transition band $f_{\mathrm{t}}^{\mathrm{R}}$ is shown in light grey. These plots show the coherence between symmetric and asymmetric cells, tonehole pair characteristic frequencies f_{c}^{Π}, and the reflection coefficient cutoff transition band $f_{\mathrm{t}}^{\mathrm{R}}$ when the resonator is acoustically regular.

The asymmetric division algorithm is applied to the geometry of a Buffet Crampon alto saxophone. Successful division of the lattice is only possible for select fingerings, all in the bottom range of the instrument. The reason for this is that several of the lowest toneholes have highly irregular spacing, and the asymmetric division fails to find a division of these cells for the eigenfrequencies possible for the upstream cells. This implies that the method of asymmetric division may be better suited for resonators that are highly acoustically regular, and application to the saxophone must be treated carefully. However, if the lowest three holes are excluded from the algorithm, division is possible for most notes. Division across all fingerings is possible when only the first 5 tonehole pairs (6 toneholes) of each fingering is included in the algorithm. The division for fingerings C and G♯ are shown in Figure 5.10, and their measured input impedance and reflection functions are provided in Figures 5.4 and 5.5, respectively. As before, the cutoff transition band $f_{\mathrm{c}}^{\mathrm{R}}$ is shown in light grey. The characteristic frequencies of the first three cells are marked by circles (black, grey, white, respectively), the average of the three by a triangle and the average of the whole lattice by a square.

Figures 5.4 and 5.5, corresponding to the high C and G♯ fingerings, appear to be quite different. However, the results of the asymmetric division are quite similar: the C

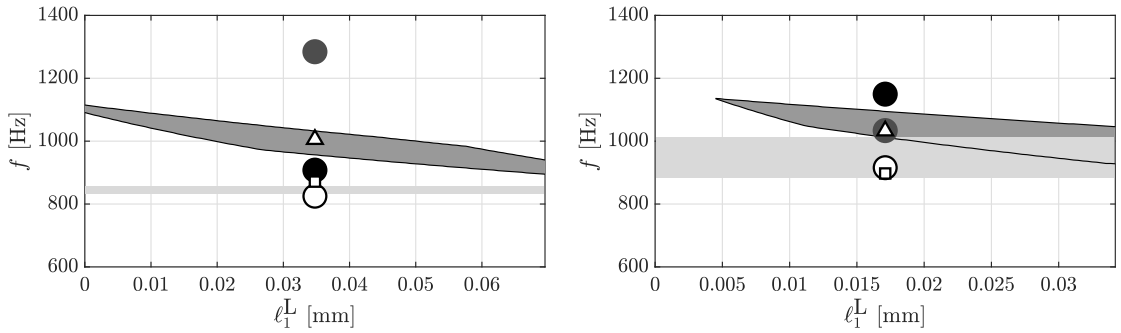

Figure 5.10: Comparison of three analysis methods. Successful asymmetric division (dark grey region) of an alto saxophone high C on left (written pitch, 311 [Hz]) and G♯ on right (written pitch, 246 [Hz]) fingerings for different initial cell length ℓ_1^{L}. The first three tonehole pair cell characteristic frequencies f_{c}^{Π} are denoted ● ● ○. The average of the first three Π-cells and of the entire lattice are provided by △ and □. The cutoff transition band $f_{\mathrm{t}}^{\mathrm{R}}$ is shown in light grey.

fingering division ranges between 940 and 1120 [Hz], and the G♯ fingerings between 930 and 1140 [Hz]. The difference in the range of initial lengths ℓ_1^{L} is not important because it is simply an arbitrary length of the resonator upstream from the first tonehole used to initiate the algorithm. As long as the algorithm arrives at a successful solution, the initialization does not matter because the degree of acoustic regularity is related to the span of possible global cutoff frequencies, and not the initial length ℓ_1^{L}. Therefore, although the continuum of successful divisions appear quite different for the two fingerings, the span of admissible global cutoff frequencies are quite similar.

The cutoff transition band $f_{\mathrm{t}}^{\mathrm{R}}$ is very narrow for the high C and relatively broad for the G♯. This is also evident in Figures 5.4, 5.5, and 5.7. Compared with other fingerings, the severity of the drop in the reflection function for the C fingering is unusually abrupt, and the width of the cutoff transition band varies considerably between fingerings.

5.3.3 Observations

Each type of analysis ($f_{\mathrm{t}}^{\mathrm{R}}$, f_{c}^{Π}, and asymmetric division of $f_{\mathrm{c}}^{\mathrm{T}}$) applied to the saxophone has advantages and disadvantages, and provides a different nuance to wave propagation in conical lattices. All three methods demonstrate an increasing cutoff for increasing notes in the first register as seen in Figure 5.7, which is consistent with observations of the input impedance of each note. This implies that all of these methods can be used to analyze the cutoff frequency of an alto saxophone, and the choice depends on the specific requirements of the study.

The cutoff frequency transition band and Π-cell calculations are likely the easiest methods to analyze a lattice, requiring either an input impedance measurement or the lattice geometry. These avoid complications that can arise using asymmetric division, such as the choice of how many cells to include when attempting to divide a highly

irregular lattice. The transition band is particularly appealing in the case of real woodwind instruments because it directly measures a cutoff behavior of the resonator, with no assumptions about acoustic regularity. However, it is not clear how well this method would work for other instruments, and it is possible that the thresholds would need to be adjusted for different instrument families.

5.4 Conclusion

This article provides some insights into why the cutoff frequency due to the toneholes of the saxophone is understudied compared with other instruments. The impossibility to define symmetric cells in a conical geometry is a difficulty that hinders all attempts of analytical study. An acoustic regularity can be defined to overcome the inherent geometric irregularity of a conical tonehole lattice, which can be used to design lattices to have a desired local cutoff. Even then, intrinsic acoustical characteristics of cones lead to more diffuse cutoff behavior than with cylinders. For real instruments, the influence of the bell, particularly for the lowest notes on the instrument, may contribute to the diffuse cutoff. Further work on this topic could include an investigation into the parameters that influence the efficiency of the cutoff, particularly for non-cylindrical resonators.

It is generally assumed that the cutoff remains fairly constant for different fingerings of a given instrument. Benade provides figures showing this phenomena for both cylindrical and conical instruments; the oboe, bassoon, and clarinet [3]. As seen here, the cutoff of the saxophone varies considerably across the range of one octave. Many notes, particularly in the higher range of the register starting around F (written pitch, 208 [Hz]), have only two impedance peaks to collaborate with the reed. Below F some notes have three or four strong impedance peaks, while the lowest notes with only one or two holes open have many more undisturbed impedance peaks. It would be interesting to study this in terms of perceived homogeneity of the timbre in the radiated sound field for different notes on the instrument. In link with sound production features, future studies could evaluate the role of the instrument maker in consciously setting the cutoff properties of the tonehole lattice, notably in compromise with the other design parameters.

Appendix

Table 5.2 provides the geometries for the two acoustically regular lattices used in this article. Both are used to test the asymmetric iterative division algorithm, Figure 5.9, described in Section 5.3.2. The simulated input impedance and reflection coefficient of the first resonator, shown in Figure 5.1, demonstrates the methodology of designing a conical resonator with an acoustically regular lattice presented in Section 5.2. The equivalent figure for the second resonator is not included to omit redundancy.

Both resonators have an apex angle $\theta = 0.028$ [rad] and in input radius $a_{\text{in}} = 6.25$ [mm], corresponding to the geometry of the alto saxophone analyzed in Section 5.3. The equations governing an acoustically regular lattice provide a wide range of options for the geometry of the toneholes. The geometries presented here attempt to follow general trends of an alto saxophone, although they are necessarily different because the saxophone is not acoustically regular.

Table 5.2: Dimensions of two acoustically regular resonators with different first impedance peak and theoretical global cutoff frequencies. Both resonators have an apex angle $\theta = 0.028$ [rad] and input radius $a_{\text{in}} = 6.25$ [mm]. The distance from the input to the n^{th} hole is denoted $w_n = r_n - x_1$, where x_1 is determined from the the apex angle and input radius.

Resonator 1: f_1 = 177 [Hz], f_c = 750 [Hz]				
hole n	w_n [mm]	a_n [mm]	b_n [mm]	h_n [mm]
1	712.9	26.2	10.5	13.2
2	744.5	27.1	12.3	15.4
3	779.4	28.1	14.4	17.0
4	818.0	29.2	16.5	17.9
5	860.6	30.4	18.9	18.0
6	907.7	31.7	21.5	17.4
7	959.7	33.1	24.3	15.8
8	1017.3	34.7	27.4	13.2
9	1080.9	36.5	30.8	9.6
10	1151.2	38.5	34.6	4.8
end	1188.0	395.2	—	—
Resonator 2: f_1 = 304 [Hz], f_c = 1000 [Hz]				
hole n	w_n [mm]	a_n [mm]	b_n [mm]	h_n [mm]
1	355.7	15.6	6.2	14.9
2	376.7	16.2	7.2	16.3
3	400.0	16.8	8.2	17.2
4	425.7	17.5	9.3	17.8
5	454.1	18.3	10.6	17.8
6	485.5	19.1	11.9	17.4
7	520.3	20.1	13.4	16.4
8	558.6	21.1	15.0	14.8
9	601.0	22.2	16.8	12.7
10	647.9	23.5	18.8	9.9
end	672.5	24.2	—	—

Chapter 6

Conclusion and future work

This dissertation contributes to the general knowledge of how the tonehole lattice cutoff frequency affects the sound production and radiation of woodwind instruments, presented through three peer reviewed articles in addition to previously unpublished results. This research serves two interests: the academic goal of fundamental research and the industry goal of scientifically guided instrument design, for which an attempt is made to treat both aspects in each chapter. Due to the article style composition of this manuscript, some global ideas that are presented individually across different and are grouped and synthesized here.

- A thorough theoretical exposition of periodic acoustic waveguides as applied to woodwind-type resonators is provided in Chapter 2. The detailed comparison between academic resonators and a real clarinet demonstrates the applicability of the theory to real instruments, which provides context for interpreting the results of prior studies in addition to guiding future research on the topic.
- The design protocol of the academic resonators proposed for cylinders in Chapter 3 and for cones in Chapter 5 for which it is possible to independently vary the first input impedance peak frequency and the cutoff frequency is, to the author's knowledge, a significant contribution to this field. These resonators can be used to study the effect of the cutoff from an academic perspective in addition to being incorporated as a design criteria for new instruments by instrument manufacturers.
- Collectively, Chapters 3 and chapter 4 provide quantitative results linking the effect of cutoff on sound production and radiation for cylindrical resonators. The cutoff frequency has a direct impact on the spectral characteristics of the pressure waveforms in the mouthpiece and the radiated soundfield, demonstrated for the first time using both simulations and measurements.
- The derivation of acoustically periodic conical waveguides is, to the author's knowledge, a new development in the analysis of periodic media. It is conceivable that this result could be adapted to other areas of acoustics.
- This work contributes the interpretation of acoustically irregular lattices to describe woodwind resonators. Acoustic regularity is an important link between geometri-

cally regular academic lattices and geometrically irregular woodwinds resonators. This notion is easily applied to some instruments, such as the clarinet, but is insufficient to describe instruments like the saxophone which are neither geometrically nor acoustically regular. Discussing the saxophone from the perspective of its deviation from acoustic regularity helps frame that instrument within the context of tonehole lattice cutoff frequencies. In particular, a resonator that has an acoustically irregular lattice can still exhibit cutoff type behavior when there is a slow evolution of the local cutoff frequencies of neighboring cells in the lattice.

– As part of studying acoustically irregular lattices, this work defines and explores the utility of multiple cutoff descriptors. This is useful because no agreed-upon definition of the cutoff exists for finite, lossy resonators. While none of the solutions proposed in this dissertation are appropriate for all types of resonators, they contribute as a set of objective cutoff descriptors which can be applied to real resonators for which the theory of periodic media is only approximate.

These projects were completed using a combination of analytical formulations, simulation, and experimental work, each chosen to identify a different aspect of the cutoff frequency, or to validate the results found using one of the other methods. The results demonstrate that the effect of the cutoff on the passive response of a resonator as well as sound production and radiation can be identified by all three types of study, each of which highlights different aspects of its influence.

While the results of these projects clearly demonstrate in quantitative terms how the cutoff effects woodwind type instruments, an emerging theme is that the cutoff of real instruments is often ambiguous and approximate. This is because instruments were not historically designed to be acoustically regular, and the analysis of woodwind resonators from the perspective of periodic waveguides sometimes succeeds, and other times fails. Furthermore, there are other factors that can contribute to a cutoff type behavior that is not due to the lattice of toneholes. This does not diminish the importance of the cutoff or invalidate the interpretation of woodwind resonators as periodic waveguides, but it is important to keep this distinction clearly in mind.

Preliminary results for two additional studies are provided in Appendix A and Appendix B. The first is a complementary study for Chapters 3 and 4, linking the internal and external acoustic pressure in terms of a transfer function. One goal of this project is to 'complete' the description for how the cutoff affects sound production and radiation, acting as bridge between the two studies. Appendix B presents preliminary results that complement Chapter 5, this time with applications to the bassoon. This work demonstrates that the methods developed for the saxophone are robust when applied to another instrument, an important result that exemplifies the generality of the methodology.

Developing both of these appendices is a natural place to begin for future research. For example, as an extension of Appendix B, an attempt could be made to identify more robust descriptors that work with a greater number of instruments, or to describe differences between instruments in the same family such as the various saxophones. The descriptors could be made more illustrative by incorporating multiple bands of the reflection coefficient in order to quantify the efficiency, or severity, of the lattice cutoff. Additionally, the descriptors could be used for automated detection of the cutoff. This

could be used to incorporate the cutoff in an optimization cost function for numerically aided instrument design.

There are many additional research topics that could continue the work in this dissertation. Some of these remain very close to the core topics treated here, while others are broader and would require considerable more work and collaboration with researchers in adjacent fields. As mentioned in Chapter 2, the role of the bell as a surrogate tonehole lattice is not fully established. It has already been mentioned that the bell likely influences sound production much like a lattice for the lowest notes of the instrument, but this could be developed to see how the bell differs from a lattice in terms of radiation.

It would also be interesting to trace the evolution of the cutoff frequency from historical to modern instruments, as was done for flutes [24, 116] and other acoustic quantities for stringed instruments [117]. Baroque, classical, and modern flutes have successively higher cutoffs due to an increase in the number and average radius of toneholes, and it is not unreasonable to expect this trend to be true for other woodwinds. This type of study could demonstrate (unconscious?) strategies adopted by manufacturers to achieve a satisfactory instrument, appropriately balancing competing requirements such as proper intonation, ease of playing, ergonomics, and radiation. This would be interesting to do in tandem with a study the interaction between the cutoff and reed resonance. From a broader perspective, one could ask if the perceptual effects of the cutoff evolution is mirrored in other instruments families, such as the strings or percussion, or even in evolving musical styles.

Lastly, and perhaps the most interesting, is to evaluate the effect of the cutoff on perceived characteristics of an instrument through subjective listening experiments. For example, one could try to map musician adjectives to the radiated sound of instruments with different cutoffs. Another open question relates to the importance of cutoff on perceived homogeneity across the first register of an instrument: each note of the clarinet has nearly the same cutoff, while the cutoff varies substantially across the register of the saxophone. How this influences perceived characteristics, and whether one or the other is a desirable trait, is unknown.

In a very general sense, this dissertation began with the general assumption that the cutoff has a large influence on the perceived characteristics of a woodwind instrument. The different studies provided in this manuscript demonstrate quantitative links between the cutoff on linear characteristics of a resonator and its effect on sound production and radiation. Future work should evaluate the perceptual importance of these effects, in addition to incorporating the cutoff as a design parameter while developing new instrument and modifying existing models.

Supplementary material A

Passive response of resonators: simulations and measurements

In Chapter 4, the effect of the cutoff on the radiated sound field is evaluated using *in situ* measurements under playing conditions. This is defended as a reasonable measurement protocol when the experiment is designed to give musically relevant results. However, some aspects of the effect of cutoff on radiation that constitute a more basic acoustical description of the resonator are obscured in that type of experiment. In particular, the effect of cutoff on external characteristics, such as radiation efficiency and directivity, are purposely ignored in Chapter 4. These topics are addressed in the current appendix.

In contrast with Chapter 4, the effect of the cutoff frequency on basic radiation properties is more easily studied by stimulating the resonator in the absence of auto-oscillation and under anechoic conditions, while keeping the source and receivers stationary in space. This allows for a detailed picture of the transfer between internal and external acoustic variables, with a much greater frequency resolution than that provided by the harmonics of an instrument under playing conditions. The measurement protocol is considerably more involved: the resonator is stimulated by a compression driver, a connection piece is 3D printed, multiple microphones must be calibrated, and the data acquisition equipment and amplifiers are in a control room while the measurements are performed in an anechoic chamber. However, the added effort is justified because it provides a deeper understanding of the effect of cutoff on radiation in addition to validating the simulations used in Chapter 4 [118]. The measurement results combined with an analytic simulation encourages additional simulation techniques, for which preliminary results are reported at the end of the appendix.

Additional comments

The remainder of this appendix is a partial reproduction and substantial extension of the conference proceedings:

E. Petersen and R. Rosser. External sound field simulations and measurements of woodwind resonators. In *Proceedings of ISMA 2019 International Symposium on Music Acoustics*, pages 58–61, 2019 International Symposium on Musical Acoustics, Detmold, Germany, Sept. 2019.

Comments:

The methodology and results presented here are currently in an unfinished state. In particular, additional details on the measurement procedure and the BEM simulations are needed to complete the description. However, the results appear promising and relevant to the main text of this dissertation, and are therefore worth reporting within the context of an appendix. The author intends to further develop the work.

A.1 Simulation of external soundfield

In order to predict the radiating characteristics of a resonator, the transfer function between a source inside the resonator and an external observation point is simulated. The simulation relies on the Transfer Matrix Method with external Interactions (TMMI) [28], a variant of the classic Transfer Matrix Method (TMM). This is the same method used in Chapter 4, but adapted in order to be compared with measurements.

The TMMI is designed to simulate the input impedance of a resonator by assuming a fictitious flow source $U^s(\omega)$ and calculating the resulting pressure and flow $P_n(\omega)$ and $U_n(\omega)$ at each n^{th} radiating aperture, accounting for the mutual radiation load between sources that radiate into the same space. An intermediate transfer function between the source flow and tonehole flow is

$$H_n^{\text{U}}(\omega) = U_n(\omega)/U^s(\omega), \tag{A.1}$$

where U^s has equal amplitude and phase for all frequencies. It is numerically equivalent to calculate a transfer function using a source pressure P^s with equal amplitude and phase for all frequencies

$$H_n^{\text{P}}(\omega) = U_n(\omega)/P^s(\omega). \tag{A.2}$$

Ignoring the presence of the body of the resonator, the holes can then be approximated as an array of monopole sources. The pressure at some observation point O is the summation of the contributions of each U_n, accounting for a propagation delay and spherical spreading:

$$P_O(r,\theta,\omega) = \sum_{n=1}^{N} j\omega\rho \frac{H_n^{\text{P}}(\omega)P^s(\omega)}{4\pi r_n} e^{j(\omega t - kr_n)}, \tag{A.3}$$

where r_n is the distance between the n^{th} hole and O [30, 189]. This model assumes anechoic conditions and ignores absorption in air. The corresponding transfer function is

$$H_O^{\text{P}}(r,\theta,\omega) = \frac{P_O(r,\theta,\omega)}{P^s(\omega)}. \tag{A.4}$$

While it may be more physically relevant to calculate $P_O(r,\theta,\omega)$ from a flow source term $U^s(\omega)$, the remainder of this appendix uses a pressure source term $P^s(\omega)$ which is more convenient for comparing with measurements.

A.2 Experimental design

The simulated transfer functions are validated by measurements performed in the LMA anechoic chamber. Internal and external pressures corresponding to the simulated $P_O(r,\theta,\omega)$ and $P^s(\omega)$ are measured, from which the transfer functions are calculated in the form of Eq. (A.4). Note that in this case the source term $P^s(\omega)$ does not have equal amplitude and phase for all frequencies as it does in the simulations. The resonators used in the current appendix are the same as those used for the *in situ* measurements in Chapter 4, although only the results corresponding to the resonator with a 1000 [Hz] cutoff are pre-

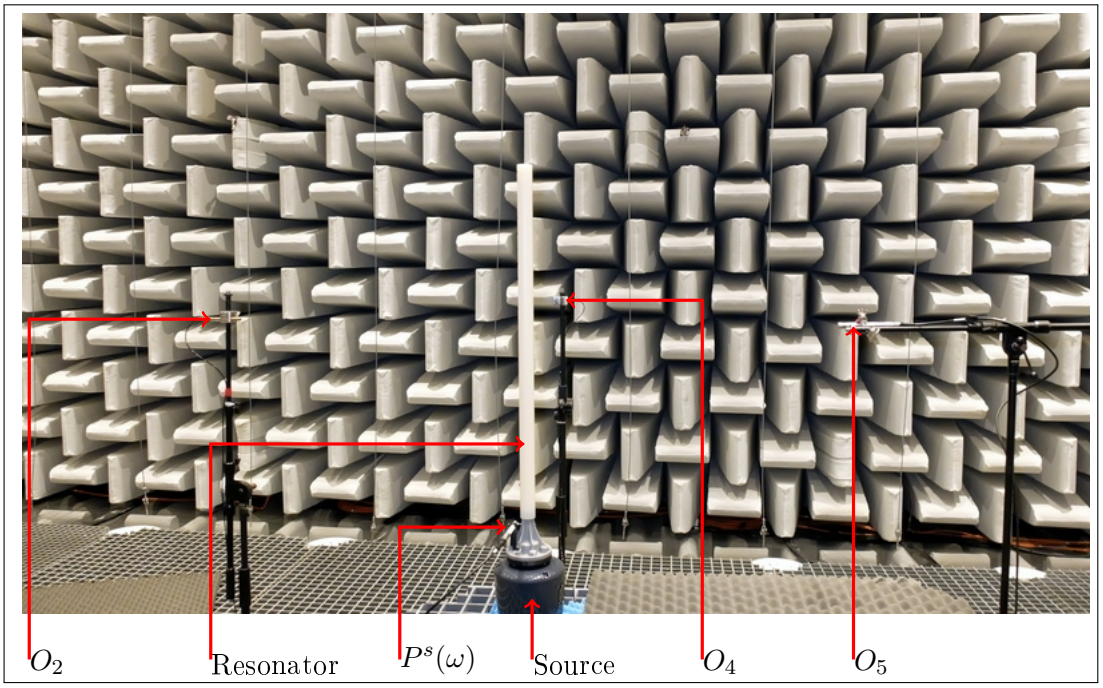

Figure A.1: Experimental installation with camera facing along the $-x_2$ axis; the perspective is the opposite from that shown in Figure Figure A.2. The resonator is positioned vertically (lattice on the upper half) on top of the compression chamber and adapter piece ensemble and microphones O_2, O_4, and O_5 are visible. There are absorption wedges under the grated floor. The equipment is supported on a grated table, covered with a sheet of foam.

sented here in order to be compared with additional simulations in Section A.4. However, the trends observed on the radiation of this resonator are representative of the resonators with 1500 [Hz] and 2000 [Hz] cutoffs.

The resonators are connected to a compression chamber using a 3D printed adapter piece shown in Figure A.1. There is a six [cm] section of cylinder with a 7.45 [mm] interior radius that is inserted into the part of the resonator that accepts a mouthpiece, with a microphone mounted at the midpoint. Upstream from the cylindrical portion the adapter flairs slowly to match the mouth of the compression driver. The pressure measured by the interior microphone is treated as the source pressure $P^s(\omega)$ in Section A.1. The radiated pressure was measured at five external locations, the positions of which are shown in Fig. A.2.

The anechoic chamber has acoustic wedges on all four walls as well as the ceiling and floor. However, the metal grating that allows the experiment installation was not removed, which could introduce diffraction. Foam was placed on the ground between the table and the furthest microphone in an effort to mitigate this problem. The resonator/adapter piece/compression driver ensemble was placed on a grated table, along with the microphone conditioners, also covered in foam. The rest of the data acquisition chain was located in a pilot room. Microphone calibration was verified using a 1 [Pa] at

1 [kHz] pistonphone.

A.2.1 Reference coordinates

The resonator is positioned vertically with the lattice above the leading duct. The coordinate system is referenced relative to the center of the first open tonehole, on the 'surface' of the exterior of the resonator. The center of the n^{th} tonehole (for $n = 1$ to 10) is located at [0, 0, (n-1)0.0326] [m]. The center of the termination is located at [-0.0163, 0, 0.3097] [m], where the negative x_1-coordinate offset relative to the toneholes is due to the radius and wall-thickness of the resonator. The equivalent monopole source terms described in Section A.1 are centered at these coordinates.

Note that the transfer functions to locations O_2, O_4, and O_5 should all be very similar due to the approximate rotational symmetry of the resonator. Deviation from this rotational symmetry is due to the non-zero x_1 coordinate of the termination of the resonator, any directivity that may exist for the toneholes, and diffraction due to the body of the resonator. The analytic simulations are only able to account for the first of these three causes.

All the observation points except O_3 have negative x_3-coordinates because this setup was also used for other resonators with different tonehole locations. The resonators were changed but the microphone locations remained fixed. For each resonator, the coordinate system is defined relative to the first tonehole, leading to the unintuitive negative x_3 values. Furthermore, the reported microphone coordinates likely have a large degree of error. This is one aspect of the measurement setup that needs improvement. However, the results in Section A.3 suggest that these discrepancies are not very detrimental.

A.2.2 Excitation signal and processing

Pure sinusoidal excitation signals sent to the compression driver are used to stimulate the resonator from 100 Hz to 4000 Hz in steps of 10 Hz. The internal sound pressure level is approximately 120 [dB], between the levels typically used to measure the linear input impedance and nonlinear playing conditions. This signal is used instead of a frequency sweep because the radiation from the resonator is very weak: the coherence function calculated using a sweep type signal was only robust in the vicinity of the impedance peaks [120]. The measured signals are band filtered from 50 Hz to 6000 Hz and windowed to retain only the stable portion of the signal $p^s(t)$. Peak amplitudes of the i^{th} harmonic are extracted using synchronous detection

$$P_O(r, \theta, \omega_i) = |2 < p_O(r, \theta, t) \cdot e^{j\omega_i t} >|, \tag{A.5}$$

for the external measurements and

$$P^s(\omega_i) = |2 < p^s(t) \cdot e^{j\omega_i t} >|, \tag{A.6}$$

for the internal measurement. This method is valid because the frequencies are precisely known and stable. In the following analysis only the fundamental frequency ($i = 1$) is considered because there is very little energy at higher harmonics. As with the simula-

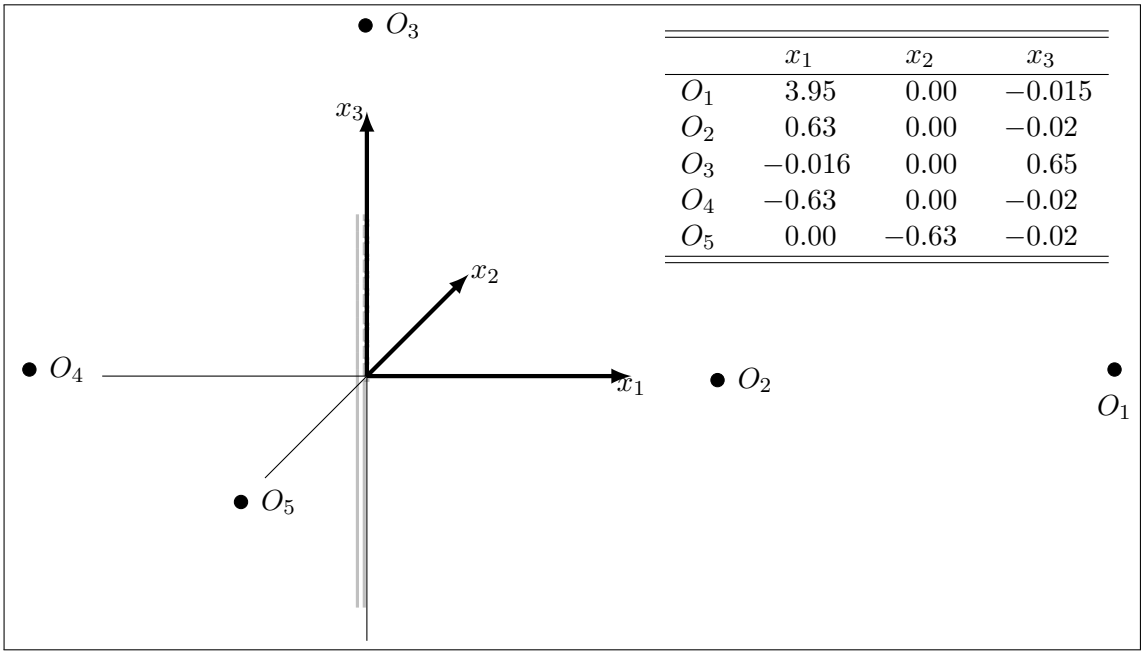

	x_1	x_2	x_3
O_1	3.95	0.00	−0.015
O_2	0.63	0.00	−0.02
O_3	−0.016	0.00	0.65
O_4	−0.63	0.00	−0.02
O_5	0.00	−0.63	−0.02

Figure A.2: The reference coordinate system is centered in the location of the first tonehole with the lattice extending along the positive x_3 axis. The schematic is to scale except point O_1, which is farther in the room than it appears here. All units are in meters.

tions, the measured transfer function between internal and external pressure is defined by Eq. A.4.

A.2.3 Internal and external pressure

The measurement results of the resonator with a cutoff at 1000 [Hz], processed using Eqs. A.5 and A.6, are shown in Figure A.3. Due to a limitation of hardware, the five microphone locations were divided into two configurations: O_1, O_2, and O_3 (left panel), followed by O_2, O_4, and O_5 (right panel). In addition to the internal microphone, position O_2 remains fixed between the two configurations as a control.

This relatively unprocessed representation of the data is informative about the radiation characteristics of these academic resonators. Most striking is their inefficient radiation, with approximately 40 to 90 [dB] difference between the internal microphone and the microphones less than 1 [m] away from the first open tonehole. The very similar measurements at low frequencies demonstrates the monopole radiation below cutoff, where the vertical offset of O_1 is due to spherical spreading. The strong directivity lobe perpendicular to the lattice at cutoff is seen by the high amplitudes measured by all microphones except O_3, which is not in same plane. The right panel shows slight frequency dependent differences between O_2, O_4, and O_5. This is likely due to the asymmetry discussed in Section A.2.1

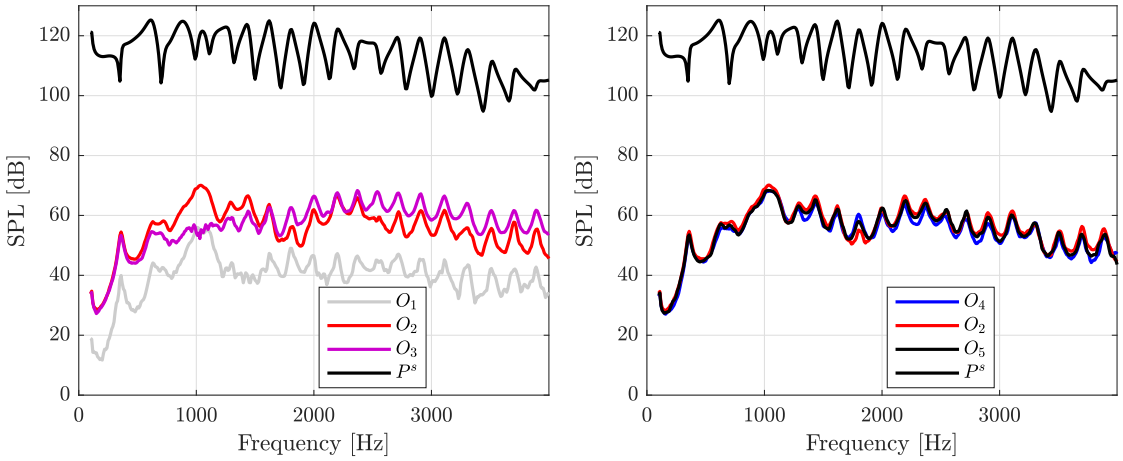

Figure A.3: Measured pressures for internal and external microphones. Two rounds of measurements correspond to two microphone configurations (see text for details). The black curves and the red curves correspond to microphones that are identical for the two configurations. The pressures shown in the right panel correspond to the nearly axis-symmetric locations.

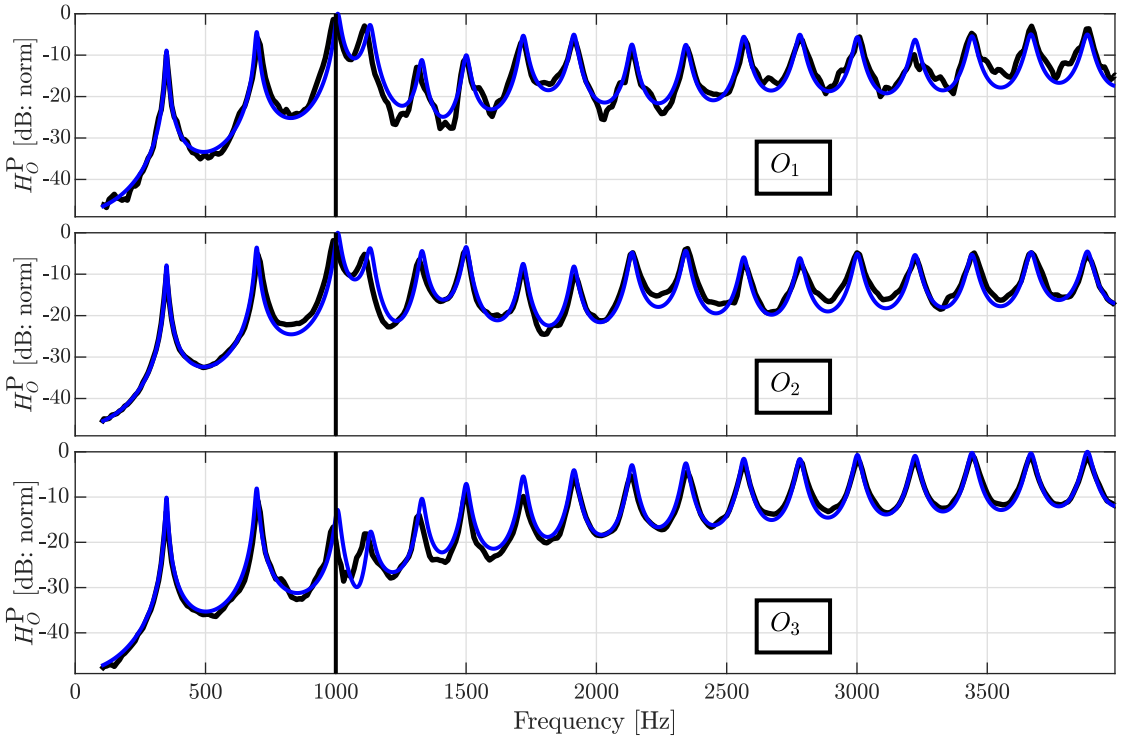

Figure A.4: Transfer function results for simulations in blue and measurement results in black for positions O_1, O_2, and O_3.

A.3 Simulation and measurement results

The simulated (Eq. (A.4)) and measured transfer functions for locations O_1, O_2, and O_3 are plotted in Figure A.4. Each panel is normalized by the maximum of the simulated curve. The simulations are in good agreement with the measurements. Around the cutoff, the simulations tend to predict peaks at slightly higher frequencies than those that are measured. The cause of this is unknown, although similar discrepancies are seen between the simulated and measured input impedance. It is not unreasonable to expect the frequencies for which there is a large transition in acoustic response of the resonator to be particularly sensitive to model errors such as assumed radiation impedance and the model of the tonehole acoustic mass, for instance.

There are also some discrepancies at high frequencies for O_1. This appears to be measurement noise. Figure A.3 shows that the sound pressure level measured by this microphone at those frequencies is approximately 40 [dB]. Furthermore, the metal grating of the floor in the anechoic chamber was not removed for these measurements, possibly leading to diffraction [121]. Despite these differences, the simulations compare favorably with the measurements.

There are two subtleties worth a reminder at this point: the first is the difference between transfer functions that use pressure and transfer functions that use flow as the interior variable, while the second relates to how the reference plane of the internal microphone affects the results. Physically, the resonator/adapter piece/compression driver has an acoustic response that relates to the entire ensemble of equipment. Input impedance peaks (at low frequencies) of this system occur for frequencies where $U_1(\omega)$ is large and $U^s(\omega)$ is small, corresponding to the quarter wave resonator model. These peaks also correspond to peaks in the transfer function $H_O^{\mathrm{U}}(r,\theta,\omega) = P_O(r,\theta,\omega)/U^s(\omega)$ because the radiation strength of a simple source n is proportional to its flow $U_n(\omega)$. In contrast, the transfer function $H_O^{\mathrm{P}}(r,\theta,\omega) = P_O(r,\theta,\omega)/P^s(\omega)$ has peaks when $P_O(r,\theta,\omega)$ is large and $P^s(\omega)$ is small. This condition corresponds to a half-wave length interpretation, such that the first peak in $H_O^{\mathrm{P}}(r,\theta,\omega)$ should be approximately double the frequency of the first peak in $H_O^{\mathrm{U}}(r,\theta,\omega)$.

This is reflected in the measurements and simulations: the first peak in $H_O^{\mathrm{P}}(r,\theta,\omega)$ occurs around 350 [Hz] while the first input impedance peak at the plane of the driver is about 165 [Hz]. This introduces the second subtlety. It is normal that the first peak in $H_O^{\mathrm{P}}(r,\theta,\omega)$ is at a frequency that is more than double the first input impedance peak frequency for two reasons. The first is that there is a cross section change between the adapter piece and the resonator, which makes the quarter- and half-wave resonator descriptions less accurate. The second reason is that the physical resonance of the ensemble is determined from the surface of the vibrating membrane, where as the internal acoustic variable $P^s(\omega)$ is measured about 10 [cm] downstream from the membrane. The effective quarter-wave length of the whole system from the loudspeakers perspective is slightly longer than the effective half-wave length measured by the internal microphone, resulting in a first maximum of $H_O^{\mathrm{P}}(r,\theta,\omega)$ that is more than double the first maximum of $H_O^{\mathrm{U}}(r,\theta,\omega)$. These are not meant to be new observations, but serve as a reminder when interpreting the following figures.

A.4 Preliminary results: additional simulations

The simulation and measurement results presented in Sections A.1, A.2, and A.3 are part of a project that is not yet complete. This work is complemented by additional numerical simulations for which preliminary results are presented in the current section. These numerical simulations are based on internal LMA boundary element method (BEM) codes known as FELIN. A detailed explanation of how these codes differ from commercial BEM software packages is provided in a recent Journal of the Audio Engineering Society [122].

A.4.1 Mutual radiation impedance

The numerical method is first used to estimate the mutual impedance between apertures radiating into the same space in order to compare with the analytic model. In the TMMI simulation, mutual impedance between the n^{th} and m^{th} $(m \neq n)$ toneholes is

$$Z_{nm} = jk\rho c \frac{e^{-jkd_{nm}}}{4\pi d_{nm}}, \tag{A.7}$$

where d_{nm} is the distance between the two apertures (see [28] Eq. 16). The factor 4 in the denominator corresponds to radiation in full space and can be replaced by a factor 2 for radiation in half space. The mutual impedance of nearby toneholes is greater than those that are distant. An N by N radiation impedance matrix has self impedance terms $(m = n)$ on axis and mutual impedance terms off axis, which can be set to zero to neglect their contribution.

The numerical BEM computation reconstructs the elements of the N by N matrix from the geometry of the resonator. The surface is divided into a mesh and the pressure at the surface of the n' element plus any contribution from the m' element is

$$P_{n'}(\omega) = Z_{n'n'}(\omega)U_{n'}(\omega) + Z_{n'm'}(\omega)U_{m'}(\omega) \tag{A.8}$$

where $Z_{n'm'}(\omega)$ is the mutual impedance between the two elements. The total pressure at the n' element is the sum of its own contribution and all other m' elements. Elements that are not at the location of a tonehole have a velocity equal to zero. Due to the fine mesh necessary to resolve frequencies above cutoff, the number of elements n' and m' is much greater than the analytic N by N matrix.

It is assumed that at any point in time the pressure is uniform across the surface of a tonehole, equal to the average of the constituent elements. Additionally, the velocity is assumed to be constant across the surface of the tonehole and equal to the average of the flow at each element divided by its area. These terms are used to reconstruct the N by N mutual impedance matrix using a numerical simulation that does not assume each tonehole acts as a monopole while also accounting for the presence of the resonator.

There are now four distinct impedance matrices to account for radiation into the same space: the analytic expression for mutual impedance in full space radiation (Eq. A.7 with a factor 4), the analytic expression for mutual impedance in half space radiation (Eq. A.7 with a factor 2), ignoring mutual impedance by using a diagonal matrix, and the numerically calculated mutual impedance matrix.

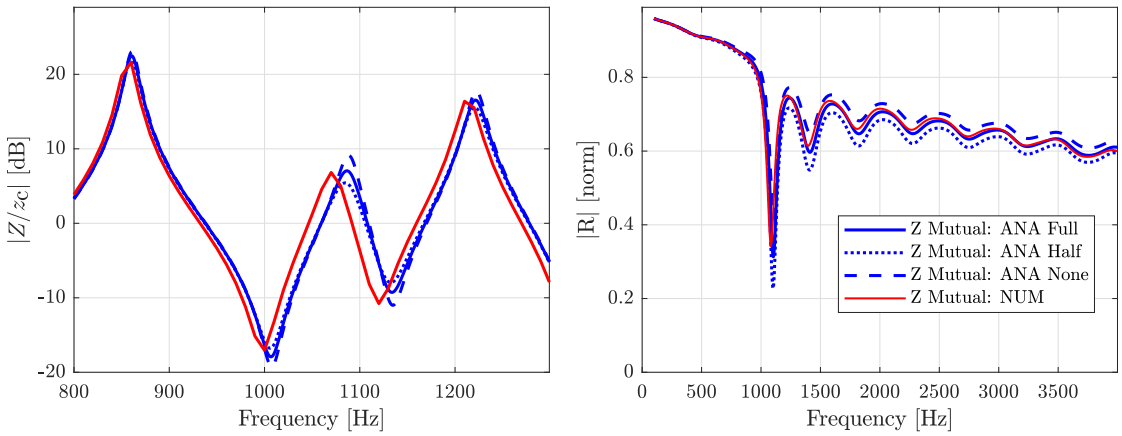

Figure A.5: Input impedance and reflection coefficient modulus using four mutual impedance approximations: analytic for radiation in full space, half space, no mutual impedance, and a numerically calculated mutual impedance.

The rounded form the resonator is approximated using only flat surfaces such that the cross-section is a decagon. This allows the toneholes to fit entirely within one surface. The surface of this object, including the toneholes, is described by a N=5524 element mesh. The impedance matrix is calculated at a rate of approximately one frequency per 15 minutes.

A.4.2 The influence of mutual impedance on internal variables

The input impedance and reflection coefficient can be calculated by the TMMI using these four mutual impedance approximations. Figure A.5 shows the input impedance modulus focusing on the frequency range around cutoff on the left panel and the reflection coefficient modulus over a larger frequency range on the right panel. Several trends emerge: above cutoff, the input impedance peaks calculated using the numerical mutual impedance terms are shifted approximately 10 [Hz] lower in frequency compared with the analytic results, corresponding to approximately 20 cents at 1000 [Hz] The resonances above cutoff are related to the total length of the resonator, so appears that the numerical model predicts a slightly longer effective acoustic length at the termination of the lattice. It is not appropriate to compare peak amplitudes between the numerical and analytic simulations because the numerical values were calculated for 10 [Hz] frequency steps, and do not fully resolve the input impedance peaks.

Due to the greater computational efficiency of the analytic method the simulations are calculated with 1 [Hz] frequency steps, which allows for a comparison of the peak amplitudes for the three analytic mutual impedance hypotheses. In particular, below cutoff they are all nearly identical, with less than 0.1 [dB] difference in amplitude for the first input impedance peak. At and above cutoff the input impedance peak amplitudes vary by 3-4 [dB]. Accounting for no mutual impedance results in the highest peaks and accounting for radiation in a half space results in the most attenuated peaks. This

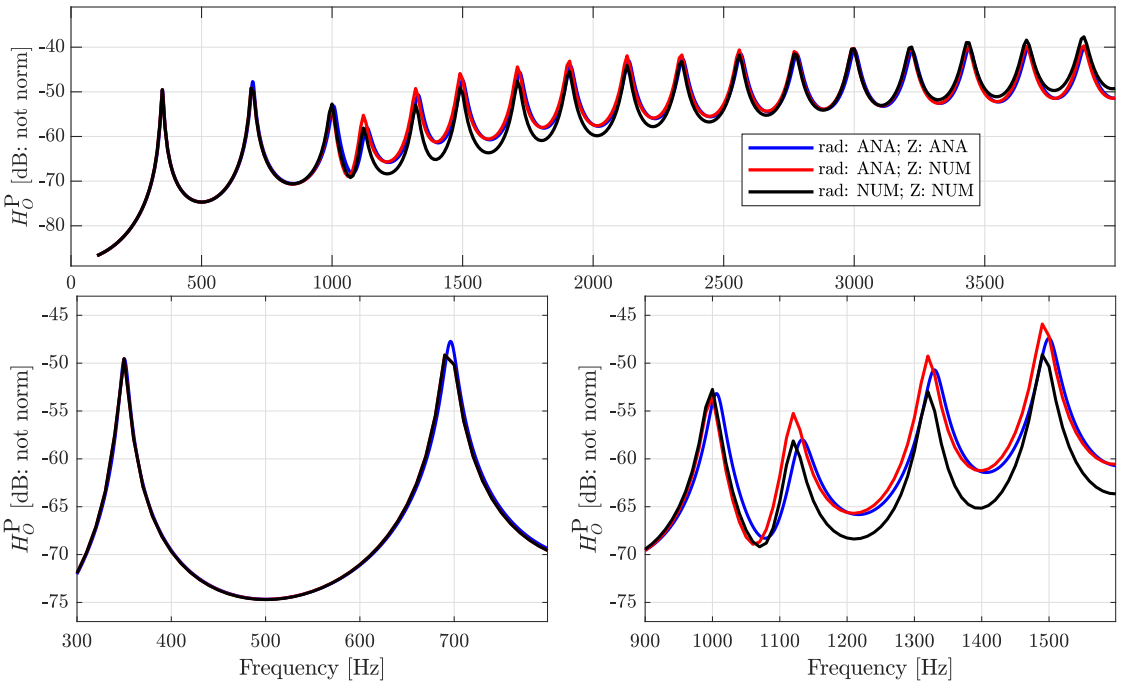

Figure A.6: Simulated transfer functions for location O_3 using a monopole radiation model with analytic mutual impedance (blue), monopole radiation model with numeric mutual impedance (red), and numeric radiation model with numeric mutual impedance (black). Bottom panels are expanded views of top panel.

particular resonator is a subdued example of these differences due to the relatively large spacing between toneholes. Figure 3.4 in Chapter 3 shows a more extreme example.

The reflection coefficient modulus shows that, above cutoff, the numerical results appear to be bounded by the most extreme analytic assumptions: that of no mutual impedance and that of half space radiation. As for the input impedance modulus, the exact amplitude of deep dips may be misleading due to insufficient frequency resolution of the numerical method. A suitable interpolation of the numerical mutual impedance will be useful for future analysis.

These are some examples of how the mutual radiation impedance conditions can effect simulations of internal variables. It may also be of interest to study the effect of the mutual impedance model on phase and group velocity within the lattice.

A.4.3 Diffraction due to resonator body

The BEM codes can also be used in a hybrid approach to estimate the effect of diffraction due to the presence of the resonator on the transfer functions between internal and external pressure. As a reminder, the simulations in Section A.1 calculates the flow in each tonehole using the TMMI. Then, the flow in each tonehole is replaced by a monopole with an equivalent flow, ignoring both the body of the resonator and any directivity that

the tonehole may have. The external pressure is then simply the sum of each monopole contribution assuming wave propagation in free space. To improve this simulation, the radiation portion of the simulation is performed using the BEM codes which account for the body of the resonator. This is a hybrid approach because the tonehole flow is provided by the TMMI calculations. The transfer functions can now be simulated using any of the four mutual impedance estimations with either the analytic and numerical radiation models.

Figure A.6 shows the results for location O_3 using the analytic radiation model and analytic mutual impedance (assuming full space radiation), the analytic radiation model with the numerical mutual impedance, and the numerical radiation model with numerical mutual impedance. The bottom panels show a closer view for frequencies well below cutoff (left) and frequencies near cutoff (right).

Below cutoff, all three mutual impedance estimations and both radiation models simulate essentially the same transfer functions. Above cutoff, the differences between the black, blue, and red curves can be attributed to the effect of the mutual impedance models or radiation models. The difference between the blue and red curves demonstrates a relatively small influence of the mutual impedance models on the transfer function. The larger offset of the black curve indicates a greater impact due to the radiation model. As for the internal variables, the numerical mutual impedance calculations result in peaks that are shifted lower in frequency by about 10 [Hz], seen on both the black and red curves.

In order to quantify the vertical offset created by each simulation, a descriptor based around the root-mean-square (rms) value of each peak region is defined. The transfer function is separated into bands that are defined by the local minima between peaks, and the rms value is calculated for each peak band. This is viewed as a crude approximation of the difference in simulated radiation efficiency. This construction is useful because a simple subtraction of one transfer function curve from another yields distorted results due to the offset of the peak frequencies.

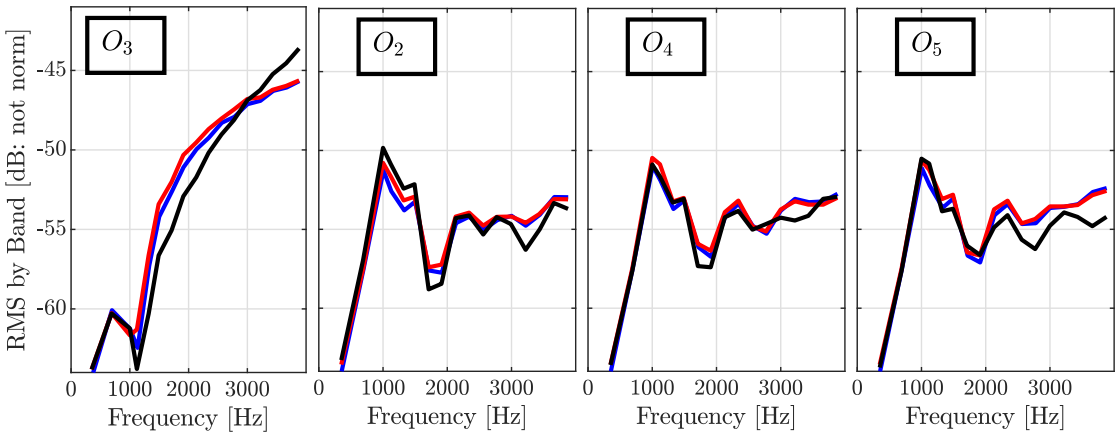

Figure A.7: Root-mean-square of peak bands for locations O_3, O_2, O_4, and O_5. The colors correspond to the same mutual impedance and radiation models in Figure A.6.

The results are shown in Figure A.7 for positions O_3, O_2, O_4, and O_5, where the colors correspond to the legend in Figure A.6. In all four panels the blue and red curves are more similar to each other than to the black curve, except possibly at the cutoff, indicating that the radiation model has a greater influence on this descriptor than the mutual impedance model.

The right three panels correspond to the microphone locations for which the analytic radiation model is least suited, as discussed in Section A.2.1. For these locations, the three microphones are in the same plane, equidistant from the origin of the coordinate system. The analytic radiation model predicts nearly symmetric radiation about x_3-axis, where any deviation from symmetry is due to the termination of the lattice located at [0, 0, -0.0163] [m]. The slight differences between the red curves (or blue curves) across these three panels indicates the slight deviations that the analytic radiation model is able to predict due to the offset of the termination of the lattice. The change of the black curve across the right three panels demonstrates the relatively large differences that the numerical radiation model is able to simulate because it accounts for any directivity of the toneholes and diffraction from the resonator body.

A.5 Discussion and future work

The results in Sections A.3 and A.4 are generally coherent with one another. The first shows that the analytic simulations match the measurements reasonably well. A deeper analysis to determine if the numerical simulations provide a better match with the measurements is an ongoing aspect of this project. However, a major conclusion of these results is lost when quantifying the differences between the simulations: all of them match the measurements with reasonably accuracy, but the analytic simulation in Section A.1 is both easier to implement and executes on the order of 10^6 times faster than the numerical method. From this perspective, the desired results will determine which method is most appropriate for a given study.

Related to this, one complication that arises when comparing different mutual impedance and radiation models is the coarse frequency spacing of the numerical simulations. These could be overcome by launching a numerical simulation for approximately five weeks. A better option may be to use a peak fitting scheme to interpolate between data points, the method that will likely be employed in the continuation of this project. This will facilitate a more detailed analysis of peak frequency and amplitude, possibly demonstrating that two of the three results (two simulation methods, one measurement) are more similar than the third.

In addition to refining the numerical simulations, the project would benefit from some additional measurements. In particular, an additional measurement location O_6 located at [0.00, 0.63,-0.02], corresponding to the 'mirror' image of O_5, would be interesting because both the analytic and numerical radiation models predict identical results O_5. Any measured difference will indicate what room effects might be present in the measurements. However, the differences could arise from a large number of causes such as asymmetry of the measurement table, the presence of the microphone conditioners (already covered with foam), microphone calibrations. These sources of error, which were reasonable to ignore before, could complicate the analysis.

It would also be interesting to repeat the measurements using sound pressure levels corresponding to *forte* playing levels of a clarinet. The measurements presented here were repeated at internal sound pressure levels approximately 10 [dB] above and below those shown in Figure A.3 without a substantial change in the resulting transfer functions. However, internal sound pressure levels corresponding to *forte* playing levels, at perhaps 170 [dB], have not yet been tested. This could have an impact on the transfer functions due to nonlinear behavior of the toneholes. However, this would require a review of the experimental setup to prevent possible damage to the equipment.

Another extension of this project is to further exploit the custom BEM codes, which are designed to calculate the radiation modes of an object [123, 124, 125]. The modes are weighted by near field measurements and are then used to simulate far field radiation patterns. As before, this is a hybrid approach in that uses measurements to calibrate the numerical model. This would provide more detailed directivity patterns than those that can be calculated from Eq. (A.4), accounting for the directivity of the toneholes and diffraction from the body of the resonator. However, this methodology is an active area of research and it is unknown how it will perform when applied to musical instrument type sources. If successful, it may be a useful when very detailed simulations are necessary, for example in auralizations.

Supplementary material B

Cutoff of the bassoon

Chapter 5 derives the theory of wave propagation in periodic media for the case of a conical resonator, and then applies it to the bore of a saxophone. In order to better understand the saxophone as a periodic waveguide, it was helpful to develop several additional methods to analyze the acoustical periodicity (and deviation from acoustical periodicity) of the tonehole lattice. The conclusion is that the bore of a saxophone has some properties that allow it to be treated as an acoustically regular conical resonator, but that a more nuanced approach recognizes the gradual change in cutoff frequency across the range of the resonator as a defining acoustic characteristic that distinguishes it from other woodwind instruments.

The purpose of this supplementary material is to present some preliminary results of a study determining the generality of these methods when applied to other woodwind resonators. Here, the bassoon is chosen as the object of analysis for both scientific and practical reasons. In order to compare with the results from the saxophone, only conical instruments were considered. Furthermore, the bassoon has a very modest bell profile which, for reasons detailed in Chapter 2 (Section 2.5.3), is beneficial when trying to isolate the effects of the tonehole lattice cutoff from other geometric influences. A practical reason for choosing the bassoon is that much of the experimental data, including detailed geometry measurements, input impedance measurements, and radiated sound using an artificial mouth, had already been collected by Vincent Turcotte, a collaborator on the project.

Additional comments

The remainder of this appendix is a partial reproduction and partial extension of the conference proceedings:

E. Petersen, V. Turcotte, and T. Colinot. Objective metrics to identify the tonehole lattice cutoff frequency of conical instruments, Forum Acusticum, Lyon, France, Dec. 2020 (originally April, 2020).

Comments:

The notation has been modified from the original proceedings to be consistent with Chapter 5.

The methodology and results presented here are currently in an unfinished state. The author expects to further develop the work in this appendix for an upcoming article.

B.1 Review and development of quantitative cutoff descriptors

In this section, the tonehole lattice cutoff frequency of a bassoon is quantitatively estimated using the methods proposed in Chapter 5. The methods developed for the saxophone are modified in order to be applied to the bassoon which, although also conical, has a very different geometry from the saxophone. In particular, the apex angle of the bassoon is approximately half that of the saxophone, resulting in a much smaller change in cross-section across the length of the main bore. Additionally, the flare of the bell is less pronounced on the bassoon. Lastly, the bassoon is approximately 2.5 times longer than an alto saxophone, folding back on itself at the boot joint in order to be manageable by the musician. This leads to some peculiarities regarding the toneholes, such as chimneys that are several centimeters long and multiple toneholes for the same note in addition to acoustical effects [126]. Given the considerable differences with the saxophone, it is not clear *a priori* how well the methods developed in Chapter 5 will work when applied to the bassoon, a question that is explored in this section.

B.1.1 Bassoon specific modifications of quantitative descriptors developed for the saxophone

The three descriptors developed in Chapter 5 to determine the cutoff frequency of a geometrically irregular tonehole lattice are the geometrically determined T-cell resonance $f_{\mathrm{c}}^{\mathrm{T}}$ found by asymmetric division of the lattice, the Π-cell characteristic frequencies f_{c}^{Π}, and the empirically derived cutoff transition $f_{\mathrm{t}}^{\mathrm{R}}$. For a review of these terms see Chapter 5 Table 1.

The three descriptors are modified in order to be applied to the bassoon. Due to the strong geometric variation of the lattice, the asymmetric division is successful when only the first three open toneholes are included in the algorithm. This is in contrast with the saxophone, for which the lattice can be divided accounting for six toneholes. Considering only the first three toneholes of the lattice is a weaker application of the asymmetric division, although the results in Chapter 5 suggest that the first several toneholes have the largest influence on the cutoff behavior of a lattice, providing some justification for this modification.

The transition band definition is also modified in order to work with the input impedance measurements of the bassoon, which differ considerably from the alto saxophone studied in Chapter 5, in part due to larger losses associated with a small average cross-section of a long acoustical duct. The input impedance of the first register fingerings of the bassoon are measured using an impedance measurement system adapted for woodwind instruments [127]. The reflection coefficient of the resonator is obtained from the input impedance

$$R(\omega) = \frac{Z(\omega)/Z_\theta(\omega) - 1}{Z(\omega)/Z_\theta(\omega)^* + 1}, \tag{B.1}$$

where the $*$ denotes the complex conjugate and

$$Z_\theta(\omega) = \frac{\rho c}{S} \frac{1}{(1 + 1/j(\omega/c)x)}, \tag{B.2}$$

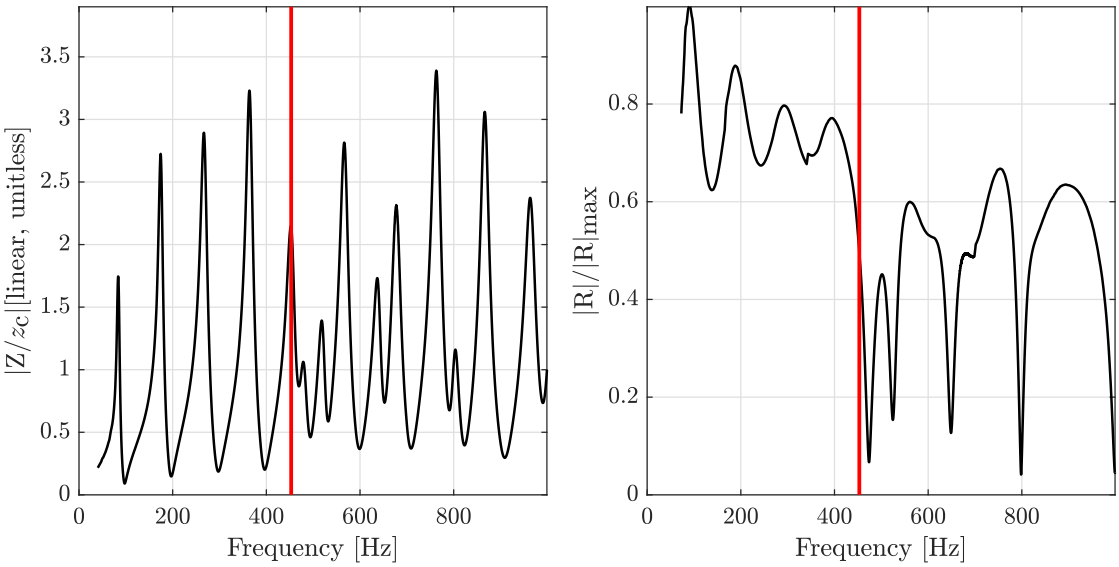

Figure B.1: Measured input impedance modulus (left) and reflection coefficient modulus (right) for the E fingering of the bassoon. The cutoff descriptor defined by Eq. (B.3) is marked by a vertical red line, and corresponds to the asterisks in Figure B.2.

is a frequency dependent characteristic impedance accounting for wave propagation in a conical bore with an input half-angle θ and missing length x.

The alternative definitions provided in Eqs. (B.1) and (B.2) are introduced as an attempt to understand the ripples in the reflection coefficient at low frequencies under the hypothesis that they are due to spherical wave propagation in the conical duct. As seen in Figure B.1, this new definition does not completely mitigate the rippling at low frequencies. One possible explanation is that the CTTM sensor measures the input impedance at the plane where the conical bore is conjoined to the cylindrical cavity of the measurement device, where there may be a combination of propagating and evanescent modes. This is an interesting topic for further investigation.

In contrast with Chapter 5, the reflection coefficient transition band is replaced by a single value. This is intended to simplify the results shown in Figures B.1 and B.2. The threshold is set at half of the maximum value of the reflection coefficient modulus $|R(2\pi f)|_{\max}$, and the estimate of the cutoff $f_{\mathrm{t}}^{\mathrm{R}}$ is the lowest frequency such that

$$|R(2\pi f_{\mathrm{t}}^{\mathrm{R}})| = \frac{1}{2}|R(2\pi f)|_{\max}. \tag{B.3}$$

Because the reflection coefficients calculated from the input impedance measurements do not achieve unity below the cutoff, possibly due to greater losses along the long bore of the instrument or the normalization of the input impedance, the threshold is defined relative to the maximum value.

The results of this descriptor applied to the E fingering (82 [Hz]) are marked as a red line in Figure B.1. The descriptor is defined from the reflection coefficient modulus

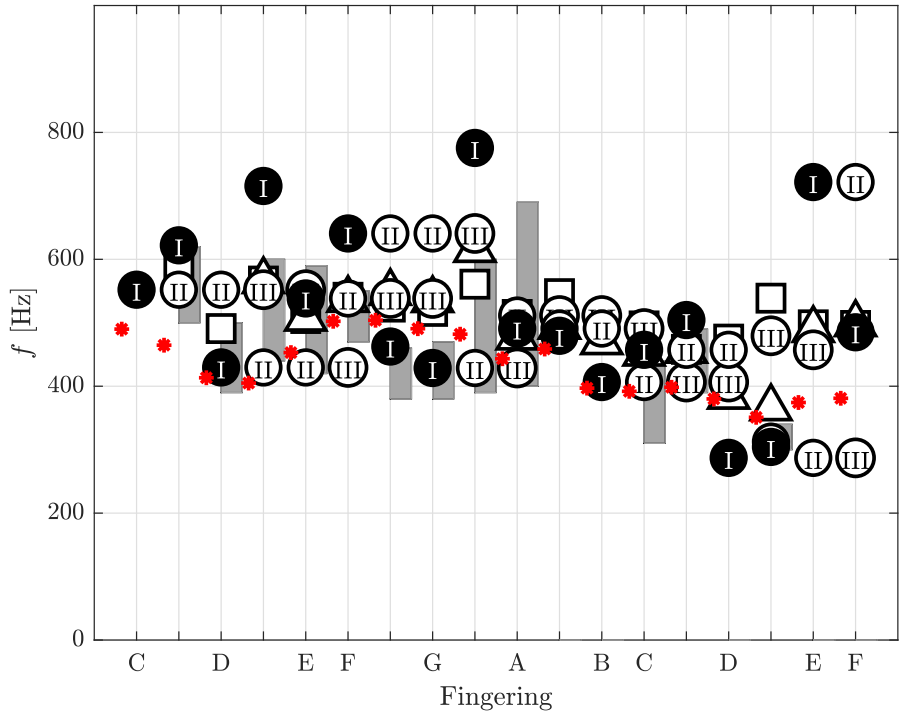

Figure B.2: Comparison of the three cutoff estimations applied to the bassoon. Circled I, II, III correspond respectively to the characteristic frequency f_c^{Π} of the first, second and third Π-shaped cells. For each fingering, triangles mark the average of the first three characteristic frequencies and squares mark the average of all characteristic frequencies. Gray bars show the intervals of successful test cutoff values in the asymmetric division algorithm. The red asterisks mark the reflection coefficient f_t^R defined by Eq. (B.3). The relatively constant cutoff across fingerings is in contrast with the results of the saxophone, Chapter 5 Figure 7, noting that the orientation of fingerings is reversed.

(right panel) but also plotted on the input impedance modulus (left panel).

B.1.2 Comparison of descriptors over first register

The three cutoff descriptors are computed for 18 fingerings in the first register of the bassoon, from C (65 [Hz]) up to F (175 [Hz]). The two lowest fingerings, producing to the notes B♭ (58 [Hz]) and B (62 [Hz]), are excluded because they only have zero and one open tonehole. Figure B.2 shows that the cutoff metrics overlap reasonably well for most fingerings. A full study would be needed to know whether this is the case for other instruments, and how it depends on the chosen thresholds. The asymmetric division algorithm provides a cutoff interval finer than the spread of characteristic frequencies for most fingerings. Overall, the cutoff estimates show an almost constant trend, between 400 and 600 Hz, for all of the fingerings, which is coherent with previously reported values [3,

128, 129]. Note that the trend is markedly different on another conical woodwind, the saxophone, where the cutoff increases progressively for higher fingerings [6].

B.2 Conclusions

The cutoff frequency estimates developed for the saxophone can be used to characterize the cutoff of the bassoon with relatively minor adaptations. The results for the bassoon show that both local and global type cutoff estimates are coherent with one another, and demonstrate that the cutoff falls within 400 and 600 [Hz] across the range of the first register. The homogeneous cutoffs across fingerings is in accordance with the results reported by Benade [3]. This is a useful result because it shows that the new descriptors match existing results for the bassoon, which bolsters their use on the saxophone, an instrument for which research of the cutoff has been rarely published.

This work adds to the results in Chapter 5 by applying previously developed cutoff descriptors to a bassoon. As in Chapter 3, digital synthesis was used to evaluate the effect of the cutoff on sound production of acoustically regular conical lattices. However, those results will be presented at a conference and are not reported here because the current author is not the first author of the submission [130].

Bibliography

[1] A. H. Benade. On the mathematical theory of woodwind finger holes. *J. Acoust. Soc. Am.*, 32:1591–1608, 1960.

[2] L. Brillouin and M. Parodi. *Wave propagation in periodic structures.* Dover Publications, NY, USA, 1946.

[3] A. H. Benade. *Fundamentals of Musical Acoustics.* Oxford University Press, London, 1976.

[4] A. H. Benade and S. N. Kouzoupis. The clarinet spectrum: theory and experiment. *J. Acoust. Soc. Am.*, 83(1):292–304, 1988.

[5] A. H. Benade and S. J. Lutgen. The saxophone spectrum. *J. Acoust. Soc. Am.*, 83:1900–1907, 1988.

[6] E. Petersen, T. Colinot, J. Kergomard, and P. Guillemain. On the tonehole lattice cutoff frequency of conical resonators: applications to the saxophone. *Acta Acust.*, 4(4):13, 2020. doi: 10.1051/aacus/2020012.

[7] A. H. Benade and D. J. Gans. Sound production in wind instruments. *Annals of the New York Academy of Sciences*, 155(1):247–263, 1968. doi: 10.1111/j.1749-6632.1968.tb56770.x.

[8] A. H. Benade. *Sound Generation in Winds, Strings, Computers: Papers by Benade, Chowning, Hutchins, Jansson, Alonso Moral Given at Seminars of the Committee for the Acoustics of Music.* Kungl. Musikaliska Akademiens skriftserie: Kungliga Musikaliska Akademien. Kungl. Musikaliska Akademien, 1980. ISBN 9789185428182.

[9] M. Chotteau. The isospectrum clarinet system. Master's thesis, Case Western Reserve University, 1971.

[10] W. E. Worman. Self-sustained oscillations in clarinet-like systems—quantitative results. *J. Acoust. Soc. Am.*, 48(1A):89–89, 1970. doi: 10.1121/1.1975391.

[11] A. H. Benade. Acoustic criteria and procedures for adjusting tone and response in woodwinds. *J. Acoust. Soc. Am.*, 1A(48):89–89, 1970.

[12] W. E. Worman. *Self-sustained nonlinear oscillations of medium amplitude in clarinet like systems.* PhD thesis, Case Western Reserve University, 1971.

[13] N. H. Fletcher. Mode locking in nonlinearly excited inharmonic musical oscillators. *J. Acoust. Soc. Am.*, 64(6):1566–1569, 1978. doi: 10.1121/1.382139.

[14] V. Debut, J. Kergomard, and F. Laloe. Analysis and optimisation of the tuning of the twelfths for a clarinet resonator. *Applied Acoustics*, 66, 2005. doi: 10.1016/j.apacoust.2004.08.003.

[15] J. Kergomard. *Internal field and external field of wind instruments.* PhD thesis, Université Paris 6 (in French), 1981.

[16] D. H. Keefe. *Woodwind Tone Hole Acoustics and the Spectrum Transformation Function.* PhD thesis, Department of Physics, Case Western Reserve University, 1981.

[17] D. H. Keefe. Woodwind air column models. *J. Acoust. Soc. Am.*, 88:35–51, 1990.

[18] S. C. Thompson. The effect of the reed resonance on woodwind tone production. *J. Acoust. Soc. Am.*, 66(5):1299–1307, 1979. doi: 10.1121/1.383448.

[19] D. H. Keefe and S. Waeffler. The influence of clarinet and saxophone reed responses on sound production. *J. Acoust. Soc. Am.*, 94(3):1833–1834, 1993. doi: 10.1121/1.407785.

[20] D. H. Keefe and R. H. Cronin. A linearized model of bassoon sound production: The role of auxiliary fingerings. *J. Acoust. Soc. Am.*, 99(4):2456–2457, 1996. doi: 10.1121/1.415474.

[21] P. Dickens, R. France, J. Smith, and J. Wolfe. Clarinet acoustics: Introducing a compendium of impedance and sound spectra. *Acoustics Australia*, 35:17–24, 2007.

[22] E. Moers and J. Kergomard. On the cutoff frequency of clarinet-like instruments. Geometrical versus acoustical regularity. *Acta Acust united Ac*, 97:984–996, 2011.

[23] A. Chaigne and J. Kergomard. *Acoustics of Musical Instruments.* Springer-Verlag, New York, 2016. (English translation).

[24] J. Wolfe and J. Smith. Cutoff frequencies and cross fingerings in baroque, classical, and modern flutes. *J. Acoust. Soc. Am.*, 114(4):2263–2272, 2003.

[25] J. O. Noreland, J. Kergomard, F. Laloe, C. Vergez, P. Guillemain, and A. Guilloteau. The logical clarinet: Numerical optimization of the geometry of woodwind instruments. *Acta Acust united Ac*, 99, 2012. doi: 10.3813/AAA.918641.

[26] M. E. McIntyre, R. T. Schumacher, and J. Woodhouse. On the oscillations of musical instruments. *J. Acoust. Soc. Am.*, 74:1325–1345, 1983.

[27] N. H. Fletcher and T. D. Rossing. *The physics of musical instruments.* Springer New York ; London, 2nd edition, 1998. ISBN 0387983740 0387983759.

[28] A. Lefebvre, G. P. Scavone, and J. Kergomard. External tonehole interactions in woodwind instruments. *Acta Acust united Ac*, 99:975–985, 2013.

[29] E. Petersen, P. Guillemain, J. Kergomard, and T. Colinot. The effect of the cutoff frequency on the sound production of a clarinet-like instrument. *J. Acoust. Soc. Am.*, 145(6):3784–3794, 2019.

[30] A. Pierce. *Acoustics: An Introduction to Its Physical Principles and Applications*, volume 34. Springer, 1989. ISBN 0883186128. doi: 10.1063/1.2914388.

[31] W. P. Mason. A study of the regular combination of acoustic elements, with applications to recurrent acoustic filters, tapered acoustic filters, and horns. *The Bell System Technical Journal*, 6(2):258–294, 1927.

[32] Juliette Chabassier and Robin Tournemenne. About the transfert matrix method in the context of acoustical wave propagation in wind instruments. Research Report RR-9254, INRIA Bordeaux, 2019.

[33] M. Born, E. Wolf, A. B. Bhatia, P. C. Clemmow, D. Gabor, A. R. Stokes, A. M. Taylor, P. A. Wayman, and W. L. Wilcock. *Principles of Optics: Electromagnetic Theory of Propagation, Interference and Diffraction of Light*. Cambridge University Press, 7th edition, 1999.

[34] S. Félix, J.-P. Dalmont, and C. J. Nederveen. Effects of bending portions of the air column on the acoustical resonances of a wind instrument. *J. Acoust. Soc. Am.*, 131(5):4164–4172, 2012. doi: 10.1121/1.3699267.

[35] V. Easwaran, V.H. Gupta, and M.L. Munjal. Relationship between the impedance matrix and the transfer matrix with specific reference to symmetrical, reciprocal and conservative systems. *Journal of Sound and Vibration*, 161(3):515 – 525, 1993. doi: 10.1006/jsvi.1993.1089.

[36] J. Backus. Acoustic impedance of an annular capillary. *J. Acoust. Soc. Am.*, 58(5): 1078–1081, 1975. doi: 10.1121/1.380767.

[37] V. Dubos, J. Kergomard, A. Khettabi, J.-P. Dalmont, D. H. Keefe, and C. J. Nederveen. Theory of sound propagation in a duct with a branched tube using modal decomposition. *Acta Acust united Ac*, 85:153–169, 1999.

[38] D. H. Keefe. Theory of the single woodwind tone hole. *J. Acoust. Soc. Am.*, 72(3): 676–687, 1982. doi: 10.1121/1.388248.

[39] D. H. Keefe. Acoustic streaming, dimensional analysis of nonlinearities, and tone hole mutual interactions in woodwinds. *J. Acoust. Soc. Am.*, 73(5):1804–1820, 1983. doi: 10.1121/1.389404.

[40] Antoine Lefebvre and Gary P. Scavone. Characterization of woodwind instrument toneholes with the finite element method. *J. Acoust. Soc. Am.*, 131(4):3153–3163, 2012. doi: 10.1121/1.3685481.

[41] A. G. Webster. Acoustical impedance and the theory of horns in the phonograph. *Proceedings of the National Academy of Sciences of the United States of America*, 5(7):275–282, 1919.

[42] E. Eisner. Complete solutions of the "webster" horn equation. *J. Acoust. Soc. Am.*, 41(4B):1126–1146, 1967. doi: 10.1121/1.1910444.

[43] J. Kergomard and A. Garcia. Simple discontinuities in acoustic waveguides at low frequencies: Critical analysis and formulae. *Journal of Sound and Vibration*, 114 (3):465 – 479, 1987. doi: 10.1016/S0022-460X(87)80017-2.

[44] F. Silva, P. Guillemain, J. Kergomard, B. Mallaroni, and A.N. Norris. Approximation formulae for the acoustic radiation impedance of a cylindrical pipe. *Journal of Sound and Vibration*, 322(1):255–263, 2009. ISSN 0022-460X.

[45] R. L. Pritchard. Mutual acoustic impedance between radiators in an infinite rigid plane. *J. Acoust. Soc. Am.*, 32(6):730–737, 1960.

[46] E. Skudrzyk. *The Foundations of Acoustics*. Springer, 1971.

[47] George Walter Stewart and Robert Bruce Lindsay. *Acoustics : a text on theory and applications / by George Walter Stewart and Robert Bruce Lindsay.* Chapman & Hall, London, 1930.

[48] C. E. Bradley. Time harmonic acoustic bloch wave propagation in periodic waveguides. Part I. Theory. *J. Acoust. Soc. Am.*, 96(3):1844–1853, 1994.

[49] H. Helmholtz. *On the Sensations of Tone*. Dover Books on Music. Dover Publications, 2013. ISBN 9780486315461.

[50] M. Abramowitz and I. A. Stegun. *Handbook of Mathematical Functions with Formulas, Graphs, and Mathematical Tables*. Dover, New York, ninth dover printing, tenth gpo printing edition, 1964.

[51] Petersen, Erik Alan, Colinot, Tom, Guillemain, Philippe, and Kergomard, Jean. The link between the tonehole lattice cutoff frequency and clarinet sound radiation: a quantitative study. *Acta Acust.*, 4(5):18, 2020.

[52] D. A. Russell, J. P. Titlow, and Y.-J. Bemmen. Acoustic monopoles, dipoles, and quadrupoles: An experiment revisited. *American Journal of Physics*, 67(8):660–664, 1999. doi: 10.1119/1.19349.

[53] S. Weinzierl, M. Vorländer, G. Behler, F. Brinkmann, H. von Coler, E. Detzner, J. Krämer, A. Lindau, M. Pollow, F. Schulz, and N. R. Shabtai. A database of anechoic microphone array measurements of musical instruments, 2017.

[54] J.M. Eargle. *In: Electroacoustical Reference Data*. Springer, Boston, MA, 1994. Chapter: Directional Properties of Woodwind Instruments.

[55] A. H. Benade. From instrument to ear in a room: direct or via recording. *J. Audio Eng. Soc.*, 33(4):218–233, 1985.

[56] A. H. Benade and C. O. Larson. Requirements and techniques for measuring the musical spectrum of the clarinet. *J. Acoust. Soc. Am.*, 78(5):1475–1498, 1985.

[57] H. Bach. Directivity of basic linear arrays. *IEEE Transactions on Antennas and Propagation*, 18(1):107–110, 1970. ISSN 0018-926X.

[58] A. H. Benade. Equivalent circuits for conical waveguides. *J. Acoust. Soc. Am.*, 83 (5):1764–1769, 1968.

[59] A. Guilloteau, P. Guillemain, J. Kergomard, and M. Jousserand. The effect of the size of the opening on the acoustic power radiated by a reed woodwind instrument. *Journal of Sound and Vibration*, 343:166–175, 2015. ISSN 0022-460X. doi: 10.1016/j.jsv.2015.01.020.

[60] J. Wolfe. http://newt.phys.unsw.edu.au/music/, Accessed 2020. Website about musical acoustics.

[61] A. H. Benade and D. H. Keefe. The physics of a new clarinet design. *The Galpin Society Journal*, 49:113–142, 1996.

[62] J. O. Noreland, J. Kergomard, F. Laloe, C. Vergez, P. Guillemain, and A. Guilloteau. The logical clarinet: Numerical optimization of the geometry of woodwind instruments. *Acta Acust united Ac*, 99, 2012. doi: 10.3813/AAA.918641.

[63] E. G. Richardson. Adjustable resonators and orchestration. *Nature*, 139:157, 1937.

[64] M. Schroeder, T. Rossing, F. Dunn, W. Hartmann, D. M. Campbell, and N. Fletcher. *Springer Handbook of Acoustics*. Springer, 2007. ISBN 0387304460, 9780387304465. doi: 10.1007/978-0-387-30425-0.

[65] J. H. M. Disselhorst and L. van Wijngaarden. Flow in the exit of open pipes during acoustic resonance. *Journal of fluid mechanics*, 99:293–319, 1980. ISSN 0022-1120. doi: 10.1017/S0022112080000626.

[66] J.-P. Dalmont, C. Nederveen, V. Dubos, S. Ollivier, V. Méserette, and E. Sligte. Experimental determination of the equivalent circuit of an open side hole: Linear and non linear behaviour. *Acta Acust united Ac*, 88:567–575, 2002.

[67] Muttalip Temiz, Ines Lopez Arteaga, and Avraham Hirschberg. Non-linear behavior of tone holes in musical instruments: An experimental study. In *Conference Française d'Acoustique CFA 2016. Le Mans, France*, 2016.

[68] M. Atig, J.-P. Dalmont, and J. Gilbert. Saturation mechanism in clarinet-like instruments, the effect of the localised non-linear losses. *Applied Acoustics*, 65, 2004. doi: 10.1016/j.apacoust.2004.04.005.

[69] J. Pätynen and T. Lokki. Directivities of symphony orchestra instruments. *Acta Acust united Ac*, 96:138–167, 2010.

[70] A. Hirschberg, J. Gilbert, A. P. J. Wijnands, and A. M. C Valkering. Musical aero-acoustics of the clarinet. *Journal de physique IV (proceedings)*, 04, 1994. doi: 10.1051/jp4:19945120.

[71] A. Myers, R. W. Pyle, J. Gilbert, D. M. Campbell, J. P. Chick, and S. Logie. Effects of nonlinear sound propagation on the characteristic timbres of brass instruments. *J. Acoust. Soc. Am.*, 131(1):678–688, 2012. doi: 10.1121/1.3651093.

[72] N. Fletcher. Air flow and sound generation in musical wind instruments. *Annu. Rev. Fluid Mech*, 11:123–146, 1979. doi: 10.1146/annurev.fl.11.010179.001011.

[73] J. Backus. Input impedance curves for the reed woodwind instruments. *J. Acoust. Soc. Am.*, 56(4):1266–1279, 1974.

[74] A. H. Benade. On woodwind instrument bores. *J. Acoust. Soc. Am.*, 31(2):137–146, 1959. doi: 10.1121/1.1907682.

[75] M. Barthet, P. Guillemain, R. Kronland-Martinet, and S. Ystad. From clarinet control to timbre perception. *Acta Acust united Ac*, 96:678–689, 2010.

[76] V. Chatziioannou, S. Schmutzhard, and M. Pàmies-Vilà. Investigating clarinet articulation using a physical model and an artificial blowing machine. *Acta Acust united Ac*, 105:682–694, 2019.

[77] Theodore A Wilson and Gordon S Beavers. Operating modes of the clarinet. *J. Acoust. Soc. Am.*, 56(2):653–658, 1974.

[78] A. Almeida, D. George, J. Smith, and J. Wolfe. The clarinet: How blowing pressure, lip force, lip position and reed "hardness" affect pitch, sound level, and spectrum. *J. Acoust. Soc. Am.*, 134:2247–55, 2013. doi: 10.1121/1.4816538.

[79] J. Adrien. *The missing link: Modal synthesis.* MIT Press, Cambridge, MA, 1991. In G. DePoli, A. Picialli, and C. Roads, editors, Representations of Musical Signals.

[80] R. T. Schumacher. Ab initio calculations of the oscillations of a clarinet. *J. Acoust. Soc. Am.*, 65(S1):S73–S73, 1979. doi: 10.1121/1.2017413.

[81] S. E. Stewart and W. J. Strong. Functional model of a simplified clarinet. *J. Acoust. Soc. Am.*, 68(1):109–120, 1980. doi: 10.1121/1.384635.

[82] T. Grothe and J. Baumgart. Assessment of bassoon tuning quality from measurements under playing conditions. *Acta Acust united Ac*, 101(2):238–245, 2015. doi: 10.3813/AAA.918822.

[83] P. Guillemain, C. Vergez, D. Ferrand, and A. Farcy. An instrumented saxophone mouthpiece and its use to understand how an experienced musician plays. *Acta Acust united Ac*, 96, 2010. doi: 10.3813/AAA.918317.

[84] P. Guillemain, J. Kergomard, and T. Voinier. Real-time synthesis of clarinet-like instruments using digital impedance models. *J. Acoust. Soc. Am.*, 118(1):483–494, 2005. doi: 10.1121/1.1937507.

[85] J. Gilbert, J. Kergomard, and E. Ngoya. Calculation of the steady-state oscillations of a clarinet using the harmonic balance technique. *J. Acoust. Soc. Am.*, 86(1):35–41, 1989.

[86] G. R. Plitnik and W. J. Strong. Numerical method for calculating input impedances of the oboe. *J. Acoust. Soc. Am.*, 65(3):816–825, 1979.

[87] R. Causse, J. Kergomard, and X. Lurton. Input impedance of brass musical instruments–comparison between experiment and numerical models. *J. Acoust. Soc. Am.*, 75(1):241–254, 1984.

[88] P. Rucz. A finite element approach for the calculation of self and mutual radiation impedances of resonators. *J. Acoust. Soc. Am.*, 143(4):2449–2459, 2018.

[89] H. Fürstenberg. Noncommuting random matrix products. *Trans. Am. Math. Soc.*, 108:377–428, 1963.

[90] P. W. Anderson. Absense of diffusion in certain random lattices. *Phys. Rev.*, 109: 1492–1505, 1958.

[91] J. C. Le Roux, M. Parchebat, and J.-P. Dalmont. A new impedance sensor for industrial applications. *Conf. Proceedings: Acoustics 2012*, 2012.

[92] P. Guillemain. A digital synthesis model of double-reed wind instruments. *EURASIP Journal on Applied Signal Processing*, 7:990–1000, 2004.

[93] W. L. Coyle, P. Guillemain, J. Kergomard, and J.-P. Dalmont. Predicting playing frequencies for clarinets: A comparison between numerical simulations and simplified analytical formulas. *J. Acoust. Soc. Am.*, 138(5):2770–2781, 2015.

[94] B. Gazengel, J. Gilbert, and N. Amir. Time domain simulation of single reed wind instrument. From the measured input impedance to the synthesis signal. where are the traps? *Acta Acust united Ac*, 3:445–472, 1995.

[95] P. Guillemain, J. Kergomard, and T. Voinier. Real-time synthesis of clarinet-like instruments using digital impedance models. *J. Acoust. Soc. Am.*, 118:483–494, 2005.

[96] F. Avanzini and M. Walstijn. Modelling the mechanical resonse of the reed-mouthpiece-lip system of a clarinet. Part I. A one-dimensional distributed model. *Acta Acust united Ac*, 90:537–547, 2004.

[97] M. Walstijn and F. Avanzini. Modelling the mechanical resonse of the reed-mouthpiece-lip system of a clarinet. part ii: A lumped model approximation. *Acta Acust united Ac*, 93:435–446, 2007.

[98] S. Bilbao, A. Torin, and V. Chatziioannou. Numerical modeling of collisions in musical instruments. *Acta Acust united Ac*, 101:155–173, 2015.

[99] J.-P. Dalmont, P. Guillemain, and P.-A. Taillard. Influence of the reed flow on the intonation of the clarinet. In *Acoustics 2012*, 2012.

[100] J.-P. Dalmont, B. Gazengal, J. Gilbert, and J. Kergomard. Some aspects of tuning and clean intonation in reed instruments. *Applied Acoustics*, 46:19–60, 1995.

[101] J. Dalmont, J. Gilbert, and S. Ollivier. Nonlinear characteristics of single-reed instruments: Quasistatic volume flow and reed opening measurements. *J. Acoust. Soc. Am.*, 114(4):2253–2262, 2003.

[102] E. Petersen, P. Guillemain, J. Kergomard, and T. Colinot. See supplementary material at https://doi.org/10.1121/1.5111855 for synthesized mouthpiece waveforms as audio for pressure, mm. (1)–(3), acoustic flow, mm. (4)-(6), and time derivative of pressure plus flow, mm. (7)–(9) (an approximation of radiated sound), for resonators with cutoff frequencies of 1000, 1500, and 2000 Hz., 2019.

[103] E. G. Shower and R. Biddulph. Differential pitch sensitivity of the ear. *J. Acoust. Soc. Am.*, 3:275–287, 1931.

[104] S. McAdams, J. W. Beauchamp, and S. Meneguzzi. Discrimination of musical instrument sounds resynthesized with simplified spectrotemporal parameters. *J. Acoust. Soc. Am.*, 105(2):882–897, 1999.

[105] K. Buys, D. Sharp, and R. Laney. Developing and evaluating a hybrid wind instrument. *Acta Acust united Ac*, 103(5):830–846, 2017.

[106] T. Grothe and S. Amengual Garí. Measurement of "reed to room" transfer functions. *Acta Acust united Ac*, 105:899–903, 2019. doi: 10.3813/AAA.919370.

[107] J. Buick, M. Atig, D. Skulina, D. M. Campbell, J.-P. Dalmont, and J. Gilbert. Investigation of non-linear acoustic losses at the open end of a tube. *J. Acoust. Soc. Am.*, 129:1261–72, 2011. doi: 10.1121/1.3543987.

[108] J. Jordania. *Garland Encyclopedia of World Music Volume 8 - Europe: Part 3: Music Cultures of Europe: Bulgaria.* Routledge, New York, 1981.

[109] V. Chatziioannou and M. Van Walstijn. Estimation of clarinet reed parameters by inverse modelling. *Acta Acust united Ac*, 98(4):629–639, 2012.

[110] T. Colinot, L. Guillot, C. Vergez, P. Guillemain, J.-B. Doc, and B. Cochelin. Influence of the "ghost reed" simplification on the bifurcation diagram of a saxophone model. *Acta Acust united Ac*, 105(6):1291–1294, 2019.

[111] A. Almeida, D. George, J. Smith, and J. Wolfe. The clarinet: How blowing pressure, lip force, lip position and reed "hardness" affect pitch, sound level, and spectrum. *J. Acoust. Soc. Am.*, 134:2247–55, 2013. doi: 10.1121/1.4816538.

[112] J.-P. Dalmont, J. Gilbert, and S. Ollivier. Nonlinear characteristics of single-reed instruments: Quasistatic volume flow and reed opening measurements. *J. Acoust. Soc. Am.*, 114(4):2253–2262, 2003. doi: 10.1121/1.1603235.

[113] S. Karkar, C. Vergez, and B. Cochelin. Oscillation threshold of a clarinet model: A numerical continuation approach. *J. Acoust. Soc. Am.*, 131:698–707, 2012. doi: 10.1121/1.3651231.

[114] F. Silva, J. Kergomard, C. Vergez, and J. Gilbert. Interaction of reed and acoustic resonator in clarinetlike systems. *J. Acoust. Soc. Am.*, 124(5):3284–3295, 2008. doi: 10.1121/1.2988280.

[115] T. Grothe and P. Wolf. A study of sound characteristics of a new bassoon as compared to the modern german bassoon. In *Stockholm Music Acoustics Conference*, 2013.

[116] D. K. Bowen, K Buys, M. Dart, and D. Sharp. Assessing the sound of a woodwind instrument that cannot be played. *Applied Acoustics*, 143:84–99, 2019.

[117] H. T Nia, A. D. Jain, Y. Liu, M.-R. Alam, R. Barnas, and N. C. Makris. The evolution of air resonance power efficiency in the violin and its ancestors. *Proceedings of the Royal Society A: Mathematical, Physical and Engineering Sciences*, 471 (2175):20140905, 2015. doi: 10.1098/rspa.2014.0905.

[118] P. Dietrich. *Uncertainties in Acoustical Transfer Functions: Modeling, Measurement and Derivation of Parameters for Airborne and Structure-borne Sound.* Aachener Beiträge zur Technischen Akustik. Hochschulbibliothek der Rheinisch-Westfälischen Technischen Hochschule Aachen, 2013. ISBN 9783832596057.

[119] E. Petersen and R. Rosser. External sound field simulations and measurements of woodwind resonators. In *Proceedings of ISMA 2019 International Symposium on Music Acoustics*, pages 58–61, 2019.

[120] S. Müller and P. Massarani. Transfer-function measurement with sweeps. *J. Audio Eng. Soc*, 49(6):443–471, 2001.

[121] P. Woloszyn. *Acoustic diffraction patterns from regular to fractal structures: application to the Sierpinski carpet.* Fractals in Engineering. New Trends in Theory and Applications. Springer Verlag, 2005.

[122] M. Sanalatii, P. Herzog, R. Guillermin, M. Melon, N. Poulain, and J.-C. Le Roux. Estimation of loudspeaker frequency response and directivity using the radiation-mode method. *Journal of the Audio Engineering Society*, 67:101–115, 2019.

[123] A. Sarkissian. Acoustic radiation from finite structures. *J. Acoust. Soc. Am.*, 90 (1):574–578, 1991. doi: 10.1121/1.401231.

[124] S. J. Elliott and M. E. Johnson. Radiation modes and the active control of sound power. *J. Acoust. Soc. Am.*, 94(4):2194–2204, 1993. doi: 10.1121/1.407490.

[125] K. A. Cunefare and M. N. Currey. On the exterior acoustic radiation modes of structures. *J. Acoust. Soc. Am.*, 96(4):2302–2312, 1994. doi: 10.1121/1.410102.

[126] D.B. Sharp, H.A.K. Wright, and W. Ring. An acoustical investigation into the effect of the crook profile on the sound produced by the bassoon. *Acta Acust united Ac*, 89(1):137–144, 2003.

[127] J.-P. Dalmont and J.-C. Le Roux. A new impedance sensor for wind instruments. *J. Acoust. Soc. Am.*, 123:3014, 2008. doi: 10.1121/1.2932617.

[128] F. Fransson. *The source spectrum of double-reed wood-wind instruments.* Prog. Status Rep. R. Inst. Technol. Stock., 1966.

[129] J. Meyer. *Acoustics and the Performance of Music*. Springer, 2009. ISBN 978-0-387-09516-5. doi: 10.1007/978-0-387-09517-2.

[130] T. Colinot, E. Petersen, and P. Guillemain. The effect of the tonehole lattice cutoff frequency on sound production for conical resonators. In *Forum Acusticum, Lyon, France*, 2020.

The research goal of this dissertation is to evaluate how the tonehole lattice cutoff frequency affects the sound production and radiation of woodwind instruments. Below the cutoff, waves entering the tonehole lattice are evanescent, where as above cutoff waves can propagate freely within the lattice. Therefore, the low frequency response of the resonator that determines the playing frequency of a woodwind is set by the length between the reed and the first open tonehole, while the high frequency response is governed by the remaining open toneholes downstream on the instrument. A study of the cutoff frequency that separates these two bands is, in effect, a study of how this 'unused' portion of the tonehole lattice may influence the sound of the instrument. Following the work of Benade in the 1960s, studies on this subject have been rare, despite its central importance to the sound of woodwind instruments. This dissertation includes analytical, numerical, and experimental advances on the subject of the cutoff frequency, approached in three published studies. In the first, cylindrical academic resonators are analytically designed to have specific cutoffs while maintaining the same first resonance frequency. They are then compared using digital synthesis based on a physical model of the instrument. The cutoff is found to have a modest impact on sound production, evaluated using the pressure and flow waveforms within the mouthpiece, where the greatest effect is a randomization of the relative amplitude of even and odd harmonics above the cutoff. There is little evidence that the 'ease of playing' of the resonators is affected by the cutoff. In the second study, the academic resonators are played by a musician using a clarinet mouthpiece during *in situ* measurements. The radiated sound demonstrates a 'region of reinforced spectra,' for which there is an amplitude increase of both even and odd harmonics around the cutoff of each resonator. The third study derives the cutoff theory for conical resonators and introduces new quantitative descriptors to estimate the cutoff of acoustically irregular lattices. An analysis of the saxophone demonstrates that the cutoff varies considerably over the first register of the instrument. The results also demonstrate ways in which the theory of wave propagation in periodic media can succeed or fail when applied to real instruments. Preliminary results for two additional studies are presented. In the first, the methods developed for the saxophone are applied to another conical instrument, the bassoon. The results show that, compared with the saxophone, the cutoff of the bassoon is homogeneous across different fingerings of the first register. In the second, the effect of diffraction from a simplified resonator is evaluated using a boundary element method. The results are compared with a simplified analytical radiation model and anechoic measurements, showing that the more efficient simple model is generally sufficient. This dissertation demonstrates ways in which the cutoff affects both internal waveforms and, more importantly, the radiated soundfield of woodwind-type instruments. It also advances the theoretical basis for incorporating the cutoff into a tonehole lattice conception, which is of practical use for instrument manufacturers.
Key words: musical acoustics; periodic waveguides; woodwinds; tonehole lattice cutoff frequency

---

L'objectif de cette thèse est de contribuer à évaluer comment la fréquence de coupure créée par un réseau de trous latéraux ouverts dans un instrument de musique de la famille des bois agit sur la production et le rayonnement du son produit par ces instruments. En dessous de cette fréquence de coupure, les ondes pénétrant dans le réseau de trous ouverts sont évanescentes, tandis qu'au delà de cette fréquence les ondes peuvent se propager dans le réseau. Par conséquent, la réponse basse fréquence du résonateur qui détermine la fréquence de jeu est directement reliée à la longueur entre l'anche et le premier trou ouvert, tandis que la réponse à haute fréquence est déterminée par le réseau de trous ouverts. Une étude de la fréquence de coupure séparant ces deux bandes de fréquence correspond donc à comprendre comment cette partie "inutilisée" du résonateur joue sur le son produit. Depuis les travaux de Benade dans les années 1960, les études sur ce sujet ont été rares bien qu'il s'agisse d'un sujet central sur le son des instruments à vent. Ce manuscript comprend des études analytiques, numériques et expérimentales relatives à la fréquence de coupure et est étayé par trois articles de revues. Tout d'abord, des résonateurs cylindriques "académiques" sont conçus analytiquement de sorte à fixer leurs fréquences de coupure tout en maintenant la première fréquence de résonance constante. Ces résonateurs sont ensuite comparés en utilisant une synthèse numérique reposant sur un modèle physique de fonctionnement. Un premier résultat est que la fréquence de coupure a très peu d'effet sur la production du son, calculée grâce à la pression et au débit interne dans l'embouchure de l'instrument. Au delà de la fréquence de coupure, on assiste à une répartition aléatoire des amplitudes des harmoniques pairs et impairs. Il y a donc très peu d'effet de cette fréquence de coupure sur la "facilité de jeu" d'un instrument. Dans une seconde étude, les résonateurs sont réalisés physiquement et joués par un musicien grâce à l'ajout d'un bec de clarinette. Le spectre externe présente une région où il y une augmentation du niveau des harmoniques, tant pairs qu'impairs, au voisinage de la fréquence de coupure. La troisième étude étend la théorie de la fréquence de coupure au cas de résonateurs coniques et introduit de nouveaux descripteurs pour estimer la fréquence de coupure de réseaux acoustiquement irréguliers. Une analyse sur le saxophone montre que la fréquence de coupure évolue de note à note au long du premier registre. Nous montrons également dans quelle mesure la théorie de propagation d'ondes dans des milieux périodiques peut fonctionner ou échouer dès lors que l'on s'intéresse à un instrument existant. Des résultats préliminaires de deux autres études dont également présentés. La première concerne le basson, pour lequel on applique les méthodes développées pour le saxophone. Les résultats montrent que, contrairement au saxophone, la fréquence de coupure reste quasiment constante tout au long du premier registre. La deuxième concerne l'utilisation d'éléments finis de frontière (BEM) pour étudier la diffraction d'un resonator muni de trous. Ce calcul est comparé avec celui produit par un calcul analytique simple et une expérience en chambre anéchoïque, qui montre qu'un modèle simple est suffisant. Dans cette thèse, nous montrons comment la fréquence de coupure agit sur les formes d'onde et le spectre de la pression et du débit internes et plus significativement sur le champ rayonné. Nous avançons également sur les bases théoriques permettant d'inclure ce critère dans un objectif de conception, à destination des facteurs.
Key words: acoustique musicale; guides d'onde periodiques; instrument de la famille des bois; fréquence de coupure d'un reseau du trous latéraux